Neuronal microRNAs in inflammation-induced neurodegeneration

Dissertation

zur Erlangung der Würde des Doktors der Naturwissenschaften

des Fachbereichs Biologie, der Fakultät für Mathematik, Informatik

und Naturwissenschaften der Universität Hamburg

vorgelegt von

Iris Winkler

aus Gütersloh

Conducted at

Institute of Neuroimmunology and Multiple Sclerosis

(INIMS) Center for Molecular Neurobiology Hamburg

(ZMNH) University Medical Center Hamburg-Eppendorf

(UKE)

Chair: Prof. Dr. Thomas Oertner

Supervisor and referee: Prof. Dr. Manuel Alexander Friese

Referee: Prof. Dr. Christian Lohr

Date of defence: 28. August 2020

Table of Contents

List of Figures

List of Tables

Abbreviations

AAV	Adeno-associated virus
ACh	Acetylcholine
AGO	Argonaute
ALS	Amyotrophic lateral sclerosis
AMO	Anti-miRNA oligonucleotide
AMPA	α-amino-3-hydroxy-5-methyl-4-isoxazole propionic acid
AP-1	Activator protein 1
AP5	2-Amino-5-phosphonopentanoic acid
AraC	Cytosine arabinoside
ASO	Antisense oligonucleotides
Bac	Bacterial artificial chromosome
BBB	Blood-brain barrier
BDNF, *Bdnf*	Brain-derived neurotrophic factor
Bp	Base pairs
BSA	Bovine serum albumin
Ca^{2+}	Divalent calcium
CaMKII	Calcium/Calmodulin dependent kinase II
cAMP	Cyclic adenosine monophosphate
CASK II	Ca^{2+}-calmodulin-dependent kinase II
CCL2	CC-Chemokine-Ligand 2
ChAT, *Chat*	Acetyl choline transferase
CHX	Cycloheximide
CIS	Clinically isolated syndrome
Cnp	2',3'-cyclic nucleotide 3' phosphodiesterase
CNS	Central nervous system
CPEB3, *Cpeb3*	Cytoplasmic polyadenylation element-binding protein 3
CREB	cAMP response element-binding protein
CS	Conserved sites
CWCS	Cumulative weighted context++ score
DC	Dorsal column
DCs	Dendritic cells

Dcun1d4	DCN1-like protein 4
DGCR8	DiGeorge syndrome critical region
DIV	Day in vitro
DPBS	Dulbecco's PBS
DRG	Dorsal root ganglion
dsRNA	Double strand RNA
DTT	Dithiothreitol
EAAT	Excitatory amino acid transporters
EAE	Experimental autoimmune encephalomyelitis
EBV	Epstein-Barr-virus
EDSS	Expanded disability status score
EDTA	Ethylenediaminetetraacetic acid
EPSC	Excitatory postsynaptic current
ER	Endoplasmic reticulum
EV	Extracellular vesicle
FACS	Fluorescence-activated cell sorting
Fam199x	Sequence similarity 199, X-linked
FC	Fold change
FC	Flow cytometry
FCS	Fetal calf serum
FDR	False discovery rate
FluC	Firefly luminescence
FSC	Forward scatter
FSC-A	Forward scatter area
FTD	Frontotemporal dementia
GABA	γ-aminobutyric acid
GAPDH	Glyceraldehyde-3-phosphate-dehydrogenase
GC	Gas chomatography
Gfap	Glial fibrillary acidic protein
GluA1, *Gria1*	Glutamate ionotropic receptor AMPA type subunit 1
GluA2	Glutamate ionotropic receptor AMPA type subunit 2
GluK	Kainate receptor supunit
GluN2A, *GRIN2A*	Glutamate ionotropic receptor NMDA type subunit 2A

GluN2B	Glutamate ionotropic receptor NMDA type subunit 2B
GM-CSF	Granulocyte macrophage colony-stimulating factor
GO	Gene ontology
GWAS	Genome wide association studies
HC	Healthy controls
HLA	Human leucocyte antigen
HOMER2	Homer scaffold protein 2
Hsa	Homo sapiens
HSCT	Hematopoietic stem cell transplantation
I.p.	Intraperitoneal
I.v.	Intravenous
IEG	Immediate early genes
IFN-γ	Interferon gamma
iGluR	Ionotropic glutamate receptor
IL-β	Interleukin beta
iMN	Inflamed motor neuron
IP	Immunoprecipitation
iSC	Inflamed spinal cord
KCl	Potassium chloride
LNA	Locked nucleic acid
LSM	Laser scanning microscope
LTP	Long-term potentiation
m^7G	7-methylguanosine
MAIT	Mucosa-associated invariant T cell
MCI	Mild cognitive impairment
mGluR	Metabotropic glutamate receptors
MHC	Major histocompatibility complex
miRAP	miRNA tagging and affinity-purification
miRNA	microRNA
Mmu	Mus musculus
MN	Motor neurons
MOG	Myelin oligodendrocyte glycoprotein
MRE	miRNA response element

MS	Multiple sclerosis
MTg-AMO	Multiple-target anti-miRNA oligonucleotide
mTOR	Mammalian target of rapamycin
N2a	Neuro-2A
NDS	Normal donkey serum
NF	Neurofilament
NFκB	Nuclear factor 'kappa-light-chain-enhancer' of activated B cells
NK	Natrual killer cell
Nlg1	Neuroligin 1
NMDA	N-methyl-D-aspartate
NO	Nitric oxide
Nxph1	Neurexophilin-1
PBMC	Peripheral blood mononuclear cell
PBS	Phosphate buffered saline
PCA	Principal component analysis
PCR	Polymerase chain reaction
PFA	Paraformaldehyde
PIP	Phosphatidyl inositol-phosphate
PKA	Protein kinase A
Poly (A) tail	Polyadenylate tail
PPAR	Peroxisome proliferator-activated receptor
PPMS	Primary progressive multiple scleoris
PRG	Plasticity-related gene
PSD	Postsynaptic density
PSD-95, *Psd-95*	Postsynaptic density protein 95
PTEN	Phosphatase and tensin homolog
Ptprc (CD45)	Receptor-type tyrosine-protein phosphatase C
PTX	Pertussis toxin
PV	Parvalbumin
Q	Glutamine
qRT-PCR	Quantitative real-time polymerase chain reaction
R	Arginine
RIS	Radiologically isolated syndrome

RISC	RNA-induced silencing complex
RluC	Renilla luminescence
RNA	Ribonucleic acid
RNS	Reactive nitrogen species
Robo	Roundabout
ROS	Reactive oxygen species
RRMS	Relapsing-remitting multiple scleoris
RT	Room temperature
S.c.	Sub-cuntanous
SC	Spinal cord
Sc-miR	scrambled miRNA
SD	Standard deviation
SEM	Standard error of the mean
Sesn3	Sestrin 3
Slit2	Slit guidance ligand 2
snoRNA	Small nucleolar RNA
SNP	Single nucleotide polymorphism
SPMS	Secondary progressive multiple scleoris
Sprr1a	Small proline-rich protein 1A
SSC	Sideward scatter
SSC-A	Sideward scatter area
St6gal2	ST6 beta-galactoside alpha-2,6-sialyltransferase 2
Stat3	Signal transducer and activator of transcription 3
SUMO	Small ubiquitin modifier
SYN1, *Syn1*	Synapsin 1
Syt1	Synaptotagmin 1
TAE	Tris-acteate EDTA
tAGO2	AGO2-GFP
TARBP	TAR RNA-binding protein
TBI	Traumatic brain injury
Tbp	TATA-binding protein
TDP-43, *TARDBP*	TAR DNA-binding protein 43
TE	Tris-EDTA

T_H cell	T helper cell
TLC	Thin-layer chromotography
TLR7	Toll-like receptor 7
TNF-α	Tumor necrosis factor alpha
TRAP	Translating ribosome affinity-purification
T_{Reg} cell	Regulatory T cell
TTX	Tetrodotoxin
UKE	University Medical Center Hamburg-Eppendorf
UMAP	Uniform manifold approximation and projection
UNG	Uracil-N-glycosylase
VGLUT	Vesicular glutamate transporter
VH	Ventral horn
Wasl	WASP like actin nucleation promoting factor
x_{c-}	Cysteine/glutamate antiporter

1 Introduction

1.1 Multiple sclerosis

Multiple sclerosis (MS) is considered a primarily inflammatory, demyelinating disease of the central nervous system (CNS), mainly caused by inappropriately activated, autoreactive T cells crossing the blood-brain barrier (BBB) and penetrating the CNS parenchyma[1]. On the basis of observed 'glial scars' (astrocytic fibrillary gliosis) in post-mortem samples, MS established as being a disseminating plaque-like sclerosis approximately 150 years ago[2,3]. However, MS is nowadays conceptualized as a highly heterogenous and complex disease[4]. Besides peripheral and central immune cell activation MS is accompanied by atrophy, neuroaxonal damage and synaptic and neuronal loss[5-7]. Around 2.5 million patients worldwide are suffering from fully to partially reversible neurological disability comprising monocular visual loss, limb weakness, sensory loss, double vision or ataxia, eventually manifesting in non-reversible impaired mobility and cognition[4,8]. The average disease onset of MS, being the most prevalent chronic inflammatory disease of the CNS[9] is around the age of 30[10]. The disease is classified in either a more inflammatory relapsing-remitting or a more neurodegenerative progressive disease course[11], but rarer variations have been reported[4]. Around 15% of MS patients are afflicted with the progressive course of onset[12], whereas approximately 80% of patients undergo the secondary progressive MS after 10-20 years post diagnosis[10]. Further, 50% of patients require a permanent use of a wheelchair after 25 years of the initial diagnosis[10]. Currently, there is no cure for MS and scientists are engaged with disentangling the distinct roles of the immune system and those contributing to disease progression[10]. Certainly, it is debated whether the initial cause is intrinsic or extrinsic to the CNS[13,14] and whether heterogenous clinical presentations can be classified as a single disease[10]. Relating thereto or not, a specific etiologic cause has not been identified yet. Multiple causes have been discussed and investigated, considering MS a multifactorial and multicellular disease[12].

1.1.1 Epidemiology

The multifactorial character of MS is displayed by a range of environmental and genetic factors that have been described to be involved in the epidemiology[15,16]. Environmental factors seem to rather play a role in triggering disease and modulating disease penetrance, most likely in combination with other risk factors like genetic predisposition, than on their own[10]. Debated environmental factors include but are not limited to vitamin D deficiency, temperature, latitude, infections, smoking, trauma, and obesity[15]. Nevertheless, many of these associated environmental risk factors still require validation due to weak experimental design or analyses.

Viral infections, especially with Epstein-Barr-virus (EBV) have been heavily discussed in being involved in MS epidemiology[12]. In a recent meta-analysis immunoglobulin G seropositivity to EBV and a preceding infectious mononucleosis together with smoking were the most significantly correlating environmental factors associated with MS susceptibility among 44 others in more than 1000 examined individuals[15]. However, the mechanisms underlying these observations still remain enigmatic[17].

Besides viral infection and their role in MS, microbiota and their toxins were debated[18]. The idea that bacteria play a role in MS epidemiology manifested by the observation that modulation of the gut microbiome influences the development of clinical disability in the MS mouse model experimental autoimmune encephalomyelitis (EAE)[19,20] and on shaping the overall immune response[18]. Direct contribution of microbiota was reported for the starting phase of human autoimmune diseases[19], whereas its role in MS slowly emerges. It was reported that specific bacterial strains are deregulated in humans afflicted with MS and further shown to have an effect on CNS specific autoimmunity[21]. However, the microbiome rather shapes the immunological landscape and is therefore probably more involved in driving inflammatory responses in MS than being the initial cause[18,19]. Nevertheless, the microbiome can also impact on neurological dysfunction[22,23] and influence the disease progression as shown in a mouse model of MS[24].

Another complex factor that seems to be involved in MS epidemiology is sex. This idea evolved from the observation that up to three quarter of MS patients are women[12]. Whatever factor the female preponderance represents is still unclear, but the influence of female hormones is under investigation[4,25]. However, this observation applies more to the relapsing-remitting than to the progressive disease type[17] and might underlie similar pathophysiological features that drive the higher susceptibility of women to develop autoimmune diseases in general[26]. Interestingly, protective effects from relapses in women[27] and amelioration of clinical symptoms in EAE during pregnancy have been reported, implying changes of immune tolerance mechanisms by shifting the T cell repertoire to regulatory T cells (T_{Reg})[28]. Also, a series of reports indicate that in relapsing-remitting MS (RRMS) men accumulate disability faster than women. However, no sex ratio for primary progressive MS (PPMS) was verified and the time to progress to the expanded disability status score (EDSS) 6 was similar for men and women[29,30]. Therefore, sex differences seem to play a more prominent role in the inflammatory stages of MS.

The probably most discussed factors for MS predisposition are of genetic origin. Clearly, MS is not an inheritable genetic disease on its own, however monogenic twin studies revealed a genetic component ranging from 30%-50%, whereas people with a first-degree relative afflicted with MS have a 2-4% risk of disease development[12]. Most genetic variants that cause disease or define

disease severity occur as single nucleotide polymorphisms (SNPs) within protein-coding or non-coding regions and might affect mRNA and protein expression, modification, localization and function[31]. Therefore, various genome wide association studies (GWAS) have been performed that focused on the identification of SNPs in order to reveal genetic variants that might influence on the development or severity of MS. GWAS have revealed over 200 loci associated with MS susceptibility, whereas the main association mapped to the major histocompatibility complex (MHC) cluster, which is related to immune function[32]. The MHC cluster is a gene-dense region with various immune response loci including the human leucocyte antigen (HLA) genes[33,34], encoding for molecules that are involved in antigen presentation to T cells. Among them the highest risk variant HLA-DRB1*15:01 that conferred a 3-fold increased risk of developing MS[35]. Another GWAS focused on genetic variants that mapped to disease severity, but no HLA susceptibility loci were confirmed, implying that these variants are rather involved in development of MS than in driving disease progression. Unfortunately, no genome-wide association with disease severity could have been made[36]. However, overrepresentation of gene variants involved in glutamate signaling like *GRIN2A*, encoding subunit 2 of the N-methyl-D-aspartate (NMDA) receptor and the postsynaptic protein homer scaffold protein 2 (*HOMER2)* were associated with CNS damage in MS patients[37], indicating that these gene variants could influence neurodegeneration in MS. Another study illuminated genetic predisposition for glutamate excitotoxicity-related neurodegeneration in MS by associating genetic variants to high glutamate levels in the patient brains[38]. Interestingly, MS patients that exhibited a higher number of associated gene variants involved in glutamate biology showed higher atrophy than patients without these variants, implying that they might be involved in driving MS progression[38]. Intriguingly, the top associated marker in this study was a genetic variant within a non-coding region, but its functional impact was not studied and is yet unknown. Other GWAS also revealed very prominent numbers of non-coding gene variants being implicated in MS, however, interpretation of these data was yet constrained due to technical limitations and absent knowledge about the function and site of action of non-coding elements[39]. Therefore, genetic variants in non-coding regions might play a larger role in predisposing for MS than thus far expected.

Taken together, it might appear that a combinatorial incidence of different environmental factors together with divergent states of genetic predisposition make the diverse appearance, course and outcome of MS, which might over time unify in progression. Further, immune related gene variants seem to rather influence MS development, whereas glutamate signaling associated alleles may impact on MS severity. However, recent insights into genetic variants at non-coding

sites that might drive the development and progression of MS stress the urgency to better understand their functional relevance.

1.1.2 Neurodegeneration

Neurodegeneration describes the structural and functional impairment and loss of neurons and neuronal connections in primary neurodegenerative diseases, which hallmarks are toxic formation, aggregation or propagation of proteins[40,41]. However, neurodegeneration is also a feature of MS and the best correlate for clinical disability[6,42]. Initially, CNS-inflammation was considered to be the cause of neurodegeneration[6]. However, a variety of neuropathological evidence indicates atrophy in early MS[43], at time of diagnosis[42] and sometimes even before white matter lesions were identified[44]. Concordantly, cognitive impairment occurs in early phases of RRMS and PPMS as well as in patients with radiologically isolated syndrome (RIS) and clinically isolated syndrome (CIS)[7]. Intriguingly, cognitive deficits were also observed in the preclinical phase of EAE[45], implying that neurodegeneration can occur quite early with response of the immune system or prior to CNS-inflammation. Also, time post diagnosis rather predicts disease progression and disability than total number or frequency of relapses[46]. This observation was further confirmed by a study that showed no influence on irreversible disability between primary progressive patients and those with a superimposed remitting-relapsing disease course over time[30]. Therefore, inflammatory and neurodegenerative events in MS are nowadays seen as being rather intermingled[47] than cause and consequence. This uncoupling of relapses and disability progression is further supported by the observation that disease progression over time is not strongly influenced by the current immunomodulatory therapies[10]. For MS no specific neuroprotective treatment is available to neither halt neurodegeneration nor disease progression once progression has started[6]. Nevertheless, relapse frequency and progression in the early disease increases the probability of occurrence and latency of entering the progressive phase, which might be deferred by immunomodulatory treatment[46,48]. However, it still remains extremely challenging to disentangle neurodegenerative from inflammatory events to identify those factors that 'truly' drive progression. One of the main reasons certainly is that the initial cause of MS is still unknown as well as its tissue origin[13,14]. Additional impediments are the lack of appropriate biomarkers to define neurodegeneration, poor subtype classification of MS as well as the use of EAE models that are biased towards autoimmunity[10,49,50]. The etiology of MS will most probably not be resolved with the help of EAE models, but understanding inflammation-induced neurodegeneration might help develop neuroprotective therapy.

1.1.3 Immunopathology

The multicellular character of MS is displayed by the dynamic interplay between the immune system, neurons and glial cells. Cells of the immune system, represented by the innate and adaptive immune system, almost every CNS resident cell type including neurons, microglia, astrocytes, oligodendrocytes and their precursor cells have been described to contribute to MS pathophysiology[10,12]. The engagement and functional contribution of different immune cell types in RRMS were comprehensively described in regard to its two-step like disease character with initial focal inflammatory lesions and progression of the disease with less and diffuse inflammation at later stages[10,12].

It is well described that early and acute RRMS lesions are mainly accompanied by macrophages, helper $CD4^+$ T cells (particularly T_H1 and T_H17) and cytotoxic $CD8^+$ T cells[49]. $CD4^+$ T cells mainly drive immune responses in EAE[49], whereas $CD8^+$ T cells were identified at higher frequencies in the CNS parenchyma in humans and correlate with axonal damage[51]. Also, deficiency of functional suppression mediated by T_{Reg} cells was shown to contribute to the deleterious actions of autoreactive T cells in MS[52]. Mucosa-associated invariant T (MAIT) cells are a subset of $CD8^+$ T cells and believed to exert a prominent role in MS pathophysiology[53], since they are successfully depleted by effective immunotherapy[54]. Also, an impairment of regulatory $CD8^+$ T cells was shown in MS patients[55]. Monocytes and macrophages were reported to be involved in demyelination and myelin regeneration in MS[56-58]. Further, B cells were shown to be variable in numbers throughout disease development, especially antibody producing plasma B cells were found at increased numbers at later progressive stages, often within tertiary lymphoid structures[59]. Their production of antibodies in the CNS is used as a feature for MS diagnosis (oligoclonal bands)[60]. However, it is unlikely that MS represents an antibody-mediated disease, since its clinical representation lacks the uniformity, which is observed for antibody-mediated autoimmune diseases[61]. Also, CNS autoantigens have never been identified in MS patients rather than multifaceted intracellular targets, probably sequestered proteins originating dying cells[62].

The uncoupling of inflammation and disease progression in MS becomes more prominent in the chronic phase of RRMS. It was proposed that adaptive immune cell exhaustion could be responsible for the inflammatory ease[63], whereas neurodegeneration might still be fueled by chronic inflammation[10]. However, for the primary progressive disease the adaptive immune system plays a minor role[48]. Chronic inflammation in MS is different in composition of immune cells; shows chronic inactive or smoldering lesions, activated astrocytes and microglia[12] and is therefore more similar to primary neurodegenerative disease[12]. However, astrocytes and microglia also contribute to MS in early stages[64]. Interestingly, microglia have been reported to

be activated even before CNS lesions were formed in immunized marmosets[65]. Microglia were ascribed a neuroprotective as well as neuro-deleterious role in CNS-inflammation[65]. Microglia were shown to release pro-inflammatory cytokines and activate reactive astrocytes that lack the ability to exert neuroprotective function, thereby promoting neurodegeneration[66,67]. Conversely, many reports show their neuroprotective contribution by removal of synapses, removal of debris, neurotrophic support and repair of neuroaxonal damage[68]. The highest number of microglia were found in the hippocampus of EAE mice and it is very likely that they exert region-specific function[7,69,70]. A dual role was also reported for astrocytes, which deliver neurotrophic support and control glutamate homeostasis in the CNS, thus being directly implicated in mediating glutamate excitotoxicity[71]. Further, astrocytes build the glial limitans of the BBB and therefore play a huge role in regulating peripheral immune cell infiltration[72]. They were also reported to attract peripheral immune cells by secretion of chemokines and recruitment of microglia by excretion of granulocyte macrophage colony-stimulating factor (GM-CSF) and CC-Chemokine-Ligand 2 (CCL2)[73]. Interestingly, activated microglia and astrocytes are also found outside of inflammatory lesions and were related to synaptic and dendritic changes, cognitive impairment and neurological dysfunction in MS patients, conceiving them important contributors to MS immunopathology that modulate neurodegeneration at early and later stages of the disease[74-76].

Finally, all cell populations described above contribute to inflammation-induced neurodegeneration by release of glutamate and neurotoxic factors, production of reactive oxygen species (ROS), reactive nitrogen species (RNS) and cytokines, all together inducing innumerable molecular changes that promote neuronal and axonal dysfunction and cell death[6,77].

1.1.4 MS mouse models

The first attempts to mimic rabies-associated encephalomyelitis by immunization with CNS tissue in marmosets and rodents established the idea of MS being a primarily autoimmune disease attacking specific antigens of the CNS[50,78]. EAE derived from these experiments and is the most frequently used animal model of MS[79]. EAE is actively induced in primates and rodents by immunization with CNS antigens, mainly peptides originating the myelin sheets, which surround neuronal axons to deliver neurotrophic support, physical protection and particularly accelerate electronic transmission along the axon (saltatory conduction)[79,80]. Different models ranging from relapsing-remitting, to spontaneous, acute and chronic EAE strongly depend on the genetic background and the immunization agents[79]. Also, an adoptive transfer of CNS antigen-specific $CD4^+$ T cells induces EAE[81]. A very eminent EAE model is induced in C57BL/6 mice using the myelin oligodendrocyte glycoprotein $(MOG)_{35-55}$ in complete Freund's adjuvant containing inactivated *Mycobacterium tuberculosis* and additional injections of pertussis toxin to enhance

clinical symptoms[82]. The clinical monophasic course of this chronic EAE model is very well described and the immunopathology has been studied in detail. One to two weeks after the immunization, autoreactive $CD4^+$ T cells enter the CNS, where they are re-activated by antigen presenting cells, recruit other immune cells and attack the myelin sheets, release cytokines and glutamate, activate astrocytes and microglia, which all results in demyelination, synaptic dysfunction, axonal and neuronal impairment and loss[6,82]. The consequential disruption of coordination, sensory and mainly motor functions determine clinical disability, which can be assessed by a scoring system covering mild to severe symptoms[82,83]. Many aspects of EAE are similar to MS pathology, sharing immunological, neuropathological and clinical features[79], but due to the strong artificial immunization and interspecies differences translational research requires carefully planned control experiments[84]. Most therapeutic interventions for MS that emerged from EAE studies are immunomodulatory[85]. However, many therapeutic targets that have been proven effective or promising in ameliorating EAE, had no or rather deleterious effects in humans[84]. Another limitation clearly is that EAE is not suited to study MS epidemiology, therefore little to no progress was made in understanding how and where MS is generated in the body, even though EAE is studied for almost 70 years now[50,85]. Yet, no treatment to alleviate long term disease progression by EAE-derived drug targets was achieved[12]. Nevertheless, EAE seems to be a suitable tool to investigate the effects of inflammation-induced neurodegeneration. Neuronal epigenomic, transcriptomic, and proteomic changes can be investigated *in vivo* and *ex vivo* to understand the pathophysiology of synaptic, axonal and neuronal demise[6,47]. Two strategies emerging from such studies appear particularly promising to develop neuroprotective therapy in MS, which is to enhance neuron intrinsic defense mechanisms and to repress deleterious pathways that are induced upon massive inflammatory stress[6].

1.2 Inflammation-induced synaptic neurodegeneration

1.2.1 Synaptopathy

Synapses are the building elements of plasticity in the CNS and changes in structural connections, synaptic transmission, generation and loss happen both in healthy and pathological conditions[47]. Altered synaptic transmission can comprise an imbalance between γ-aminobutyric acid (GABA)ergic and glutamatergic signaling or synaptic dysfunction or degeneration, together termed synaptopathy[86-88]. Removal of surplus synapses (synaptic pruning) and synaptic removal upon injury (synaptic stripping), along with differential expression of synaptic proteins are observed during development and memory consolidation, but also in CNS diseases like MS, Huntington's, Alzheimer's, amyotrophic lateral sclerosis (ALS), autism and schizophrenia[47]. Synaptopathy is an important feature of grey matter atrophy in MS patients and is known to entail

excitotoxic damage, causing cognitive and motor impairments[89]. Altered synaptic transmission and loss can also occur in early MS and EAE, indicating that synaptic structures are particularly sensitive to the inflammatory microenvironment and early targets of neurodegeneration, therefore constituting promising structures for neuroprotective treatment[47,90]. Relating thereto glutamate receptor blocker have been proven effective to prevent spine loss in EAE and reduce the number of apoptotic synapses[91]. Further, besides ionotropic glutamate receptors (iGluRs) also other components affecting glutamate signaling have been reported to be deregulated in MS and EAE as glutamate transporters[92] and metabotropic glutamate receptors (mGluRs)[93].

1.2.2 Glutamate signaling

Glutamate is the major excitatory neurotransmitter of the mammalian CNS and also the most abundant free amino acid (~5–15 nmol per kg) in the brain[94]. The highest concentrations of glutamate were found within vesicles in presynaptic nerve terminals, from where it is released by exocytosis and bound by glutamate receptors at the postsynaptic side. To prevent overactivation of glutamate receptors, glutamate is directly removed from the synaptic cleft by a very potent uptake system. This uptake system consists of the excitatory amino acid transporters (EAATs) 1–5, which are expressed by neurons and astrocytes and directly transport glutamate either back into the presynapse or into astrocytes[94,95]. Taken up by astrocytes glutamate can be metabolized to either glutamine (by glutamine synthetase), which is taken up by neurons to resynthesize glutamate (by glutamate dehydrogenase), to GABA (by glutamate decarboxylase) or to α-ketoglutarate, which is used for ATP synthesis[71]. Glutamate can bind to either ionotropic or metabotropic glutamate receptors[94]. mGluRs are categorized into three groups of G protein–coupled glutamate receptors that upon activation act on membranous ion channels or second messengers as diacylglycerol or cyclic adenosine monophosphate (cAMP)[94]. However, besides the presynaptic release of glutamate, excitatory signal transmission relies mostly on ionotropic AMPA (α-amino-3-hydroxy-5-methyl-4-isoxazole propionic acid) and NMDA glutamate receptors at the postsynaptic side and therefore plays an important role in mediating glutamate excitotoxicity[96].

1.2.3 Ionotropic glutamate receptors

iGluRs are intrinsic cation permeable channels categorized into three families namely Kainate, NMDA and AMPA receptors. Interestingly, glutamate is highly variable in conformation and is therefore able to bind with different affinity to a variability of glutamate binding sites. This characteristic of glutamate enabled the categorization of receptors and transporters by their specific affinity to different synthetized compounds[95]. iGluRs are tetrameric receptors and differ

in their permeability to cations like Na^+, K^+ and Ca^{2+} and in their electrophysiological kinetics by expression of different subunits[96]. This modular nature of iGluRs produces many different receptor combinations, which are further increased by alternative splicing and RNA editing, thereby enabling enormous molecular and functional variability that is very likely to be physiologically relevant[97] .In general, iGluRs are critical components for neuronal development, synaptic plasticity, memory and learning and are associated with a variety of neurological and psychiatric disorders[98], particularly with glutamate mediated excitotoxicity[99,100].

AMPA receptors are present at all neurons in the CNS[101]. They are responsible for the most rapid excitatory transmission and mediate the bulk of synaptic transmission during basal neuronal activity within the vertebrate CNS[98,102]. AMPA receptors are tetramers of the pore-forming homologous subunits GluA1-4[103]. Each receptor contains two agonist-binding sites and is only activated upon occupation of both sites. Upon binding, the conformation of the channel is changed, which allows entry of cations and thus alteration of the local membrane potential know as excitatory postsynaptic current (EPSC). AMPA receptors are mostly selective for Na^+ and K^+ and in some cases for Ca^{2+} [97,99]. Usually the tip of the re-entrant pore loop expresses a glutamine (Q) residue enabling Ca^{2+} permeability. Nevertheless, most neurons express and edit the GluA2 mRNA (messenger RNA) transcript causing replacement of the Q with and arginine (R), leading to Q/R heteromeric receptors selective for only monovalent ions[104].Relating thereto, AMPA receptors that lack GluA2 are Ca^{2+}permeable. However, also a Ca^{2+} independent excitotoxic function of GluA2 containing AMPAR was described, by interacting with glyceraldehyde-3-phosphate-dehydrogenase (GAPDH), leading to induction of p53 and finally to apoptosis[105].

NMDA receptor subunits GluN1, GluN2A-GluN2D, GluN3A and GluN3B were described[98], whereas most NMDA receptors are composed of two GluN1 and two GluN2 or GluN3 subunits, respectively. They often colocalize with AMPA receptors in central synapses and form the synaptic unit. However, the ratio of AMPA to NMDA receptor mediated synaptic current varies across a wide range[98]. Interestingly, some synapses seem to co-regulate AMPA and NMDA receptor subunit expression, exhibiting different open probabilities as well as contribution to synaptic currents and were described as being transcriptionally regulated upon activity[102]. NMDA receptors require besides binding of glutamate co-agonism by glycine or D-serine. Additionally, extracellular Mg^{2+} blocks the pore at resting membrane potential, which is relieved by depolarization of the membrane by either activation of AMPARs or backpropagating action potentials[106]. However, because of their high $Ca2^+$ permeability NMDA receptors are considered particularly important in triggering several different forms of plasticity, whereas abnormal expression levels and malfunction contributes to neuronal injury and death.

Finally, kainate receptors consist of five different subunits (GluK1-GluK5) and are unique in the way that besides postsynaptic expression they mostly act at the presynaptic side. Kainate receptors are considered as subtle actors in controlling glutamatergic and GABAergic neurotransmitter release[94,98,106], regulating the strength of synaptic connections and have a strong developmental and regional regulation. Kainate mediated synaptic EPSCs are much slower than AMPA mediated EPSCs[98]. Further, Kainate receptors were described as potential therapeutic targets for epilepsy and pain[107].

1.2.4 Glutamate excitotoxicity

Glutamate excitotoxicity is a dysregulation of glutamate homeostasis and transmission, leading to cellular damage and cell death[108]. Certainly, due to its complexity of involved cellular compartments and molecules, the intracellular apparatus of glutamate mediated cell toxicity is still not fully understood. However, the underlying basis is believed to be increased intracellular levels of the second messenger Ca^{2+}. Increased Ca^{2+} causes autophagic, apoptotic and necrotic events, which were induced by activation of transcription factors and immediate early genes (IEGs), Ca^{2+} dependent enzymes, protein kinases and production of ROS, nitric oxide (NO) and free radicals. Organelles such as mitochondria, the endoplasmic reticulum (ER) and lysosomes play an important role in consolidating the increase of intracellular Ca^{2+}, production of cytotoxic molecules, shutdown of energy and of decluttering machineries[108,109]. Importantly, multiple processes are controlled by intracellular Ca^{2+} signaling, which is defined by its site of entry associated with electrical activity[110,111]. Glutamate excitotoxicity was shown to be mediated mostly by activation of extrasynaptic (including perisynaptic), but not synaptic glutamate receptors[112,113]. It was shown that Ca^{2+}-influx by activation of synaptic NMDA receptors usually induces 'nuclear' cAMP responsive element binding protein (CREB) and expression of brain-derived neurotrophic factor (*Bdnf)*, thereby exerting anti-apoptotic function. Conversely, extrasynaptic NMDA receptor activation terminated in dominant CREB shut-off and blocked production of BDNF, resulting in mitochondrial damage and cell death[112]. Others reported an important role of magnitude and duration in co-activation of synaptic and extrasynaptic glutamate receptors[114]. However, the spatiotemporal relevance of glutamate receptor activation in mediating excitotoxicity by inducing different biological pathways is nowadays uncontentiously proven[113]. Extrasynaptic glutamate receptors play a particular role during neuronal development and differentiation, however their function is not fully understood yet even though they constitute a substantial population of all glutamate receptors in adult neurons[113,115]. Although, a contribution of AMPA receptors in mediating glutamate excitotoxicity was shown[116], extrasynaptic AMPA receptors mainly gained popularity by trafficking and lateral diffusion in the plasma membrane to mediate synaptic plasticity[9] rather than mediating excitotoxicity. Finally, glutamate excitotoxicity-

mediated cell death can also be divided into acute and chronic insults on the basis of slight molecular differences in expression pattern and composition of glutamate receptors, transporters and antiporters and the considerably different time course in which downstream events contribute to neuronal demise[117].

Glutamate excitotoxicity was described in MS and EAE[117,118] and in a variety of neurodegenerative diseases and seems to play a pivotal role in neuronal demise in CNS-inflammation[119]. Even though it is believed that the major mediators of glutamate excitotoxicity are glutamate receptors[100] (proven mostly by chemical inhibition in neuronal cultures *in vitro*), pharmacological inhibition thus far has been less effective than presumed and strong adverse side effects have been reported[120]. For EAE pharmacological AMPA, NMDA and Kainate blockage has been proven to exert beneficial effects on neuronal survival, whereas the translational application in MS patients had either no effect or even deteriorated neurological symptoms[118,120,121]. An explanation for this might be, besides interspecies differences, that glutamate excitotoxicity depends on the magnitude of inflammatory insults, site of activation, disease progression and age of the patients and might therefore favor different therapeutic strategies in the glutamate pathway[84,117]. However, glutamate receptors are needed to maintain normal brain function, therefore regulators of glutamate homeostasis or downstream molecules might constitute more attractive targets for neuroprotection than pharmacological inhibition of glutamate receptors[109].

1.2.5 Glutamate excitotoxicity in EAE and MS

Proposedly, glutamate excitotoxicity in EAE and MS constitutes the central link between inflammation, synaptic and neuronal degeneration[47,109]. In MS, almost all aspects of glutamate homeostasis are pathophysiological altered, suggesting glutamate toxicity an important mechanism[122]. By magnetic resonance spectroscopy it was shown that acute MS lesions contain elevated glutamate levels, which could originate infiltrating immune cells, astrocytes and microglia cells, producing but also releasing glutamate[123,124]. Contribution to the extracellular glutamate occurs by either cysteine/glutamate antiporters (x_c^-), connexin hemichannels or anion channels[55]. High glutamate levels were also reported in the CSF of MS patients[125]. Interestingly, the highest glutamate levels in MS brains were found in active lesions of CIS and RRMS patients, whereas secondary progressive MS (SPMS) patients showed a decline in glutamate and glutamine levels, which was recently proposed as biomarker for progression in theses patients[126]. Concordantly, extracellular glutamate levels in PPMS patients were similar to those of healthy controls[123], indicating different pathophysiological actions of glutamate accompanying different MS subtypes, age, sex and very likely disease stage[127]. Therefore, to decrypt different pathomechanisms of MS, it might be considered to distinguish and differentially target acute and chronic excitotoxic events.

Intriguingly, it was shown that also environmental factors could lead to an increase of glutamate release form nerve endings, thereby contributing to excessive activation of glutamate receptors[128]. Further, it was proposed that excitotoxicity might be driven by the increased loss of inhibitory inputs, thereby promoting neurodegeneration[129]. Interestingly, GABAergic parvalbumin (PV) positive inhibitory neurons were reported to be significantly reduced in post mortem motor cortex of MS patients in comparison to control brains[130]. GABAergic neuronal loss was also reported in layer II–III of the primary motor cortices of EAE mice[131].

High glutamate levels have also been detected in EAE[118]. The contribution of glutamate excitotoxic effects were proven by pharmacological inhibition of all types of ionotropic glutamate receptors in different animal models of EAE. A series of publications showed the participation of AMPA receptors in modulating clinical disability. Different antagonists were shown to be effective in reducing synaptic and neuronal damage, as NBQX, GYKI52466, fanapanel and talampanel[118,132,133]. Further, a peptide disrupting the formation of the GluA2-GAPDH complex ameliorated EAE and showed specific neuroprotective function[134]. Interestingly, it seems that especially motor neurons are selectively vulnerable to AMPA/Kainate receptor-mediated neurodegeneration, caused by an overload of mitochondrial Ca^{2+} and ROS generation[135,136]. These *in vitro* findings were validated in *ex vivo* spinal cord slices in which motor neuronal degeneration induced by chronic blockage of glutamate reuptake, was mostly protected by AMPA/Kainate receptor blockers[137,138]. Intriguingly, it was suggested that AMPA/Kainate receptors rather play a role in mediating slow (chronic) neurodegeneration as described for ALS, whereas NMDARs mediate mainly acute neuronal toxicity[139]. Further, upregulation and increased phosphorylation of GluA2-lacking AMPARs were reported in defined neuronal populations in EAE, causing synaptic and neuronal damage and could be rescued by application of NBQX. It was reported that not only the constitution of AMPAR subunits, but also phosphorylation at specific sites changes the open probability of the pore, as observed for GluA1 phosphorylation at serine residue 845 by cAMP-dependent protein kinase A (PKA)[140]. AMPARs constituting of only GluA4 subunits were described as being particularly selective for Ca^{2+}, leading to activation of activator protein 1 (AP-1), which further causes cell death[116]. Other reports show the AMPAR-mediated activation and translocation of nuclear transcription factor NFκB (nuclear factor 'kappa-light-chain-enhancer' of activated B cells) induced cell death[141,142]. However, some of these functional studies on AMPAR were performed in cell lines or primary cell cultures and exert no neuron exclusive function. For instance, it was shown that AMPARs on oligodendrocytes massively impact on neuronal integrity and survival *in vitro* and in EAE[143]. Further, AMPARs are also expressed on glial cells and undergo excitotoxic changes upon increase of extracellular glutamate, thereby augmenting neuronal glutamate excitotoxicity[144,145].

1.3 microRNA biology and function

microRNAs (miRNAs) are short RNAs (~22 nucleotides) that exert their major function by post-transcriptional regulation of gene expression[146]. miRNAs were discovered almost three decades ago and initially believed to exclusively play a role in nematodes[147]. Thus far, miRNA research exponentially increased and is meanwhile shown to play an important functional role in almost all organisms as plants, non-vertebrates and vertebrates[148]. Their major functional impact on development is nowadays uncontentiously proven[149], however they are involved in almost all biological processes and gained increased attention as they were found deregulated in numerous diseases[150-153]. The importance of miRNA deregulation in disease got apparent by ablation of factors of the miRNA biogenesis machinery, which caused hallmarks of Parkinson's' disease in dopaminergic neurons[154], Alzheimer's in CaMKII expressing neurons[155] and multiple sclerosis in oligodendrocytes[150,156]. Further, mutations in proteins of the miRNA biogenesis machinery were shown to cause neurological diseases as familiar ALS[157] and fragile X syndrome[150,158]. Intriguingly, miRNA abundance increases with organismal and cellular complexity, indicating that they also play a decisive evolutionary role[146]. Certainly, it was and still is puzzling what literally encodes for the differences between mice and human, which share approximately between 60-99% sequence identity for protein-coding genes or between human and chimpanzees, which are the closest living relatives with more than 98% genomic overlap[152,159]. The answer seems to be within the non-coding genome[160]. Relating hereto, the most striking evidence for its functional relevance is apparently that almost 98% of the human genome consists of non-coding genes that have always been considered as 'junk DNA' or 'dark matter'[161]. This view has dramatically changed, mainly as a result of recent technological advances and bioinformatic tools[160,161]. The non-coding genome between mouse and humans differs around 50%, also the major differences between the human and chimpanzee genome are within non-coding regions[152,160]. It was proposed that the generation of new cell types to form the primate brain might be ascribed to the increasing numbers of cell type specific miRNAs[162]. miRNAs are important for normal function of the nervous system, which comprises the broadest spectrum of miRNA expression among all human tissues. In line with that, 70% of all miRNAs were found to be expressed in the human brain, from which many exert neuronal function[163]. Further, miRNAs are considerably important in counteracting environmental contingencies by aligning the cell's gene expression to its own needs[164]. Computational analyses have predicted that almost 60% of protein coding genes can be regulated by miRNAs[165]. Together, miRNAs constitute important regulatory molecules, which define a certain cell identity and cell state by its own appearence[164].

1.3.1 miRNA biogenesis

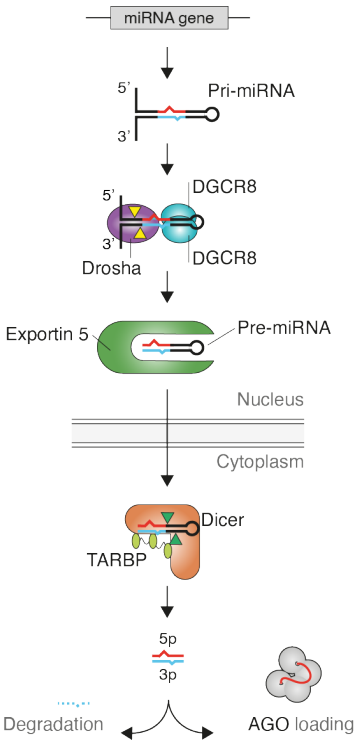

Figure 1-1 miRNA biogenesis

Scheme of miRNA biogenesis[166]. miRNAs are transcribed and exported into the cytoplasm where they are processed in multiple steps into a miRNA–miRNA* duplex. AGO proteins load one miRNA strand and assemble to RISC, in which miRNA targets are translationally inhibited. The other miRNA* strand is immediately degraded.

miRNAs are encoded within introns or long non-coding RNAs and transcribed by RNA polymerase II[167]. Often, miRNAs are encoded in polycistronic clusters under control of one promoter and transcribed as a single transcript starting with a 5' 7-methylguanosine (m^7G) cap and ending with a 3' poly(A) tail[146,168]. The primary mRNA transcript, termed pri-miRNA contains the intermediate miRNA sequence, which is around 60 nucleotides in length and folds itself back into a hairpin secondary structure termed stem loop. In a two-step enzymatic processing machinery, the mature miRNA strand is produced (Figure 1-1)[153,166,167]. The first enzyme complex is formed by RNase III enzyme Drosha and double strand (ds)RNA-binding protein DiGeorge syndrome critical region 8 (DGCR8), which together excise the stem loop from the primary transcript, thereby forming the secondary transcript named pre-miRNA. In case the pri-miRNA consisted of a miRNA cluster, more pre-miRNA transcripts can be produced in this step[169,170]. The pre-miRNA is subsequently transported out of the nucleus by Exportin 5[171] and further processed into the miRNA–miRNA* duplex by the RNase III enzyme Dicer and TAR RNA-binding protein (TARBP), consisting of two partially complementary strands originating the 5' and 3' arm of the stem loop (5p and 3p). The leading miRNA strand is preferentially loaded into Argonaute (AGO) proteins and where it is functionally active, whereas the passenger strand (miRNA*) is immediately degraded[166,172].

1.3.2 miRNA regulation

miRNAs exert their function while incorporated into a protein of the AGO family (AGO1–4), which assembles with other proteins to build the RNA-induced silencing complex (RISC). Within this complex, miRNAs bind complementary regions termed seed sequence within the 3'UTR of their mRNA targets (referred to as miRNA recognition elements, MREs) to regulate their

translation[173,174]. Usually, miRNAs inhibit translation of their target mRNAs by preventing translational initiation or by stimulation of mRNA decay[175,176]. AGO2, as the only AGO family member with endonuclease activity, can directly cleave highly complementary mRNA targets. However, AGO2 cleavage is a rather rare event in animals, whereas it constitutes the canonical miRNA-mediated mechanism of translational regulation in plants[177,178]. miRNAs are often categorized into miRNA families, which share the same seed sequence and therefore the same mRNA targets[179,180]. However, many mRNAs have long 3'UTRs, enabling a variety of different miRNAs to regulate their translation, whereas one miRNA can potentially regulate more than one mRNA target[181,182]. This miRNA paradigm impedes studying miRNA function and is probably the reason why most miRNA knockout studies showed modest or no phenotypic effects at all[183]. Interestingly it was proposed that miRNAs, which belong to a miRNA cluster, even though they have different seed regions and regulate different targets, might be involved in regulation of the same biological pathway or different pathways that a certain cell requires in order to adapt to a certain environmental alteration[182,184]. The same idea was proposed for single miRNAs that have multiple 'related' mRNA targets, forming a network that is eventually specialized for a certain cell type in order to adapt[164]. However, the regulation of a target gene by a miRNA is not only dependent on the seed sequence, but also on how the seed is constituted, how many binding sites a mRNA offers and how big the overlap between MREs for the same or different miRNAs is within a 3'UTR. But it also depends on the expression levels of the miRNA, other potential miRNAs and all its targets in a certain cell[164,179]. Interestingly, the number of miRNAs that define cell identity by its expression patterns are considerably higher than those changed upon environmental influences. It was proposed that adaptational changes in miRNA expression might be somehow limited, to not disrupt the miRNA profile that defines the cell[164]. However, another very effective way of increasing the miRNA regulatory capacity for adaptational processes is imperfect processing by Drosha or Dicer, generating different miRNA seed sequences, which exert a different target specificity[185]. Intriguingly, it was shown that pri-miRNAs with paralogous chromosomal locations are particularly susceptible for alternative processing to produce isomiRs, thereby increasing the target repertoire. However, how exactly these processes and alternatives are regulated is yet poorly understood[186].

1.3.3 miRNAs in EAE and MS

Inflammation appears to be a heavy driver of miRNA deregulation. Abnormal inflammation-induced miRNA expression was reported in a variety of cell types as peripheral and CNS resident immune cells, astrocytes, microglia and neurons[64,187,188]. Therefore, and certainly due to miRNA stability and accessibility in biofluids of patients, miRNAs became popular candidates as disease biomarkers[189]. Most miRNA studies in MS patients are biomarker studies. In MS, deregulated

miRNAs were found in peripheral blood mononuclear cells (PBMCs), serum, plasma, CSF and brain tissue[151]. Many of these reports concentrated of deregulated miRNA expression between MS patients and healthy controls[190,191]. In later studies, miRNA expression profiles were also compared between different MS subtypes, treatment versus non-treatment and other neurodegenerative diseases to predict progression and neurodegeneration in MS[191-193]. These studies aimed to improve patient stratification and drug efficacy – a yet unfulfilled desire. A recent profiling study correlated serum miRNAs with brain and spinal cord atrophy and the clinical disability score EDSS of 120 MS patients and identified a profile of positively and negatively correlating miRNAs, which were provocatively termed 'protective' or 'pathogenic'[194]. However, the functional impact of these miRNAs, whether they exhibit cell type or tissue-specific function or contribute to MS pathophysiology is largely unknown[194]. Most biomarker studies report only few miRNAs, some seem to be differentially regulated in other diseases or in many cell types at the same time[189]. It was presumed that most circulating miRNAs are coming from apoptotic or necrotic cells and are therefore rather disease unspecific[195]. However, various reports show miRNA circulation within extracellular vesicles (EVs) as exosomes that can be actively or passively exo- and endocytosed and signal between cells and tissues[196-198]. It was shown that upon cytokine stimulation astrocytes excrete EVs containing miRNAs that regulate the expression of neuronal genes involved in neurotrophic signaling[199]. Recently it was reported that miR-146-5p, which is deregulated in MS, is released from microglia and regulates synaptic synaptotagmin (*Syt1*) and neuroligin *(Nlg1*), which probably promotes the decrease of dendritic spine density during inflammation[200]. Further it was shown that astrocytic EVs contain miRNAs that target the peroxisome proliferator-activated receptor (PPAR)-α upon intracerebral injection of interleukin (IL)-1β, enter the circulation and induce CNS infiltration of peripheral immune cells[201]. How EV-mediated miRNA transport and signaling is precisely regulated is mainly unclear, but a role in MS slowly emerges[193]. Some of the in MS patients identified miRNAs were validated in EAE and functionally investigated. Interestingly, for many miRNAs a dual role for the immune und central nervous system was reported. miR-142a-3p is strongly linked to inflammation in MS and was found upregulated in the CSF of active RRMS patients and in EAE brain[202,203]. Other studies showed induced expression of miR-142a-3p in MS blood[204]. Therefore, miR-142a-3p was proposed as a potential biomarker for RRMS. miR-142a-3p knockout mice were completely protected against EAE[202]. It was shown that one mechanism of miR-142a-3p is downregulation of EAAT1 expression in glia cells in an IL-1ß-dependent manner, thereby reinforcing glutamate excitotoxicity and neuronal impairment[202]. However, miR-142a-3p is also upregulated in $CD3^+$ immune cells in EAE and $CD4^+$ immune cell of MS patients, indicating that the absence of EAE clinical disability in miR-142a-3p knockout mice rather related to deficiency of an immune response[202,205]. Another commonly identified inflammatory miRNA in MS, miR-155-5p was also

proposed as a potential biomarker[206]. Deletion of miR-155 was shown to ameliorate EAE clinical disability by damping T_H1 and T_H17 responses[207]. An important function of this miRNA and miR-142a-3p was described in immune cells, being both involved in priming, development and differentiation of T cells and other immune cell subsets[208,209]. Interestingly, for miR-155-5p also a neuron-specific function was assigned. It appears that deletion of miR-155-5p is neuroprotective and helps axonal regeneration after injury, by regulating regeneration induced genes in the spinal cord[210]. Concordantly, a reduced expression of miR-142a-3p and miR-155-5p was detected after immunomodulatory treatment with glatiramer acetate or hematopoietic stem cell transplantation (HSCT) in MS patients[203,205], implying that therapeutic targeting of these miRNA would be immunosuppressive and neuroprotective at the same time. Another commonly identified miRNA in MS and EAE, miR-223-3p was shown to exert a neuroprotective function in EAE[211] and traumatic brain injury (TBI), by regulating expression of the glutamate receptor subunits GluA2 and GluN2B[212]. Another miRNA with synaptic function and the capability to impact on neurodegeneration was shown in *drosophila melanogaste*r. Knockout of the activity-regulated, presynaptic miR-1000, which acts on glutamate release by regulating translation of the vesicular glutamate transporter (VGLUT) was shown to induce glutamate excitotoxicity and apoptosis in the brain[213]. Moreover, specific ablation of dicer in neuronal subpopulation as well as in astrocytes and oligodendrocytes caused neurodegeneration in mice, implicating an import role of miRNAs in neurodegeneration[156,214,215].

Together, these studies indicate that miRNAs have an important neuronal function in CNS-inflammation in MS and EAE, but are most probably not disease specific. Most miRNA studies identified brain or spinal cord-induced miRNAs without deciphering cell type specific expression. The first study dedicated to identify neuron-specific miRNAs in EAE used laser caption to mechanically dissect neurons from the spinal cord and retina[188]. They showed deregulation of 14 miRNAs, which were bioinformatically predicted to target genes involved in regeneration and tissue repair[188]. However, most of these miRNAs have not been functionally validated yet.

1.4 miR-92a-3p biology and function

miR-92a-3p is the leading strand of the miR-92a–miRNA duplex, consists of 21 nucleotides (UAU UGC ACU UGU CCC GGC CUG) and is generated by *Mir92-1* within the polycistronic miR-17/92 cluster encoded by *Mir17HG* on chromosome 14 in mice[216]. However, in humans miR-92a-3p is encoded on chromosome 13 and contains an additional uracil nucleotide at the 3' end[217]. miR-92a-3p is expressed throughout the CNS[218,219] and its seed region is very well conserved among vertebrates[220]. Due to the shared seed region and the same predicted targets miR-92a-3p is

categorized into the evolutionary broadly conserved miRNA family miR-25, which harbors five members miR-25-3p, miR-32-5p, miR-92a-3p, miR-363-3p and miR-367-3p[184,221]. It is not fully understood how miRNAs from the same seed family regulate the same targets and pathways, but most likely they exert different target specificities, which are determined by variances in their sequence and differential cell type-specific expression[222]. However, also miR-92a-3p exerts various functions in different cell types and tissues[223].

1.4.1 miR-17/92 cluster

The miR-17/92 cluster is the best studied miRNA cluster and gained its popularity due to its high expression and functional role in development and progression of several cancer. Therefore, miR-17/92 is also referred to as Oncomir-1. Nevertheless, the miR-17/92 cluster has also been associated with other diseases[184]. Intriguingly, homozygous deletion of the whole cluster in mice is postnatally lethal[224]. Besides association with autoimmunity, the cluster seems to have an important role in neurological and neurodegenerative diseases[225]. Deregulation of the cluster has been observed for MS[226], EAE[227], Alzheimer's[228], ALS[229], autism[230] and neuropathic pain[231].

The miR-17/92 cluster is transcribed as a primary transcript comprising the 6 mature miRNAs miR-17, miR-18a, miR-19a, miR19b and miR-92a[184]. A role of the miR-17/92 cluster was shown in immune system regulation and differentiation, particularly for B cells[224]. However, the single expression of each cluster member in tissues and different cell types at different stages of organismal development or in disease is only partially investigated[184]. A serial knockout of each cluster miRNA attributed the major role in B cell development to miR-17 and miR-18, whereas a knockout of mir-92a alone had no effect on immune cell development and number of B cells[232]. Further, it was shown that miR-92a is expressed in $CD4^+$ T cells, whereas its expression is much lower than for miR-17 and miR-20a[233]. Besides an immunological role it was shown that the cluster regulates axon outgrowth in cortical neurons[234] and regulates development and differentiation of the mouse neocortex[235]. Further, it was shown that the cluster is also implicated in adult hippocampal neurogenesis and dysfunction and was associated with anxiety and depression. Interestingly, the major phenotypic outcome of this study was attributed to miR-19a and miR-92a[219]. Hemizygous germline deletion of the miR-17/92 cluster was associated with the autosomal dominant Feingold syndrome[236]. The major features of these patients are microcephaly, digital abnormalities and relative short stature[236]. Intriguingly, a recent study showed that miR-17/92$^{\Delta 92/\Delta 92}$ mice had a skeletal phenotype with shorter stature, significantly smaller skull and tibia length, but no impairment of B cell development nor changed numbers of $CD45^+$ cells in blood and bone marrow[237]. These studies indicate that miR-92a-3p seems to have a more prominent role the in the CNS, specifically in neurons. However, it is very challenging to

study the cluster function and contribution of its miRNAs due to their complex regulation. It was reported that over 35 transcription factors can modulate expression of the cluster and it is poorly understood, how differential processing of the stem loops and maturation of single miRNAs from that cluster occurs[184]. Additionally, two paralogous cluster of the miR-17/92 cluster have been reported, miR-106a/363 and miR-106b/25 cluster, which probably cooperate on related targets and pathways[238,239]. Nevertheless, scientists are engaged to disentangle whether and how each miRNA of the clusters contributes to a certain cell type and tissue-specific function at the basal state and in various diseases.

1.4.2 miR-92a-3p in neurological diseases

In a recent MS biomarker profiling study, plasma miR-92a-3p levels correlated with lesion-based brain tissue destruction (T1:T2 weighted MRI)[194], indicating that miR-92a-3p might be involved in inflammation-induced neurodegeneration in MS. However, the expression of miR-92a-3p did not correlate with disability of the patients. In this study different MS subtypes were not discriminated, therefore attribution of miR-92a-3p upregulation to a certain MS subtype remains obscure. Also, high levels of miR-92a were identified in spinal cord homogenate of acute EAE mice, but the expression levels were not assigned to a specific cell type[240]. A direct association of miR-92a-3p, independent of the other miR-17/92 cluster miRNAs was made for a variety of neurodegenerative diseases. For Alzheimer's disease miR-92a-3p was discussed as a potential biomarker together with two other brain-enriched miRNAs miR-181c-5p and miR-210-3p[241]. miR-92a-3p was found upregulated in serum of Alzheimer's patients and those with mild cognitive impairment (MCI). Interestingly, miR-92a-3p levels were higher in MCI patients that developed Alzheimer, but were not deregulated in patients with frontotemporal dementia (FTD). However, it remains unclear how miR-92a-3p increased in biofluids of these patients and where it originated from. Also, it is mainly unknown whether miR-92a-3p is also directly associated with disease pathology of MS, EAE, MCI and Alzheimer's. However, for ALS, a direct contribution of miR-92a-3p was shown. Interestingly, miR-92a-3p was found highly downregulated in spinal cord homogenates of ALS patients[242]. Fascinatingly, AAV-delivered miR-17/92 increased lifespan of the ALS mouse model $SOD1^{G93A}$ and overexpression of the cluster could prevent motor neuronal degeneration induced in human $SOD1^{+/L144F}$ pluripotent stem cells[229].

Together, miR-92a-3p expression is associated with a variety of neurological diseases and seems to play a prominent role in the spinal cord. However, its regulation seems to be strongly dependent on the pathophysiology of the disease and is yet poorly understood.

1.4.3 Neuronal function and targets of miR-92a-3p

Overexpression of the miR-17/92 cluster in mouse cortical neurons was shown to enhance the outgrowth of axons by decreasing expression of phosphatase and tensin homolog (PTEN) and increasing the expression of mammalian target of rapamycin (mTOR). The contribution of single cluster miRNAs in regulating axonal outgrowth has not been studied yet[234]. However, miR-92a-3p was shown to be involved in regulating axon guidance and outgrowth of commissural axons in the developing chicken spinal cord by regulating the expression of roundabout (*Robo*) mRNA[243]. Further, it was demonstrated that the miR-17/92 cluster regulates motor neuronal survival and degeneration in mice by targeting the ubiquitin ligase E3, which monoubiquitinates PTEN and thereby affects its subcellular localization to the nucleus where it induces apoptosis[244]. Therefore, conditional knockout of the miR-17/92 cluster in MN induced apoptosis by overt accumulation of PTEN in the nucleus, whereas overexpression of miR-17/92 had drastically reduced nuclear PTEN levels and rescued the MNs from programmed cell death[244]. Again, the contribution of single cluster miRNAs in regulating motor neuronal survival and degeneration is still to be investigated.

miR-92a-3p also exerts synapse specific function, which is mediated by its regulation of synaptic target genes and was shown to be implicated in synaptic scaling, learning and memory. By profiling cell type-specific miRNAs from diverse neuronal subpopulations in the mouse brain it was shown that miR-92a is mostly expressed by glutamatergic neurons[218]. Further, it was demonstrated that mir-92a-3p represses the translation of cytoplasmic polyadenylation element-binding protein 3 mRNA (*Cpeb3*)[245]. The RNA-binding protein CPEB3 was shown to be highly enriched in the brain, especially in the postsynaptic density (PSD)[246]. It was described that CPEB3 represses translation of its own target mRNAs in P-bodies, but localizes to polysomes and oligomerizes due to its prion-like domain upon neuronal activation, thereby promoting translation of its targets mRNAs[247]. CPEP3 functionality is highly modified by activity-dependent post-translational modifications[248-250]. Small ubiquitin modifier (SUMO)ylation and monoubiquitination of CPEB3 were shown to regulate CPEB3 aggregation[248,249]. At the basal state, CPEB3 was shown to act as a translational repressor of postsynaptic mRNAs as glutamate ionotropic receptor AMPA type subunit 1 and 2 (*Gria1, Gria2*), *Psd-95* and *actin*[246,251,252]. After glutamate receptor stimulation in hippocampal neurons CPEB3 was shown to redistribute from the cytoplasm to the nucleus to eventually induce transcriptional changes or transport synaptic mRNAs[253]. Further, it was reported that NMDA-mediated Ca^{2+}-influx might lead to Calpain 2 activation, which cleaves the N-terminal repression motif of CPEB3, thereby abrogating its translational repression[254]. Finally, it is still under investigation whether phosphorylation of CPEB3 can also induce polyadenylation of its target mRNAs to enhance their translation as it was shown

to be the canonical function of CPEB1[250,255]. Interestingly, miR-92a-3p expression was shown to be induced upon contextual fear conditioning in the hippocampus of mice, accompanied by downregulation of CPEB3[256]. Also, injection of a miR-92a-3p inhibitor into primary neurons and into the CA1 region of the mouse hippocampus led to upregulation of CPEB3 and impairment of contextual fear conditioning[256]. Concordantly, CPEB3 knockout mice exhibited enhanced hippocampal memory in contextual fear conditioning and increased spatial memory[252].

Another fascinating synaptic function of miR-92a-3p was shown by regulation of AMPAR subunit GluA1 during synaptic scaling in rat hippocampal neurons[257]. miR-92a-3p expression was downregulated by pharmacological activity blockage with tetrodotoxin (TTX) and 2-Amino-5-phosphonopentanoic acid (AP5), which led to increased translation of *Gria1*[257].

Together, despite its attribution to different diseases and expression by different cell types, miR-92a-3p clearly exerts a neuron and synapse-specific function by regulating translation of its targets as CPEB3 in an activity-dependent manner.

1.5 Therapeutic potential of miRNAs

The idea of inhibiting RNA molecules by antisense oligonucleotides (ASOs) as therapeutic strategy has been proven effective for neurological diseases as spinal muscular atrophy or Huntington[258]. Most reports that showed successful therapeutic re-balancing of deregulated disease-associated miRNAs emerged from cancer studies[259], however evidence for neuroprotective therapeutic approaches were delivered from animal models of various neurological disease including one for MS[211,260,261]. Importantly, miRNAs exert their cell and target specificity mostly in a spatiotemporal manner[164,262] and only few exclusively restricted cell type or tissue-specific miRNAs have been identified so far[162,263]. Therefore, miRNA-associated therapy might require tissue or cell type-specific delivery. Different strategies were described that can be used to outbalance deregulated miRNA levels systematically or directly in target tissues[150]. As shown in Figure 1-2 either miRNA induction or inhibition, dependent on whether disease-associated miRNAs were up or downregulated, can be applied. For deleterious downregulation of miRNAs synthetic miRNA mimics (locked nucleic acids (LNAs) or agomiRs) might be suited that were chemically modified to increase stability and efficacy. Further, an AAV-mediated application of precursor miRNA can be utilized. This strategy might also be applicable for cell-type specific expression of the miRNA precursor by using respective promoters.

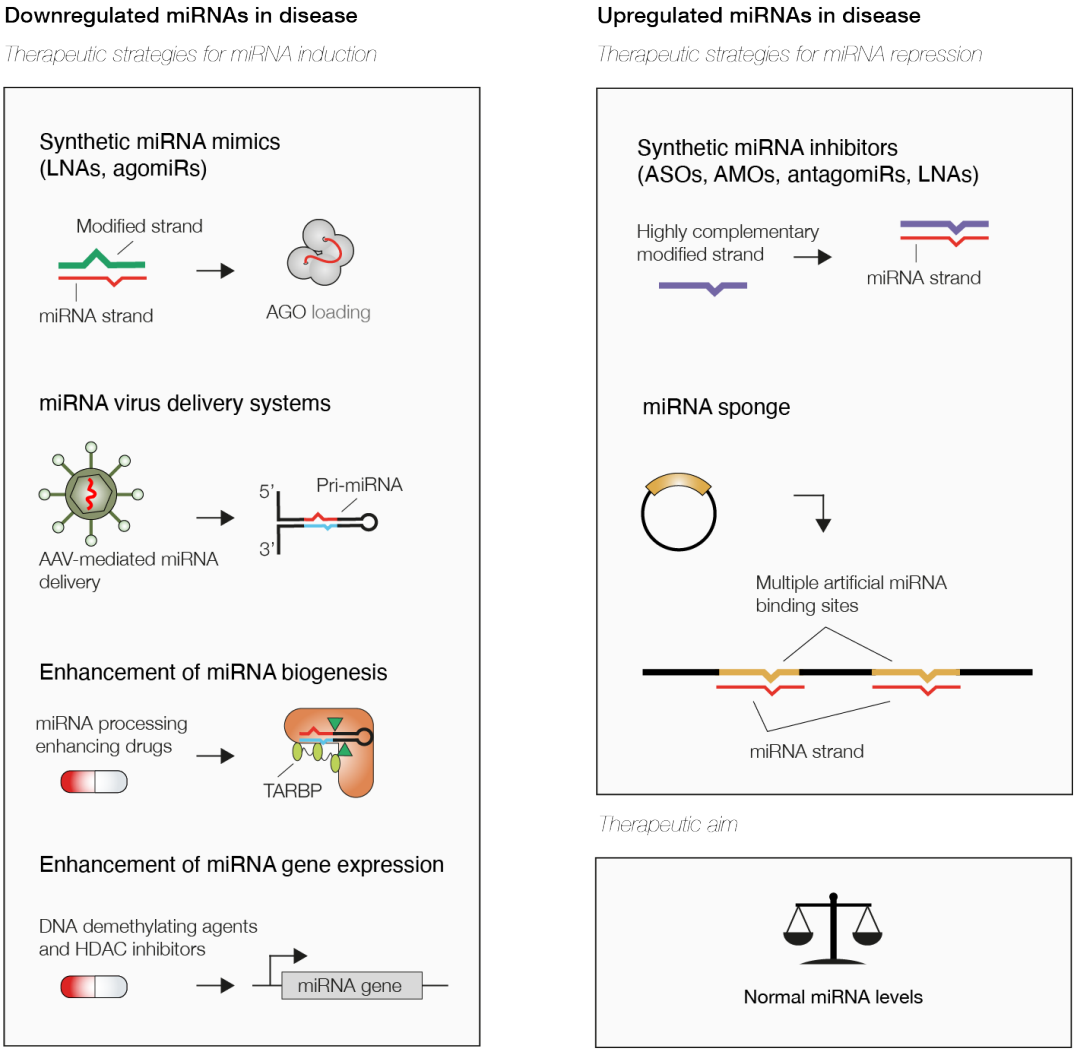

Figure 1-2 Therapeutic strategies to target deregulated miRNA in human disease

Schematic demonstration of miRNA targeting in human diseases[150]. (Left box) Therapeutic strategies that might be used to achieve upregulation of downregulated miRNAs in disease. (Right, upper box) Therapeutic strategies to inhibit upregulated miRNAs in disease. (Right, lower box) miRNA targeting is used to rebalance dysregulated miRNAs and their targets that cause disease.

However, such gene-based therapies present a range of challenges as described for viral delivery of protein-coding genes[150,264]. Also, more global miRNA-restoring approaches were made. The small molecule drug enoxacin was used to increase the expression of various downregulated miRNAs in cancer by promoting their binding to TARBP2, thereby enhancing miRNA biogenesis[265]. Another global approach was made in cancer treatment by using compounds (DNA demethylating agents or histone deacetylase inhibitors) that change the epigenetic

modification of tumor suppressor miRNAs[150,266,267], leading to inhibition of tumor growth and induction of apoptosis.

Contrarily, deleterious upregulation of miRNAs can be achieved by inhibiting miRNAs with synthetic miRNA inhibitors such as ASOs, anti-miRNA oligonucleotide (AMOs), antagomiRs and LNAs, which all differentiate in their chemical modifications, stability and efficacy. Finally, miRNA sponges that exhibit multiple artificial binding sites to 'catch' and inhibit overexpressed miRNAs might be applicable as therapeutic strategy (Figure 1-2). As discussed above the pleiotropic and multifaceted character of miRNA regulation is often compensatory[164]. In most disease not only single miRNAs, but multiple miRNAs are deregulated at the same time[150]. Therefore, the targeting of single miRNAs might not be sufficient in order to achieve successful therapy. Thus, multiple miRNA mimics could principally be applied to substitute expression of different downregulated miRNAs simultaneously. Concordantly, inhibition of different upregulated miRNAs can be achieved at once. Such an approach was made by targeting three upregulated oncogenic miRNAs in cancer by using a multiple-target AMO (MTg-AMO)[268] that was more powerful in suppression of tumor growth than inhibition of a single upregulated miRNA Currently, different miRNA delivery systems such as nanocells, nanoparticels and liposomes are developed and improved to increase stability, specificity of targeting and to minimize toxicity, which are all still challenges of miRNA-based therapy[151]. However, miRNA targeting comprises great potential not only for personalized medicine, but also for modulating impaired disease associated pathways instead of single targets[151].

1.6 Aims

MS is characterized by immune cell infiltration, axonal demyelination and neurodegeneration. Excessive activation of the glutamatergic pathway accompanies MS pathophysiology and results in neuronal stress responses that impair neuronal signaling and perpetuate neurodegeneration and consecutive neurological deficits as cognitive impairment and disability. For MS no specific neuroprotective treatment is available to neither halt neurodegeneration nor disease progression. Importantly, it is still poorly understood by which mechanisms neuronal stress responses are driven and regulated in CNS-inflammation. A fundamental mechanism to respond to changes in the cellular environment is coordination of translation by miRNAs. However, it remains unclear to which extend neuronal miRNAs orchestrate neuronal gene expression and whether they determine consecutive neurodegeneration in CNS-inflammation. Therefore, the overall aim of this work is to understand the regulatory mechanisms of neuronal miRNAs in CNS-inflammation in order to help develop new neuroprotective treatment for inflammation-induced

neurodegeneration. To achieve this overarching aim, 4 single aims were formulated in the following.

Aim 1: Profiling of neuronal miRNAs in CNS-inflammation

Aim 2: Profiling of neuronal gene regulatory networks in CNS-inflammation

Aim 3: Validation of neuronal miRNA networks

Aim 4: Deletion of miRNAs in CNS-inflammation

Together, the Identification and examination of inflammatory neuronal miRNAs should facilitate identifying relevant target genes and biological networks that foster the understanding and interference of neurodegenerative processes to develop new therapeutic neuroprotective strategies in CNS-inflammation.

2 Material

2.1 Reagents and chemicals

Table 1 Reagents and chemicals for animal experiments

Name	Company
CO_2/O_2 gas mixture (80%/20%)	SOL
DietGel® Recovery	Clear H_2O
Freud's adjuvant	Difco laboratories
Ketanest® S 25mg/ml (Ketamine)	Pfizer Pharma
Mouse/rat MOG_{35-55} peptide	Peptides & elephants
Mycobacterium tuberculosis	Difco laboratories
Nekrolyt® Salbe	CP-Pharma
Pertussis toxin (Bordetella pertussis)	Calbiochem
Rompun® 2% (Xylazine)	Bayer

Table 2 Reagents and chemicals for genotyping

Name	Company
dNTP Mix (10mM)	Thermo Scientific
DreamTaq™ Hot Start Green DNA Polymerase, 5 U/µl	Thermo Scientific
DreamTaq™ Hot Start Green PCR Master Mix (10X)	Thermo Scientific
Ethylenediaminetetraacetic acid (EDTA), 0.5 M	Sigma–Aldrich
GeneRuler 1 kb DNA Ladder	Thermo Scientific
Maxima™ Hot Start PCR Master Mix (2X)	Thermo Scientific
Maxima™ Hot Start Taq DNA-Polymerase, 5 U/µl	Thermo Scientific
$MgCl_2$	Sigma–Aldrich
Nuclease-Free H_2O	Invitrogen

Primer	Biomers
QuickExtract™ DNA Extraction Solution	Lucigen
Roti®-Safe GelStain	Carl Roth
Tris ultrapure	Applichem
UltraPure™ Agarose	Invitrogen

Table 3 Reagents and chemicals for immunohistochemistry

Name	Company
High Precision Microscope Cover Glasses	Marienfeld
Normal Donkey Serum	Merck
PAP pen 2 mm tip width (Liquid Blocker)	Sigma–Aldrich
ROTI®Mount FluorCare DAPI	Carl Roth
Superfrost Plus™ Adhesion Microscope Slides	Thermo Fisher™
Triton-X® 100 reinst	Carl Roth

Table 4 Reagents and chemicals for qRT-PCR

Name	Company
2-Mercapthoethalnol	Sigma–Aldrich
DEPC-treated water	Invitrogen
Ethanol, absolute, ≥99.8% (GC)	Sigma–Aldrich
High-Capacity RNA-to-cDNA™ Kit	Applied Biosystems
RNeasy® Mini Kit	Qiagen
TaqMan® MicroRNA Reverse Transcription Kit	Applied Biosystems
TaqMan® Universal PCR Master Mix II (2X) with UNG	Applied Biosystems
TaqMan™ Gene Expression Master Mix	Applied Biosystems
Tris-EDTA buffer (TE), 8.0 pH	Invitrogen

Table 5 Reagents and chemicals for miRAP and TRAP

Name	Company
07:0 PC (DHPC) 1,2-diheptanoyl-sn-glycero-3-phosphocholine	Avanti® Polar Lipids
1,4-Dithiothreitol (DTT)	Roche
cOmplete™, EDTA-free Protease Inhibitor Cocktail	Roche
D-(+)-Glucose, BioXtra, ≥99.5% (GC)	Sigma–Aldrich
DEPC-treated water	Invitrogen
Dynabeads™ MyOne™ Streptavidin T1	Invitrogen
Rabbit α-GFP monoclonal antibodies (19C8, 19F7)	Antibody & Bioresource Core Facility, Sloan Kettering Institute, USA
GlycoBlue™ Coprecipitant	Invitrogen
Bovine Serum Albumin (BSA), IgG-free, protease-free	Jackson ImmunoResearch
miRNeasy® Micro Kit	Qiagen
Pierce™ Recombinant Protein L, Biotinylated	Thermo Scientific
QIAzol Lysis Reagent	Qiagen
RNase-Free DNase Set	Qiagen
RNeasy® Micro Kit	Qiagen
TRIzol™ Reagent	Invitrogen
NP-40 Surfact-Amps™ Detergent Solution	Thermo Scientific
Cycloheximide (CHX), ≥ 94% (TLC)	Sigma–Aldrich
Chloroform, anhydrous, ≥99%	Sigma–Aldrich
Sodium acetate, anhydrous, for molecular biology, ≥99%	Sigma–Aldrich
Ethanol, absolute, ≥99.8% (GC)	Sigma–Aldrich
Methanol, anhydrous, 99.8%	Sigma–Aldrich
Dulbecco's PBS (DPBS) sterile filtered (1X)	Pan-biotech
$MgCl_2$ (1 M)	Invitrogen
2-Propanol, anhydrous, 99.5%	Sigma–Aldrich

2-Mercaptoethanol, suitable for cell culture, BioReagent, 99% (GC/titration)	Sigma–Aldrich
KCl (2 M)	Invitrogen
HEPES, 1M, pH 7.3, UltraPure	Thermo Scientific
HBSS, 10X, calcium, magnesium, no phenol red	Gibco
RNasin® Plus RNase Inhibitor, 10.000U	Promega
SUPERase•In™ RNase Inhibitor, 10.000U	Invitrogen
Sodium bicarbonate (NaHCO3), BioXtra, 99.5-100.5%	Sigma–Aldrich

Table 6 Regents and chemicals for cell culture and stress assays

Name	Company
Cytosine β-D-arabinofuranoside (AraC)	Sigma-Aldrich
B-27™ Supplement (50X), serum free	Gibco
(+)-Bicuculline	Sigma-Aldrich
DMEM-F12	Gibco
DMEM, high glucose GlutamMAX™ Supplement	Gibco
DPBS sterile filtered (1X)	Pan-biotech
Fetal Calf Serum (FCS)	Carl Roth
GlutamMAX™ Supplement	Gibco
HBSS, no calcium, no magnesium	Gibco
L-glutamic acid	Sigma–Aldrich
Neurobasal™ Medium	Gibco
Opti-MEM™	Gibco
Penicillin-Streptomycin (10.000 U ml^{-1})	Invitrogen
Poly-D-Lysine hydrobromide	Sigma–Aldrich
Recombinant Mouse IL-1β	BioLegend
Recombinant Murine IFN-γ	PeproTech
Recombinant Murine TNF-α	PeproTech

TrypLE™ Express Enzyme (1X)	Gibco
Trypsin-EDTA (0.05%), phenol red	Gibco

Table 7 Reagents and chemicals for miRNA target gene luciferase reporter assay

Name	Company
Dual-Glo® Luciferase Assay System	Promega
Lipofectamine 2000	Invitrogen
miRCURY LNA™ miRNA mimics	Qiagen
miTarget™ 3′ UTR miRNA Target Clones	GeneCopoeia

Table 8 Regents and chemicals for flow cytometry

Name	Company
CompBead Control Compensation Particles Set	BD
Cytofix™ Fixation Buffer	BD
DNase I from bovine pancreas	Sigma–Aldrich
FACS Clean Soution	BD
FACS Lysing Solution (10X)	BD
FACSFlow™ Sheath Fluid	BD
FACSRinse Solution	BD
Percoll®	Sigma–Aldrich
Rosewell Park Memorial Institute (RPMI) 1640 Medium	Pan-biotech
TruCount® Absolute Counting Tubes	BD

2.2 Buffers, solutions and media

Table 9 Buffers, solutions and media

Name	Ingredients
Tris-acetate-EDTA (TAE), 50X	2 M Tris
	0.05 M EDTA
	5.7% Acetic Acid
	in ddH_2O
CNS digestion solution	1 mg ml^{-1} Collagenase A
	0.1 mg ml^{-1}l DNase I
	In RPMI 1640
Dissection buffer	1X HBSS
	2.5 mM HEPES
	35 mM Glucose
	4 mM $NaHCO_3$
	100 µg ml^{-1} CHX
	In DEPC-treated H_2O
N2a medium	500 ml DMEM, high glucose, GlutaMAX™ Supplement
	10% FCS
	100 U ml^{-1} Penicillin-Streptomycin
FACS buffer	0.5% BSA
	0.02% NaN_3
	In 1X DPBS
Lysis buffer	20 mM HEPES
	5 mM $MgCl_2$
	150 mM KCl

	0.5 mM DTT
	100 µg ml^{-1} CHX
	Protease-Inhibitor (1:100)
	40 U ml^{-1} RNasin®
	20 U ml^{-1} SUPERase•In
	In DEPC-treated H_2O
Neurobasal Feeding Medium	500 ml Neurobasal™, Gibco
	100 U ml^{-1} Penicillin-Streptomycin
	10 ml B-27™ Supplement
Neurobasal Plating medium	500 ml Neurobasal™, Gibco
	12.25 µl L-glutamic acid
	100 U ml^{-1} Penicillin-Streptomycin
	10 ml B-27™ Supplement
PBS-T	1X PBS
	0.1% Triton-X
Phosphate buffered saline (PBS), 1X, 7.4 pH	137 mM NaCl
	2.7 mM KCl
	10 mM Na_2HPO_4
	1.8 mM KH_2PO_4
	In ddH_2O
Potassium chloride (KCl), 0.15 M	20 mM HEPES
	5 mM $MgCl_2$
	150 mM KCl
	1% NP-40
	0.5 mM DTT
	100 µg ml^{-1} CHX
	In DEPC-treated H_2O

Potassium chloride (KCl), 0.35 M	20 mM HEPES 5 mM $MgCl_2$ 350 mM KCl 1% NP-40 0.5 mM DTT 100 µg ml^{-1} CHX In DEPC-treated H_2O

2.3 Antibodies

Table 10 Primary antibodies for immunohistochemistry

Name	Clone	Dilution	Company
Chicken α-GFP	Polyclonal	1:500	Abcam
Goat α-ChAT	Polyclonal	1:300	Sigma–Aldrich
Guinea pig α-GFAP	Polyclonal	1:100	Synaptic Systems
Guinea pig α-Synapsin 1/2	Polyclonal	1:300	Synaptic Sytems
Mouse α-CNPase	11-5B	1:100	Sigma–Aldrich
Mouse α-SMI-31R	SMI-31	1:500	BioLegend
Mouse α-SMI-32P	SMI-32	1:500	BioLegend
Rabbit α-Iba1	Polyclonal	1:100	Abcam
Rat α-CD31	MEC 13.3	1:100	BD Pharmingen™

Table 11 Secondary antibodies for immunohistochemistry

Name	Clone	Dilution	Company
Alexa Fluor® 647 donkey α- guinea pig	Polyclonal	1:300	Jackson ImmunoResearch
Alexa Fluor® 488 Donkey α-chicken	Polyclonal	1:600	Jackson ImmunoResearch

Alexa Fluor® 488donkey α-guinea pig	Polyclonal	1:600	Jackson ImmunoResearch
Alexa Fluor® 549 donkey α-rat	Polyclonal	1:300	Jackson ImmunoResearch
Alexa Fluor® 647donkey α-goat	Polyclonal	1:300	Jackson ImmunoResearch
Alexa Fluor® 647donkey α-mouse	Polyclonal	1:300	Jackson ImmunoResearch
Alexa Fluor® 647donkey α-mouse	Polyclonal	1:600	Jackson ImmunoResearch
Cy™3 donkey α-rabbit	Polyclonal	1:300	Jackson ImmunoResearch

Table 12 Stain and Antibodies for flow cytometry

Name	Clone	Label	Dilution	Company
Armenian Hamster α-CD3e	145-2C11	PerCP-Cy5.5	1:100	BioLegend
Hamster α-CD11c	N418	APC	1:300	BioLegend
LIVE/DEAD Fixable Dead Cell Stain	–	APC-Cy7	1:1000	Invitrogen
Mouse α-NK1.1	PK136	PE	1:150	eBioscience
Rat α-CD11b	M1/70	FITC	1:300	BioLegend
Rat α-CD45	30F11	AF700	1:100	BioLegend
Rat α-CD45R (B220)	RA3-6B2	V500	1:250	BD Pharmingen
Rat α-CD8a	53-6.7	PB	1:300	BioLegend
Rat α-Ly6G	1A8	PE-Cy7	1:300	BD Pharmingen
Rat F_C Block (α-CD16/CD32)	93	-	1:1000	BioLegend

2.4 qRT-PCR primer and assays

Table 13 qRT-PCR primer and assays for miRNAs

Name	Assay ID	Company
hsa-miR-92	000430	Taqman™ by Applied Biosystems
snoRNA234	001234	Taqman™ by Applied Biosystems
hsa-miR-16	000391	Taqman™ by Applied Biosystems
mmu-miR-218-5p	mmu481001-mir	Taqman™ by Applied Biosystems
hsa-miR-138-5p	477905_mir	Taqman™ by Applied Biosystems
mmu-miR-9-5p	mmu481285_mir	Taqman™ by Applied Biosystems
mmu-miR-150-5p	mmu480947_mir	Taqman™ by Applied Biosystems
mmu-miR-384-3p	mmu481152-mir	Taqman™ by Applied Biosystems

Table 14 qRT-PCR primer and assays for mRNAs

Name	Assay ID	Company
Cpeb3	Mm01204299_m1	Taqman™ by Applied Biosystems
Gria1	Mm00433753_m1	Taqman™ by Applied Biosystems
Mir17HG	Mm03306814_pri	Taqman™ by Applied Biosystems
Tbp	Mm01277042_m1	Taqman™ by Applied Biosystems

2.5 Consumables

Table 15 Consumables

Name	Company
96 PCR Plate half skirt	Sarstedt
Biosphere® Plus Filter Tips	Sarstedt
Biosphere® SafeSeal Tubes (PCR Performance Tested)	Sarstedt
Butterfly cannula	Sarstedt
Cannulas	B. Braun
Cell Culture Dishes	Thermo Fisher Scientific
Cell scrapers, 16 cm handle length	Sarstedt
CELLSTAR® Cell Culture Multiwell plates	Greiner Bio-One
CELLSTAR® Filter Cap Cell Culture Flask	Greiner Bio-One
CELLSTAR® Polypropylene Tubes	Greiner Bio-One
ddH_2O	Centre for Molecular Neurobiology
Falcon™ Cell Strainers	Fisher Scientific
MicroAmp® Optical 384-well reaction plate	Applied biosystems
Nonstick, RNase-free Microfuge Tubes, 1.5 ml	Applied biosystems
Pasteur pipette 230 mm (glass)	Heinz Herenz Medizinbedarf
Filter tips	Sarstedt
RNase Zap™	Invitrogen
Round Bottom Polystyrene Tube, 5 ml (FACS)	Sarstedt
SafeSeal Micro tubes	Sarstedt
Serological pipettes (sterile)	Sarstedt
StarGuard® Comfort gloves	Starlab
Syringes (1 ml)	B. Braun
Syringes (3 ml)	BD

2.6 Equipment

Table 16 Equipment and Devices

Name	Company
ABI Prism 7900 HT Fast Real-Time PCR System	Applied biosystems
Bench Top Microcentrifuge	Eppendorf
Binocular Stereo Microscope	Leica
Biometra Low Voltage Power Supply	Analytik Jena
Biometra Thermocycler	Analytik Jena
Chemical fume hood	Kugel medical
Comfort Freezer (–20°C)	Liebherr
DynaMag™-2 Magnet rack	Invitrogen
Electrophoretic system	Peqlab
Epifluorescence Microscope Eclipse	Nikon
Eppendorf® Thermomixer Compact (1.5 ml block)	Sigma–Aldrich
Fume hood	Belec Vario Lab
Homogenizer Vessel (2 ml)	Satorius
Hot bead Sterilizer	FST Fine Scientific Tools
Incubator (cell lines)	Memmert
Incubator (primary neurons)	Termo Scientific
Intas Gel-documentation	Intas Science Imaging Instruments
Light Microscope	Olympus
LSM600 confocal laser scanning microscope	Zeiss
LSR II Flow cytometer	BD
Microme HM 560 Cyrostat	Thermo Fisher Scientific
myFUGE Mini Microcentrifuge	Biozym
NanoDrop™ 1000 Spectrophotometer	Thermo Fisher Scientific
Neubauer cell count chamber	Marienfeld
Perfusion System	Ismatec

Picus® Electronical Pipettes	Satorius
Pipettes	Gilson, Satorius
PlateFuge™ Microcentrifuge	Benchmark Scientific
QuantStudio™ 6 Flex Real-Time PCR System	Applied biosystems
Refrigerator (4°C)	Liebherr
Rotator	GLW Gesellschaft für Laborbedarf
Spark™ 10M multimode microplate reader	Tecan
Staining jars	Marienfeld
StainTray slide staining system	Sigma–Aldrich
Laminar flow hood	Thermo Fisher Scientific
Surgical instruments	FST Fine Scientific Tools
Trypan blue Solution (0.4%), cell culture	Sigma–Aldrich
Ultra-low Temperature Freezer (–80°C)	Sanyo
Water bath	GFL Gesellschaft für Laborbedarf

2.7 Software

Table 17 Software

Name	Company/Website (Open Source)
FACSDiva™	BD
FlowJo for Mac v10	FlowJo
ImageJ (Fiji)	https://imagej.nih.gov/ij/index.html
Prism 8 for Mac	Graph Pad Software
SparkControl plate reader software	Tecan
TBase Client 4Dv12sql	MacKeeper
ToppGene Suite	https://toppgene.cchmc.org
Venny v.21	https://bioinfogp.cnb.csic.es/tools/venny/
RQ Manager v1.2.1	Applied Biosystem
R Studio v.3.3.2	https://rstudio.com
SDS v2.4	Applied Biosystem

Adobe Photoshop CS6 v13.0 x64	Adobe Inc.
Adobe Illustrator CS6 v16.0.0	Adobe Inc.
Microsoft Excel for Mac v16.16.17	Microsoft
Microsoft Excel for Mac v16.16.17	Microsoft
STAR v2.4	http://code.google.com/p/rna-star/

3 Methods

3.1 Laboratory animals

All animas were housed and bred at the Central Animal Facility at the University Medical Center Hamburg-Eppendorf (UKE). Mice were provided with food and water *ad libitum*. Two weeks before starting an experiment, mice were transferred into the institute colony and kept in individually-ventilated cages under specific pathogen-free conditions. All experiments were approved by the local ethics committee (*Behörde für Soziales, Familie, Gesundheit und Verbraucherschutz in Hamburg*), *Tierversuchsantrag* Nr. 20/15 or Nr. 122/17 and ORG 713.

3.1.1 C57BL/6J

C57BL/6J mice were initially received from The Jackson Laboratory, USA. This mouse strain constitutes the genetic background for the utilized genetically modified mouse lines and is therefore referred to as wildtype.

3.1.2 Chat-IRES-Cre x R26-LSL-tAGO2

The *B6(Cg)-Gt(ROSA)26Sor*$^{tm1(CAG-GFP/Eif2c2)Zjh}$*/J (R26-LSL-tAGO2)* mouse strain was created by *Miao He* and colleagues[218] and purchased from The Jackson Laboratory, USA. These animals were crossed with *B6;129S6-Chat*$^{tm2(cre)Lowl}$*/J (also referred to as ChAT-IRES-Cre*) knock-in mice, purchased from The Jackson Laboratory as well.

3.1.3 Chat-EGFP/Rpl10a

The mouse strain *B6.FVB(Cg)-Tg(Chat-EGFP/Rpl10a,Slc18a3)DW167Htz/J (Chat-EGFP/Rpl10a)* was generated by *Paul Greengard and Nathaniel Heintz*[269] and purchased from The Jackson Laboratory, USA,

3.1.4 miR~17/92$^{\Delta 92}$

The *B6.Cg-Mir92-1*$^{tm1.1Aven}$*/J (miR~17/9*$^{2\Delta 92}$) knockout mouse strain was created by *Yoon-Chi*[232] and purchased from The Jackson Laboratory, USA.

3.2 Genotyping

Mouse tail biopsies were taken by the Animal Facility at the UKE prior to weaning. The tails were lysed in 50 µl QuickExtract™ DNA Extraction Solution at 65°C for 6 minutes at 500 rpm, followed by a second heating step at 98°C for 2 minutes at 350 rpm in a Thermomixer to extract genomic DNA. 2 µl of DNA template per reaction was mixed with a polymerase chain reaction (PCR) mix and replicated by the indicated conditions in a Thermal Cycler. 3% Agarose gels were prepared in 1X TAE buffer and cooked for 2 minutes until the agarose completely dissolved. Roti®-Safe GelStain was added to the agarose solution (1:500) and finally filled into gel chambers for approximately 45 minutes until the agarose polymerized. 6 µl DNA GeneRuler 1 kb DNA Ladder and 20 µl amplified PCR sample were pipetted into the gel pockets and the gel was run at 150–180 (mV) for ~20 minutes. The PCR product sizes (gel bands) of the respective genotypes were recorded by a Gel-documentation, analyzed by Adobe Photoshop CS6 and the genotypes entered into TBase Client 4Dv12sql.

3.2.1 Chat-IRES-Cre x R26-LSL-tAGO2

Chat-IRES-Cre

First, 23 µl PCR Mix per sample was generated containing 16.03 µl Nuclease-Free H_2O, 2.5 µl DreamTaq™ Hot Start Green PCR Master Mix (10X), 0.5 µl dNTPs (10 mM), 1 µl of each Cre primer (forward primer, TAA CAT TCT CCC ACC GCT AGT ACG; reverse primer, AAA CGT TGA TGC CGG TGA ACG TGC), 0.9 µl of each β-actin primer (forward primer, AGA GGG AAA TCG TGC GTG AC; reverse primer, CAA TAG TGA TGA CCT GGC CGT) and finally 0.17 µl DreamTaq™ Hot Start Green DNA Polymerase. Subsequently, the DNA template was added and the PCR was run in a thermal cycler at following conditions. 94°C for 2 minutes to activate the hot-start DNA polymerase activity, 35 cycles at 94°C for 30 seconds for denaturation of double-stranded templates or primer, 58°C for 30 second to anneal the primer and 72°C for 30 seconds to elongate the DNA templates. The PCR was stopped with a final incubation step at 72°C for 5 minutes to promote complete synthesis of all products and finally cooled down to 15°C. The PCR resulted in DNA fragments of a size of 214 base pairs (bp) (Cre) and 150 bp (β-actin).

R26-LSL-tAGO2

First, 23 µl PCR Mix per sample was generated containing 16.7 µl Nuclease-Free H_2O, 2.5 µl DreamTaq™ Hot Start Green PCR Master Mix (10X), 0.5 µl dNTPs (10 mM), 1 µl of each tAGO2 primer (forward primer, CCA AAG TCG CTC TGA GTT GTT ATC; reverse primer one, GAG CGG

GAG AAA TGG ATA TG; reverse primer two, CGG GCC ATT TAC CGT AAG), and finally 0.3 µl DreamTaq™ Hot Start Green DNA Polymerase. Subsequently, the DNA was added and PCR was run in a thermal cycler at the following conditions. 95°C for 10 minutes, 40 cycles starting with 94°C for 30 seconds, 66°C for 60 seconds (with – 0.5 °C gradual annealing per cycle) and 72°C for 30 seconds. The PCR was stopped at 72°C (10 minutes) and cooled down to 15°C. The PCR resulted in products of a size of 604 bp (*C57BL/6J*) and 300 bp (tAGO2).

3.2.2 Chat-EGFP/Rpl10a

First, 23 µl PCR Mix per sample was generated containing 16.03 µl Nuclease-Free H_2O, 2.5 µl DreamTaq™ Hot Start Green PCR Master Mix (10X), 0.5 µl dNTPs (10 mM), 0.9 µl of each eGFP primer (forward primer, CGG CGA GCT GCA CGC TGC CGT CCT C; reverse primer, CCT ACG GCG TGC AGT GC TTC AGC), 1 µl of each β-actin primer (forward primer, AGA GGG AAA TCG TGC GTG AC; reverse primer, CAA TAG TGA TGA CCT GGC CGT) and finally 0.17 µl DreamTaq™ Hot Start Green DNA Polymerase. Subsequently, the DNA template was added and PCR was run in a thermal cycler at following conditions. 94°C for 2 minutes, 38 cycles at 94°C for 30 seconds, 64°C for 30 seconds and 72°C for 30 seconds. The PCR was stopped at 72°C (5 minutes) and cooled down to 4°C. The PCR resulted in products of a size of 350 bp (eGFP) and 150 bp (β-actin).

3.2.3 miR~17/92$^{\Delta 92}$

First, 23 µl PCR Mix per sample was generated containing 15.5 µl Nuclease-Free H_2O, 2.5 µl Maxima™ Hot Start PCR Master Mix (2X), 2 µl $MgCl_2$ (5 mM), 0.55 µl dNTPs (10 mM), 1.1 µl of each primer (forward primer, GTG CTT ATA GTG CAG GTA GTG TGT; reverse primer, CAC TCC ATC AGC TCG TGA AC) and finally 0.25 µl Maxima™ Hot Start Taq DNA-Polymerase. Subsequently, the DNA was added and PCR was run in a thermal cycler at following conditions. 94°C for 2 minutes, 10 cycles at 94°C for 20 seconds, 65°C for 15 seconds (with – 0.5 °C gradual annealing per cycle) and 68°C for 10 seconds. This was followed by 30 cycles at 94°C for 15 seconds, 60°C for 15 seconds and 72°C for 10 seconds. The PCR was ended with a last reaction at 72°C for 2 minutes and cooled down to 10°C. This resulted in PCR products of a size of 408 bp (*C57BL/6J*) and 310 bp (*miR~17/92$^{\Delta 92}$*).

3.3 Immunohistochemistry

3.3.1 Perfusion

Mice were intraperitoneally (i.p.) anesthetized with an overdose (15 µl/g bodyweight) of Ketamine/Xylazine (12 mg ml^{-1}/1.6 mg ml^{-1}) in 1X PBS. After 5–15 minutes the toe reflexes were tested. After surgical tolerance was obtained, the thorax and diaphragm were opened in order to reveal the heart. A 25G butterfly cannula was connected to a perfusion system and inserted into the left ventricle without puncturing the right ventricle. To finally enable perfusion of the whole blood circulation the left atrium was opened and perfusion was started with 1X PBS (3 minutes, ~10 ml) to eliminate the blood and thereafter with 4% paraformaldehyde (PFA) for 7 minutes (~24 ml) to cross-fix the tissue. Subsequently, the spinal cord was dissected and post-fixated in 4% PFA for 30 minutes.

3.3.2 Tissue preparation

The PFA-fixated spinal cord tissue was dehydrated and cryo-protected in 30% sucrose solution in 1X PBS for at least 1–2 days at 4°C, then frozen in embedding solution (Tissue-Tek® O.C.T.™ compound) and finally cut into 12 µm thick transversal cryosections by a cryostat. The slices were stored at –80°C.

3.3.3 Staining procedure

The cryoslices were air dried and surrounded with a thin line of liquid blocker, which was dried for another approximately 15 minutes. All staining steps were carried out at room temperature (RT), except for the incubation with the primary antibody. The slices were washed in 1X PBS (5 minutes), followed by an incubation of 10% normal donkey serum (NDS) in 0.1% Triton X-100 in 1X PBS (PBS-T) for 45 minutes, in order to permeabilize the cell membrane to allow penetrance of the antibodies and to block potential unspecific binding sites. The slices were washed in 1X PBS and the primary antibody (see Table 10) was incubated in 1X PBS at in a humidified slide staining system) overnight. The next day the slices were washed three times in 1X PBS and finally incubated with the fluorophore-labelled secondary antibody (see Table 11) for 2.5 hours in the humidified chamber. Thereafter, slices were washed three times in 1X PBS, once in ddH_2O, air dried and finally embedded with Cover Glasses in mounting medium containing DAPI. The freshly mounted sliced were dried at room temperature for 2 hours and stored at 4°C. The imaging was performed with a laser scanning microscope (LSM 600, Zeiss).

3.3.4 Image analysis

All images were analyzed by *ImageJ* (https://imagej.nih.gov/ij/). The specimens were always recorded as a z-stack covering the thickness (~12 µm) of the complete slice. Cell counting was performed manually (Cell counter plugin), whereas counting of particles was executed with a counting mask (Analyze Particles command). Therefore, the confocal images were converted to 8-bit images, background fluorescence was subtracted and the pictures were smoothened. A defined threshold was set to finally convert the pictures into black and white. The watershed function was applied additionally to segment overlaying objects. All adjustments were established for each staining individually in order to ensure the best sensitivity and specificity. The cell and particle counts were finally normalized to the recorded area. The data visualization and statistics were performed by Prism8. The data are presented as mean values ± the standard error of the mean (SEM.). Differences between the examined groups were determined by Kruskal–Wallis test (uncorrected Dunn's test), $*P < 0.05$, $**P < 0.01$.

3.4 Quantitative real-time polymerase chain reaction

3.4.1 Sample preparation

In order to allow quantitative real-time polymerase chain reaction (qRT-PCR) analysis of miRNAs and mRNAs, the samples were lysed and the nucleic acids isolated according to the sample material (primary cells or tissue). cDNA transcription and qRT-PCR were sequentially performed for miRNAs and mRNAs. The total RNA content was measured by a spectrophotometer (NanoDrop, Thermo Fisher Scientific).

Primary cells

Primary cortical neurons were grown in 6-well plates at a density of 80,000 cells per cm^2 and harvested at day in vitro (DIV) 14. The cells were detached from the cell culture dish surface by two consecutive rounds of scraping (Cell scrapers) in 1 ml ice-cold 1X DPBS after two immediate washes in 2 ml 1X DPBS each. The cells were centrifuged at 3500 × g for 5 minutes, the supernatant was removed, the cell pellets snap-frozen in liquid nitrogen and finally stored at –80°C. For RNA isolation, the pellets were lysed in 350 µl RLT buffer (RNeasy® Mini Kit) containing β-mercaptoethanol (1:00) by gently pipetting up and down for ~10 times and subsequently homogenized by QIAshredder™ columns. The flow-through was finally RNA-purified with silica-gel membrane containing spin-columns (RNeasy® Mini Kit) according to the manufacturer's protocol. The RNA was eluted in 30 µl DEPC-treated H_2O and stored at –80°C.

Tissue

Mice were anesthetized and perfused with 1X PBS as described above. The brain and spinal cord were removed as well as the spleen and the lymph nodes (superficial cervical, para-aortic, axillary, brachia, inguinal[270]). 20 mg of each tissue was lysed in RLT lysis buffer (RNeasy® Mini Kit) containing β-mercaptoethanol (1:100) in a homogenizer vessel. RNA was purified from the homogenate by silica-gel membrane containing spin-columns (RNeasy® Mini Kit) according to the manufacturer's protocol. The RNA was finally eluted in 30 µl DEPC-treated H_2O and stored at –80°C.

3.4.2 miRNA qRT-PCR

miRNAs were reverse transcribed into cDNA for qRT-PCR analysis with two different protocols, pursuant to technical facilitation. According to the reverse transcription protocol utilized, different qRT-PCR probes were used. Either a miRNA-specific protocol was performed, which allowed detection of snoRNAs to normalize miRNA expression or a universal transcription protocol, which enabled detection of miRNAs exclusively. A specific probe against miR-92a-3p did not exist for the more recent and less laborious reverse transcription protocol, therefore the miRNA-specific protocol had to be used.

miRNA-specific transcription

miRNAs were reverse transcribed by the TaqMan® MicroRNA Reverse Transcription Kit and detected with TaqMan® MicroRNA Assays, consisting of a stem-looped primer for reverse transcription and sequence specific primer for quantification by qRT-PCR. For cDNA transcription, a single RT reaction mix was prepared for each sample and each miRNA or miRNA control. For each reaction, 10 ng of total RNA were reverse transcribed by MultiScribe™ Reverse Transcriptase (50 U μl^{-1}) with specific 5X RT primer according to the manufacturer's protocol. The RT product was stored at –20°C.

The qRT-PCR reaction mix was prepared with miRNA specific 20X TaqMan® MicroRNA Assays in DEPC-treated water (Invitrogen™) and TaqMan® Universal PCR Master Mix II (2X) with Uracil-N-glycosylase (UNG) according to the manufacturer's protocol. qRT-PCR reaction plates (384-well or 96-well plates) were prepared with 18.8 µl per well of qRT-PCR reaction mix. qRT-PCR was always performed in triplicates for each sample and each miRNA. In each well 1.2 µl cDNA per well was added and the qRT-PCR was run on ABI Prism 7900 HT Fast Real-Time PCR System or The Applied Biosystems™ QuantStudio™ 6 Flex Real-Time PCR System according to the comparative C_T ($\Delta\Delta C_T$) run mode. The thermal conditions were an initial 2–minute step at

50°C to activate UNG-enzyme activity followed by a 10–minute deactivation of UNG and activation of the AmpliTaq Gold™ DNA Polymerase (hot-start polymerase) at 95°C. Following, denaturation of double-stranded DNA templates was performed for 15 seconds at 95°C and primer annealing and extension was attained for 60 seconds at 60°C. The last two steps were repeated for 40 cycles.

Universal miRNA transcription

miRNAs were universally reverse transcribed by the TaqMan® Advanced cDNA synthesis Kit and detected with specific TaqMan® Advances miRNA Assays for quantification by qRT-PCR. For each sample, 10 ng of total RNA were reverse transcribed and amplified according to the manufacturer's protocol. The RT and miR-Amp product were stored at –20°C.

The qRT-PCR reaction mix was prepared with miRNA specific 20X TaqMan® Advances miRNA Assays (20X) in DEPC-treated water (Invitrogen™) and TaqMan® Fast Advanced Master Mix (2X) according to the manufacturer's protocol. qRT-PCR reaction plates (384 well) were prepared with 7.5 µl per well of qRT-PCR reaction mix. qRT-PCR was always performed in triplicates for each sample and each miRNA. In each well 2.5 µl pre-diluted (1:10) miR-Amp reaction per well was added and the qRT-PCR was run on ABI Prism 7900 HT Fast Real-Time PCR System according to the comparative C_T ($\Delta\Delta C_T$) run mode. The thermal conditions were an initial 10–minute activation of the AmpliTaq™ Fast DNA Polymerase at 95°C. Following, denaturation of double-stranded DNA templates was performed for 3 seconds at 95°C and primer annealing and extension was attained for 30 seconds at 60°C. The last two steps were repeated for 40 cycles.

3.4.3 mRNA qRT-PCR

mRNAs were reverse transcribed with the High-Capacity RNA-to-cDNA™ Kit and qRT-PCR was performed with respective TaqMan® Gene Expression Assays. For each sample, 80 ng of total RNA was universally reverse transcribed by a 20X RT Enzyme Mix (MultiScribe™) and a 2X RT Buffer Mix with oligo d(T)16 and random octamer primer in DEPC-treated H_2O according to the manufacturer's protocol. The RT product was stored at –20°C.

The qRT-PCR reaction mix was prepared with gene specific 20X FAM™ dye-labeled TaqMan® MGB probes with two unlabeled PCR primer (TaqMan® Gene Expression Assays) and 2X TaqMan™ Gene Expression Master Mix according to the manufacturer's protocol. qRT-PCR reaction plates (384-well or 96-well plates) were prepared with 8 µl qRT-PCR reaction mix per well. qRT-PCR was always performed in triplicates for each sample and each gene. In each well 2 µl cDNA was added and the qRT-PCR was run as described for miRNAs above.

3.4.4 qRT-PCR analysis

Analysis was performed with the appropriate software being SDS v2.4.1 and RQ Manager v1.2 or QuantStudio™ v1.3, respectively. miRNA expression was normalized to the small nucleolar RNA (snoRNA) sno234[271], miR-16[272] or miR-384 (from own data) and mRNA expression was normalized to the housekeeping gene Tbp[273]. The quantification of miRNA or mRNA was performed according to $2^{-\Delta\Delta CT}$, respectively. The mean C_T value of the triplicates for each miRNA or gene of each sample was calculated. The data visualization and statistics were performed by Prism8. The data are presented as box-plot whiskers from minimal to maximal value with all points shown. Differences between the examined groups were determined by Kruskal–Wallis test (uncorrected Dunn's test), $*P < 0.05$, $**P < 0.01$. Outliers were identified by ROUT outlier identification (Q = 10%).

3.5 Experimental autoimmune encephalomyelitis

3.5.1 Immunization

The multiple sclerosis mouse model experimental autoimmune encephalomyelitis was actively induced in mice with a *C57BL/6J* genetic background[82]. For this purpose, a 1:1 emulsion of myelin oligodendrocyte protein ($MOG_{35–55}$, MEV GWY RSP FSR VVH LYR NGK), diluted in 1X PBS (2 mg ml^{-1}) was homogenized for 10 minutes with Complete Freund's Adjuvant (CFA, containing 2 mg ml^{-1} M. tuberculosis) in two interconnected 3 ml Syringes. Adult mice (8–14 weeks of age) were subcutaneously (s.c.) injected with 100 µl of the $MOG_{35–55}$/CFA emulsion (200 µg per animal) into the left and right hind flank each. These injections were followed by either an intravenous (i.v.; tail vein; early and phenotypic experiments) or intraperitoneal (i.p.) injection of 100 µl pertussis toxin (PTX), solved in H_2O and diluted in 1X PBS (200 ng per animal). Two days later the PTX injection was repeated.

3.5.2 Clinical scoring

The EAE-induced animals were handled according to TVA Nr. 17–122. Mice were weighted and scored at the day of immunization, at day 2 after immunization and from day 6 on every day. The animals were supplied with food and water ad libitum and additionally provided with softened food pellets and DietGel® Recovery gel in order to overcome dehydration and diminish weight loss. Where applicable, skin irritations and infected injection sides were provided with Nekrolyt®. Animals with EAE score ≥ 4 or ≥ –25% body weight (from starting weight) were euthanized according to the regulation of the Animal Welfare Act. Clinical disability was assessed as a 5–score scale (0, no clinical symptoms; 1, paresis of the tail; 2, paresis of the hind limbs; 3, partial

paralysis of the hind limbs; 3.5, paralysis of the hind limbs; 4, paralysis of the hind limbs and paresis of the front limbs; 5, pre–morbidity or death). All symptoms were assed in 0.25 steps if required – beginning from 0.5 and ending at 5 – in order to reach a higher sensitivity of scoring clinical disability.

3.5.3 Statistical analysis of EAE clinical scores

The data visualization and statistics were performed by Prism8. The weight and EAE score were presented as mean values ± the standard error of the mean (SEM) per day. Animals with no disease symptoms, symptoms ≤ 0.5 and disease onset ≥ day 17 post immunization were excluded from the analysis. For statistical analysis of the EAE clinical course between two genotypes, the mean score of disease onset (mean disease onset of both groups) per animal was compared by two-tailed Mann–Whitney test, $*P < 0.05$, $**P < 0.01$.

3.6 miRNA tagging and affinity-purification

3.6.1 Tissue preparation

For miRNA tagging and affinity-purification (miRAP) mice were anesthetized and perfused with dissection buffer for 1 minute as described above. The cervical spinal cord of three animals were dissected (~0.7 cm) and homogenized in 1 ml lysis buffer in a glass homogenizer vessel with ~12 strokes. The homogenate was centrifuged for 10 minutes at 2000 × g at 4°C, the supernatant (800 µl) mixed with 100 µl NP-40 (10%) and 100 µl DHPC (300 mM) and incubated for 5 minutes on ice. After a 10–minute centrifugation at 20.000 × g at 4°C the supernatant was further processed to either isolate miRNAs directly (100 µl) or purify GFP-AGO2 by immunoprecipitation (IP) first, to obtain cell-type specific miRNAs (~800 µl).

3.6.2 miRNA purification procedure

miRNA tagging and affinity-purification (miRAP)[218] was applied in order to immunopurify cell-type specific miRNAs. The protocol was technically modified to achieve the highest comparability with the translating ribosome affinity-purification (TRAP)[274] method. Every step was carried out on RNaseZap™ cleaned laboratory workbenches and RNase and DNase free consumables.

Bead preparation

Magnetic bead preparation was performed in a DynaMag™ magnetic rack on ice. The magnetic beads were coupled to two different clones of monoclonal α-GFP antibodies (MSKCC, Antibody & Bioresource Core Facility) in a two–step way. Every step was carried out in Nonstick, RNase-

free Microfuge Tubes. Per IP 300 µl Dynabeads™ MyOne™ Streptavidin T1 were resuspended and washed with 1X DPBS. Subsequently, the beads were incubated with 120 µl Pierce™ recombinant biotinylated Protein L for 35 minutes while rotating. The protein L coated beads were blocked in 5 consecutive washing steps with 3% bovine serum albumin (BSA) in 1XPBS. The beads were resuspended in 1 ml 0.15 M KCl buffer containing 50 µG rabbit α-GFP antibody (19C8) and 50 µg rabbit α-GFP antibody (19F7) and incubated for 1 hour while rotating. The GFP-coupled beads were washed in 0.15 M KCl buffer three times and finally resuspended in 200 µl 0.15 M KCl buffer and stored on ice until the IP. In order to diminish technical deviations, the beads prepared for different IPs were first pooled and then spitted again.

Immunopurification

The GFP-coupled magnetic beads were resuspended, mixed with the purified spinal cord homogenate and incubated with gentle end over end rotation at 4°C overnight. The next day, the beads were washed in 0.35 M KCl buffer for four times. Subsequently, the IP and the non-immunopurified spinal cord lysate were resuspended in 700 µl QIAzol lysis reagent in order to isolate miRNAs.

miRNA isolation

The QIAzol lysates were incubated at RT for 5 minutes, vigorously shaken with 140 µl Chloroform for 15 seconds and incubated for another 3 minutes. After centrifugation at 12.000 × g for 15 minutes at 4°C the upper colorless phase was carefully removed without contamination of the other phases, mixed with 1.5 volumes of ~100% ethanol and pipetted onto RNeasy MinElute Spin columns (miRNeasy® Micro Kit). The purification of miRNAs followed according to the manufacturer's protocol. miRNAs were eluted in 14 µl RNase-free water and stored at –80°C.

3.6.3 miRNA-sequencing

Small RNA Sequencing was performed by the *Transcriptome and Genome Analysis Laboratory*, Göttingen. In total, four groups with five bio replicates each were sequenced. The spinal cord (SC) and the motor neuronal fraction (MN) form healthy animals as well as the inflamed spinal cord (iSC) and inflamed motor neuronal fraction (iMN) form EAE-induced mice. The small RNA sequencing libraries were prepared by the TruSeq Small RNA Library Prep Kit (Illumina). The libraries were pooled and sequenced on an Illumina HiSeq 4000, creating 50 base pair single-end reads.

3.6.4 miRNA-sequencing analysis

The raw read sequences (FASTQ files) were adaptor trimmed, cleaned, aligned and counted by *OASIS 2.0*[275] (by *Transcriptome Analysis Laboratory*, Göttingen). The following analyses were performed by *Dr. Dr. Jan Broder Engler*. Most of the analyses were performed in the *R environment (v.3.3.2)* using publicly available packages. The overall quality control of the samples and subsequent differential expression analysis was constructed with the R package *DESeq2*[276] based on negative binomial generalized linear models (fold change > 1.5, FDR-adjusted $P < 0.05$, minimal count ≥ 20). The principal component analysis (PCA) was generated from expression values after variance stabilizing transformation using the top 500 most variable miRNAs. Gene expression heatmaps were generated from normalized expression values using the R package *'pheatmap'* (v.1.0.8). All plotting was done using the R package *'ggplot2'* (v.2.2.1). The graphs were further processed with *Illustrator CS6*.

Target candidates of all miRNAs were computationally predicted with *TargetScanMouse 7.2*[179] (cumulative weighted context++ score (CWCS) < –0.4) and subsequently compared to the downregulated candidate mRNAs in inflamed motor neurons (TRAP, 3.7). The network diagram of the miRNA candidates and their target genes was constructed using the R packages *'network'* and *'ggnetwork'*. For overrepresentation analysis, hypergeometrical testing (FDR-adjusted $P < 0.05$) in the R environment was used.

Target candidates of miR-92a-3p were determined by analyzing all predicted targets (*TargetScanMouse 7.2*), significantly downregulated candidate genes in inflamed motor neurons and significantly downregulated candidate genes caused by miR-92a-3p overexpression (dataset from *Atsushi Sakai*[231]). These genes were visualized by a color-coded hairball graph, which was constructed using the R packages *'network'* and *'ggnetwork'*.

Gene list enrichment analyses were performed by *ToppGene Suite*[277] with default parameters. Enrichment maps[278] summarizing overlapping gene sets into interconnected clusters where each node represents a significantly regulated gene set, were constructed using the R packages *'tidygraph'* and *'ggraph'*. To increase legibility, highly interconnected gene ontology (GO) terms that gave no additional biological insight with regard to their child terms were summarized and single nodes that gave no additional biological insight not annotated.

3.7 Translating ribosome affinity-purification

3.7.1 Tissue preparation

For translating ribosome affinity-purification (TRAP) the preparation of the tissue was performed according to miRAP.

3.7.2 mRNA purification procedure

To isolate mRNAs in a cell-type specific manner TRAP[274] was performed. The bead preparation and immunopurification was performed as described for miRAP. Here, the IP and the non-immunopurified spinal cord lysate were resuspended in 800 µl TRIzol™ lysis reagent.

mRNA isolation

The TRIzol™ lysates were incubated at RT for 5 minutes, vigorously shaken with 200 µl Chloroform for 15 seconds and incubated for another 3 minutes. After centrifugation at 12.000 × g for 15 minutes at 4°C the upper colorless phase was carefully removed without contamination of the other phases, mixed with 3 M sodium acetate (1:10), an equal volume 2-Propanol, 5 µl of GlycoBlue™ Coprecipitant and finally incubated at –80°C overnight. The next day pelletizing was achieved by a 15–minute centrifugation at 15.000 × g for 15 minutes. The pellet was carefully washed two times with ice-cold 70% ethanol and finally dried for ~15 minutes. After resuspension in 100 µl RNase-free water the IP and the non-immunopurified sample were mixed with 350 µl RLT buffer with β-mercaptoethanol (RNeasy® Micro Kit), 250 µl of 100% ethanol each and pipetted onto RNeasy MinElute Spin columns (RNeasy® Micro Kit). The purification of total RNA followed according to the manufacturer's protocol. The RNA was eluted in 14 µl RNase-free water and stored at –80°C.

3.7.3 mRNA-sequencing

Sequencing of total RNA was performed by the *Transcriptome and Genome Analysis Laboratory*, Göttingen. In total, four groups with five bio replicates each were sequenced and named like for miRAP. The RNA sequencing libraries were manually prepared by the NEBNext Ultra RNA Library Prep Kit for Illumina (New England Biolabs) with minor modifications in ligation and amplification. The libraries were pooled and sequenced on an Illumina HiSeq 4000, creating 50 base pair single-end reads.

3.7.4 mRNA-sequencing analysis

The bioinformatic analysis of the RNA sequencing was performed by *Dr. Dr. Jan Broder Engler* as described previously[273]. Most of the following analyses were performed in the *R environment (v.3.3.2)* using publicly available packages. The reads were aligned to *the Ensemble mouse reference genome (mm10)* using *STAR v.2.4*[279] with default parameters, overlap with annotated gene loci was counted *with featureCounts v.1.5.1*[280] and differential gene expression was analyzed with the R package *DESeq2*[276] (fold change > 1.5, FDR-adjusted $P < 0.05$).

3.8 Cell culture

3.8.1 Primary neuronal cultures

Primary cortical mouse neurons were prepared from *C57BL/6J* prenatal mice at gestational day E16.5[281] in a semi-sterile environment with sterile dissecting instruments. After dissection of the embryonal cortices, every step was performed at sterile conditions under a laminar flow hood. Prior to preparation of cortical neurons 6-well cell culture plates were pre-coated with 10 mg ml^{-1} poly-D-lysine solution in 1X DPBS at 37°C overnight and washed two times in 1X DPBS and once in ddH_2O.

First, the pregnant mouse was anesthetized with CO_2/O_2 and subsequently decapitated. The abdomen was rinsed with 70% ethanol and the abdominal wall opened to reveal the body cavity. The uterine horns were lifted out of the cavity and removed by cutting along the mesometrium. The embryos were released by dissecting the uterus and removing the embryo sacs. The embryos were decapitated in a new cell culture dish containing 1X HBSS and the brains carefully removed. Subsequently, the hemispheres were separated, the meninges removed and the cortices dissected under a binocular. The cortices were collected in a 15 ml polypropylene tube in 1X HBSS, washed and trypsinized in 1 ml 0.05% Trypsin/EDTA solution for 6 minutes at 37°C. Subsequently, the trypsinization was stopped by adding 6 ml of DMEM/F-12 supplemented with 10% FCS and gentle mixing. After a 2-minute centrifugation at 600 × g, the medium was aspirated and the cortices finally dissociated in 1 ml plating medium by gently pipetting up and down for ~10 times each with first a 1000 µl filter tip and a narrowed Pasteur pipette afterwards. The homogenous cell suspension was filtered by using a 40 µm cell strainer and subsequently counted in a Neubauer cell counting chamber in a 1:1 trypan blue solution (0.4%). 80,000 cells per cm^2 were plated in plating medium. After 4–6 hours the medium was completely exchanged to wash off non-attached, dead cells and tissue remnants. The next day, 1 µM cytosine arabinoside (AraC) was added. 50% of the medium was exchanged every 4–5 days with pre-

warmed feeding medium. The cortical cells were cultured for 14 days in vitro in a cell culture incubator at 37°C and 5% CO_2.

3.8.2 Cell lines

The neuroblastoma cell line Neuro-2A (N2a) was purchased from ATTC Manufacturing. Mycoplasma-free N2a cells (tested by *Nina Kursave*) were cultured in filter cap cell culture flasks containing N2a medium. Cells were passaged when 80–85% confluence was obtained. For this purpose, N2a cells were quickly washed two times in ice-cold 1X DPBS and subsequently detached from the cell culture flask surface by incubation in 1 ml TrypLE™ at 37°C. The cells were collected and resuspended in 4 ml N2a medium and cultured in a new cell culture flask until passage 25–30. For experiments, µCLEAR® white 96-well cell culture plates were coated with 10 mg ml^{-1} poly-D-lysine solution in 1X DPBS at 37°C overnight and subsequently washed two times with 1X DPBS and one with ddH_2O. N2a cells were detached as described and counted in a Neubauer cell counting chamber as before. Finally, 44,117 cells per cm^2 plated in N2a medium for 1–2 days.

3.8.3 Neuronal stress assay

The stress assays were performed with primary cortical neurons at DIV 13. The cells were chronically stimulated for 24 hours. Therefore, 50% of the preconditioned cell culture well medium (1.5 ml) was removed and filtered by a 20 µm cell strainer. The medium was pipetted back into the 6-well plate containing TNF-α, IFN-γ or IL-1β (100 ng ml^{-1}) or glutamate (1 µM, 5 µM, 10 µM and 20 µM). Subsequently, the neurons were quickly washed two times in ice-cold 1X DPBS and subsequently detached from the cell culture plate surface (cell scrapers) in 1.5 ml ice-cold 1X DPBS. The neurons were pelleted by a 5–minute centrifugation for 3500 × g at 4°C. The 1X DPBS was aspirated and the neuronal cell pellets snap frozen in liquid nitrogen and stored at –80°C. Finally, the RNA was purified as described above (Methods, 3.4.1).

3.9 miRNA target gene luciferase reporter assay

3.9.1 Plasmids

The miRNA target gene luciferase reporter assay plasmids (miTarget™ 3' UTR miRNA Target Clones) were purchased from GeneCopoeia. A control vector and a reporter vector were used. The assay vectors (pEZX) consisted of a firefly gene under the control of a SV40 promotor and a renilla luciferase gene under control of a CMV promotor to control for transfection efficiency. The

full length Cpeb3 3' UTR was cloned into the firefly 3' UTR of the reporter vector, whereas the control vector had no exchanged 3' UTR.

3.9.2 Reporter assay procedure

N2a cells with a confluency of 80–95% were transfected with Lipofectamine 2000 according to the manufacturer's protocol in 40 µl Opti-MEM™ per well. Six wells (replicates) were transfected for each condition. Auto-luminescence was detected by applying one 'medium only' condition onto each experimental plate. N2a cells were either transfected with 150 ng of one miTarget™ 3′ UTR miRNA Target Clone or co-transfected together with 5 nM miRCURY LNA™ scrambled miRNA mimic or miRCURY LNA™ miR-92a-3p mimic, respectively. After 60 minutes, the Opti-MEM™ medium was replaced by 200 µl pre-warmed N2a medium. After two days, the Dual-Glo® Luciferase Assay System was used according to the manufacturer's protocol in order to consecutively record firefly and renilla luminescence in a luminometer.

3.9.3 Reporter assay analysis

The auto-luminescence was subtracted from firefly and renilla luminescence, respectively. Firefly luminescence was normalized to renilla luminescence (RluC/FluC) and the mean value of the replicates of each condition was calculated. The mean luminescence of the co-transfected replicates was normalized to the mean luminescence of the replicates transfected with plasmid only. Finally, for each plasmid the mean luminescence of miR-92a co-transfected replicates was normalized to those values of sc-miR co-transfection. Statistical significance between miR-92a and sc-miR transfection was performed by a one sample t test ($P < 0.5$).

3.10 Flow cytometry

3.10.1 Tissue preparation

Mice were induced with EAE as described above. At acute EAE (day 15 post immunization) mice were anaesthetized and perfused with 1X DPBS as described above. The brain and spinal cord were dissected, cut into small pieces and incubated in 10 ml CNS digestion solution for 60 min at 37°C in a water bath while shaking. The tissue was dissociated by 40 µm cell strainer und diluted in 1X DPBS. Subsequently, the homogenate was centrifuged at 300 × g for 10 minutes at 4°C. The supernatant was discarded and the tissue pellet was washed with 1X DPBS and centrifuged again. The immune cells were isolated from the remnant CNS tissue by a discontinuous percoll gradient. Therefore, the tissue pellet was dissolved in 4 ml percoll solution (30%). Following, 2 ml percoll solution (78%) was cautiously sub-leveled and centrifuged for 30

minutes (setting, without brakes) at 1500 × g at 4°C. The cells were isolated by carefully removing the white intermediate phase without contamination from the upper and lower phase. The cells were washed twice with 1X DPBS and the supernatant discarded. The cell pellet was dissolved in 1 ml 1X DPBS. 10% per sample was utilized to determine the absolute immune cell numbers in each CNS tissue (TruCount® Tubes). The remaining cells were used to identify different immune cell populations by sequential gating.

3.10.2 Absolute cell counting

Unspecific binding of staining antibodies by Fc receptors (CD16 and CD32) on the immune cell surface was reduced by addition of F_c block (1:1000) consisting of α-CD16/32. The cells were stained with α-CD45 (1:100) in order to identify all immune cells (20 minutes, 4°C). Afterwards, the cells were diluted in 3 volumes FACS (fluorescence-activated cell sorting) buffer and finally analyzed by flow cytometry (FC). The gating of beads and $CD45^+$ events is depicted in Results, Figure 4-12. The absolute number of cells was determined by dividing the number of beads (fixed size) by the recorded number of beads (events) and finally multiplying this value with the recorded number of $CD45^+$ events and the dilution.

3.10.3 Cell staining

Staining protocol

In order to identify the heterogenous mixture of different CNS invading and resident immune cells, the previously isolated cells were counted in a Neubauer cell counting chamber as described before and 2×10^6 cells were transferred into FACS tubes. The cells were washed in 2 ml 1X PBS, centrifuged at 350 × g for 5 minutes and subsequently resuspended in 150 µl LIVE/DEAD Fixable Dead Cell Stain solution (1:1000) in 1X PBS and incubated for 30 minutes at 4°C in the dark. The cells were washed in 3 ml 1X PBS and finally resuspended in the 100 µl staining solution in FACS buffer containing F_c block and the antibodies α-CD3ε, α-NK1.1, α-CD11b, α-CD11c, α-Ly6G, α-B220, α-CD8, α-CD45 (for concentrations see Table 12) and incubated for 30 minutes at 4°C in the dark. Subsequently, the cells were washed with 2 ml FACS buffer, followed by a 5–minute centrifugation at 350 × g. The supernatant was discarded and cells were dissolved in 150 µl Cytofix™ Fixation buffer and incubated for 20 min at room temperature in the dark. Afterwards the cells were washed in 2 ml FACS buffer and finally dissolved in 300 µl FACS buffer and stored at 4°C in the dark until FACS analysis.

Compensation

To analyze whether excitation overlap of the utilized fluorochrome-coupled-antibodies occurred, compensation control beads (α-Rat and α -Hamster Ig κ/Negative Control Compensation Particles Set) were used. Therefore, FACS tubes were filled with 25 µl of compensation beads and 75 µl FACS buffer. The dilution of antibodies applied for the cell staining was used for compensation of the emission signal as well (one tube for each antibody). After incubation for 20 min at 4°C, the compensation beads were washed in 1 ml FACS buffer, followed by a 5–minute centrifugation at 350 × g and finally resuspension in 300 µl FACS buffer.

3.10.4 FC data analysis

The acquisition of single cell events was obtained by the LSR II Flow Cytometer and events recorded by FACSDiva™ software. Further analyses and manual gatings were performed by FlowJo for Mac v10 (Results, Figure 4-12 and Figure 4-13). Statistical analysis and data visualization were performed by Prism8. Data were further processed in Adobe Illustrator CS6.

Uniform manifold approximation and projection (UMAP)

A UMAP algorithm (FlowJo plugin) was applied in order to visualize the cluster densities of different immune cell populations (identified by sequential gating) between the investigates groups. Therefore, all recorded single-cell events were concatenated to 300K events and a two-dimensional UMAP plot was constructed with default parameters. Different cell clusters were assigned according to the manually set gates by backgating.

4 Results

4.1 Profiling of neuronal miRNAs in CNS-inflammation

4.1.1 Establishment of a transgenic mouse line to study neuronal miRNAs

In order to investigate the role of neuronal miRNAs in CNS-inflammation, a genetically modified mouse line was utilized, which enabled studying miRNAs in a cell-type specific manner. For this purpose, genetic tagging of AGO protein as the functional unit of miRNAs was exploited, which allowed cell-type restricted isolation of regulatory miRNAs by immunoprecipitation (IP). The mouse line *R26-LSL-tAgo2* was generated by *Miao He* et al.[218] on a *C57BL/6J* genetic background and comprises a modified *Ago2* gene fused to a GFP- and Myc tag. The Cre/loxP binary system was utilized by inserting a floxed STOP sequence (loxP-STOP-loxP) before the tagged *Ago2* cassette into the *Gt(ROSA)26Sor (Rosa26*) locus to allow for conditional expression. To finally obtain cell-type specific expression of GFP-MYC-AGO2, a Cre recombinase driver mouse line under control of a neuron specific promotor was used. Since the spinal cord is the primarily inflamed CNS tissue in experimental autoimmune encephalomyelitis (EAE), where neuronal damage and neuronal impairment are the best correlates for clinical disability in EAE[282,283] and MS[284-286], a motor neuron specific (Chat) Cre driver line was chosen (Figure 4-1, a).

For characterization of GFP-AGO2 expression, Cre positive *ChAT-Cre × R26-LSL-tAGO2* mice and ChAT-Cre negative littermates (*R26-LSL-tAGO2*) were perfused with PFA (4%), the spinal cord was dissected and cryosections were prepared in order to co-stain motor neurons (α-ChAT antibody) and GFP-AGO2 (α-GFP antibody). GFP-AGO2 was only detected in ChAT immunoreative cells of the spinal cord from Cre positive, but not Cre negative *ChAT-Cre × R26-LSL-tAGO2* mice (Figure 4-1, b). To further analyze, if expression of GFP-AGO2 was exclusively restricted to ChAT expressing motor neurons, other cell types of the spinal cord were examined by immunohistochemistry. Neither oligodendrocytes (α-CNPase antibody), astrocytes (α-GFAP antibody), endothelial cells (α-CD31 antibody) nor microglia (α-Iba1 antibody) were detected to express GFP-AGO2 (Figure 4-1, c).

As characterization of the transgenic mouse line *ChAT-Cre* × *R26-LSL-tAGO2* showed specific expression in spinal cord motor neurons, purification of miRNAs from these cells was established by a technique called miRNA tagging and affinity-purification (miRAP)[218]. The MS mouse model EAE was induced by subcutaneous injection of $MOG_{35–55}$ peptide solved in complete Freund's adjuvant containing *M. tuberculosis* and two intravenous doses of PTX into the tail vein.

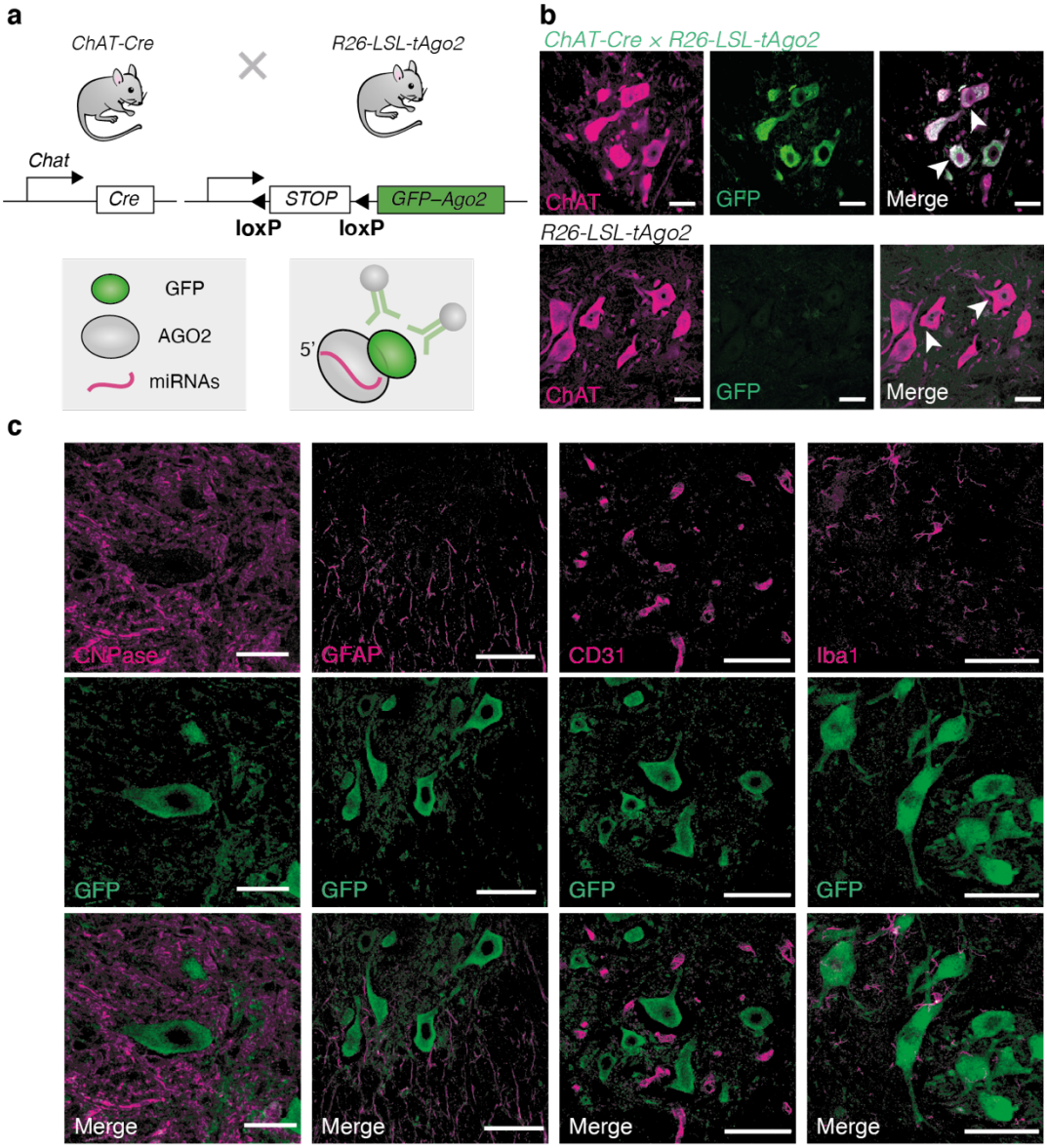

Figure 4-1 Ago-tagged Chat Cre/loxP binary system targets motor neuronal miRNAs

(a) Schematic of the mouse line used to investigate motor neuronal miRNAs. *R26-LSL-tAGO2* (GFP-MYC-AGO2 fusion protein) expression was activated in cells expressing Cre recombinase under the ChAT promotor (crossed with *ChAT-Cre* mice). (b) tAGO2 was counterstained by an α-GFP antibody and motor neurons were labelled via an α-ChAT antibody. Arrows indicate single lateral column motor neurons. Scale bar, 25 µm. (c) tAGO2 counterstaining in other cell types of the spinal cord of *ChAT-Cre* × *R26-LSL-tAGO2* mice (CNPase, oligodendrocytes; Scale bar, 25 µm. GFAP, astrocytes; CD31, endothelial cells; Iba1, microglia Scale bar, 50 µm).

For miRAP, mice were perfused with dissection buffer containing dithiothreitol (DTT) to stabilize proteins and cycloheximide (CHX) to maintain the biological state of the cell by blocking protein synthesis. The upper spinal cords of three mice were dissected and miRNAs were either purified

from lysed spinal cord (SC) directly or immunoprecipitated by α-GFP antibodies to acquire the motor neuronal (MN) miRNA (Figure 4-2, a). miRNAs were extracted by centrifugation, phenol/guanidine-based isolation and miRNA-enriching silica-membrane-based purification of total RNA. cDNA was reverse transcribed and qRT-PCR expression was normalized by miR-384-3p (Figure 4-2, b-c), which was identified here as a stable miRNA reference for healthy and inflamed SC and MN or miR-16-5p (Figure 4-2, d), which was shown to be a robust reference for miRNA qRT-PCR normalization[272]. Healthy and EAE-diseased Cre positive *ChAT-Cre* × *R26-LSL-tAGO2* mice and Cre negative littermates were used to test the sensitivity and specificity of miRAP (Figure 4-2, b–d). The fold change (FC) expression of tissue-specific miRNAs that were isolated by miRAP (MN) and miRNAs that were expressed in whole spinal cord (SC) was calculated. Motor neuronal miR-218[287] and neuronal miR-138[288] were found highly enriched in MN of healthy and EAE *ChAT-Cre* × *R26-LSL-tAGO2* mice, whereas neural miR-9[289] and hematopoietic miR-150[290] were not enriched (Figure 4-2, b–c). Further, no enrichment of any of those miRNAs was detected in Cre negative littermates (Figure 4-2, d), indicating a high specificity and sensitivity of miRAP from motor neurons.

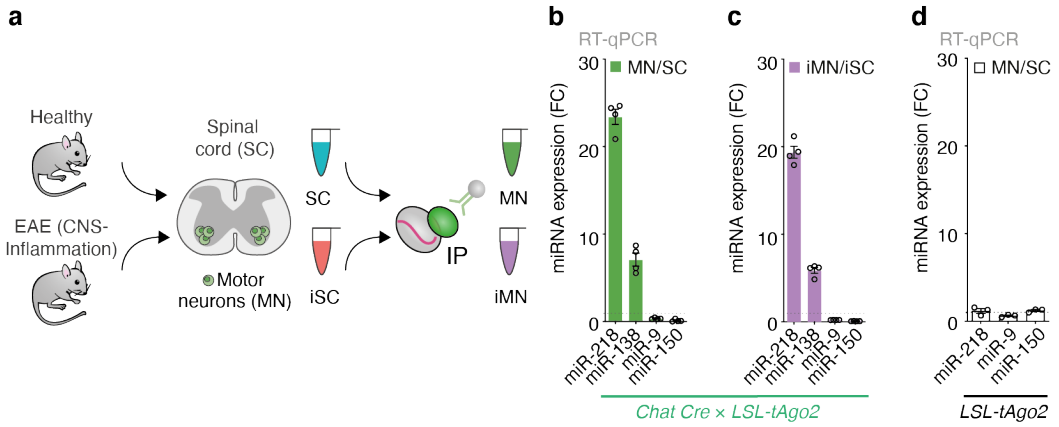

Figure 4-2 Motor neuron specific isolation of miRNAs

(a) Experimental design to identify motor neuronal miRNAs by miRNA tagging and affinity-purification (miRAP). Spinal cords of three healthy (SC) or EAE-induced mice (iSC) were either analyzed directly or processed by α-GFP-AGO2 immunoprecipitation (IP) to extract AGO2 bound motor neuronal miRNAs (MN) or (iMN), respectively. EAE was induced with $MOG_{35–55}$ in complete Freund's adjuvant containing *M. tuberculosis* and pertussis toxin. (b, c) miR-384-3p normalized expression of tissue specific miRNAs (miR-218, motor neuronal; miR-138, neuronal; miR-9, neural; miR-150, hematopoietic). IP-enrichment was calculated by fold change (FC) expression of miRNAs from MN versus SC. (d) Cre negative littermates were used as negative control. Expression data was normalized to miR-16-5p. Dotted line represents no enrichment (FC = 1).

4.1.2 Screening of neuronal miRNAs in CNS-inflammation

To elucidate whether CNS-inflammation impacts on neuronal gene expression by regulatory miRNAs, the healthy and inflamed miRNome was compared. Therefore, miRNAs were purified by the miRAP technique from healthy and EAE-induced mice and subsequently analyzed by small RNA sequencing on an Illumina HiSeq 4000 Analyzer. The samples (n = 5 per group) were prepared from healthy and inflamed spinal cord at acute EAE day 12 post immunization form *ChAT-Cre × R26-LSL-tAGO2* mice (Figure 4-3, a). Raw read sequences were adaptor trimmed, cleaned and aligned with *OASIS 2.0* (sequencing and analysis performed by *Transcriptome Analysis Laboratory,* Göttingen). The overall quality control of the samples and subsequent differential expression analysis was constructed with the R package *DESeq2* based on negative binomial generalized linear models (fold change > 1.5, FDR-adjusted $P < 0.05$, minimal count ≥ 20; analysis performed by *Dr. Dr. Jan Broder Engler*). Spinal cord miRNAs and motor neuronal miRNAs were both explored (Figure 4-3, b). In a PCA analysis biological replicates nicely clustered according to their experimental group (Figure 4-3, c), indicating a high consistency and robustness of the acquired data. As shown in Figure 4-3 d, miRAP led to successful isolation of motor neuron specific miRNAs relative to the spinal cord in both, healthy and inflamed conditions. The initial screening experiment was repeated in a second cohort (n = 4 per group), which validated 22 differentially expressed miRNA candidates in inflamed motor neurons (Figure 4-3, e). Intriguingly, all 22 miRNA candidates were upregulated by inflammation (Figure 4-3, f). Four miRNAs, namely miR-92a-3p, miR-21a-5p, miR-146b-5p and miR-143-3p showed a high expression in motor neurons even without inflammation, whereas the other candidates were all induced from either low or undetectable expression (Figure 4-3, g–h). In both data sets, the most significant induction upon CNS-inflammation among these four miRNAs was miR-92a-3p, implying an important functional role in healthy as well as inflamed motor neurons (Figure 4-3, g–h). Together, these results indicate that a strong neuronal stimulus like CNS-inflammation rather leads to induction of several regulatory miRNAs than to their repression.

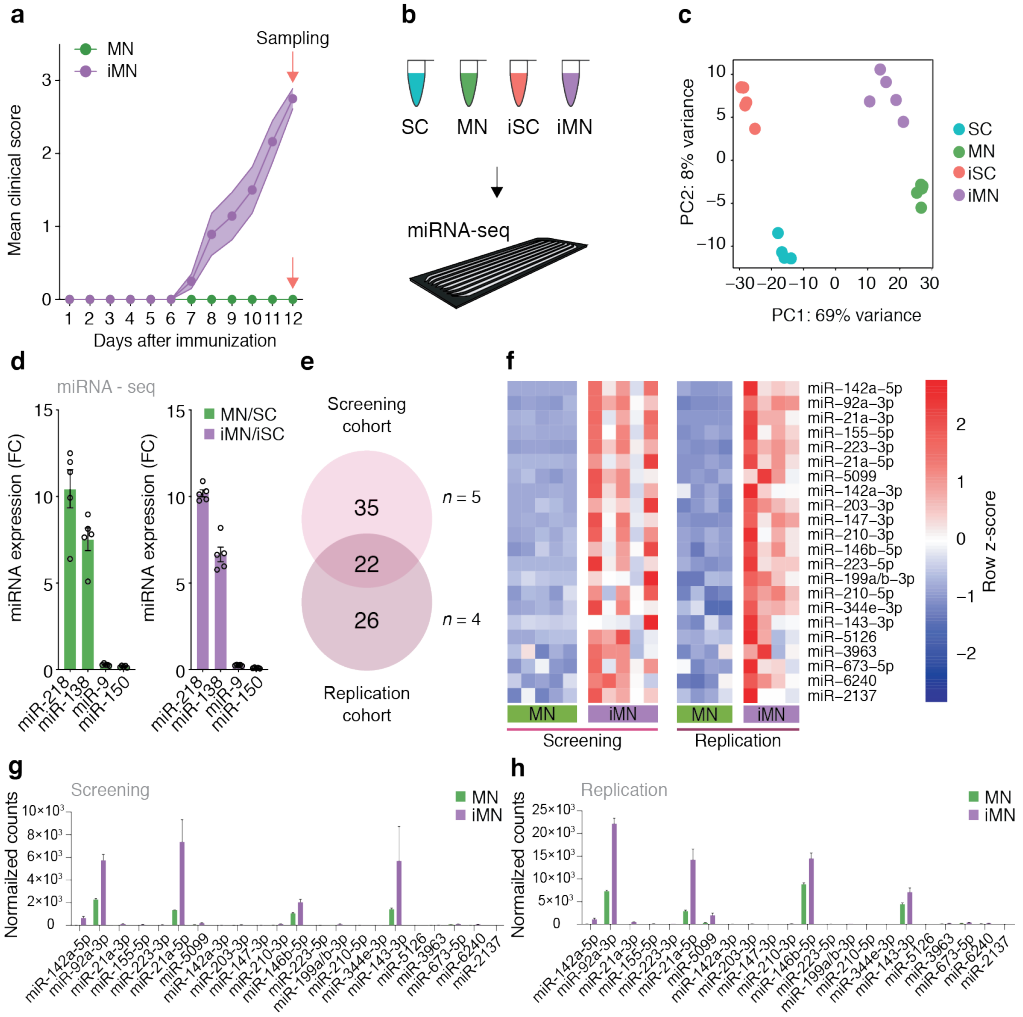

Figure 4-3 CNS-inflammation induces neuronal miRNAs

(a, b) miRAP was utilized to identify differentially expressed miRNAs in inflamed motor neurons. Samples were harvested in acute EAE (day 12 ± 1, indicated by red arrows) and sequenced on an Illumina HiSeq 4000 Analyzer. (c) Sequencing data were analyzed based on negative binomial generalized linear models (*R package DESeq2*). PCA plot shows the first two principal components of the 20 sequenced samples. (d) IP-enrichment (FC MN/SC, iMN/iSC) of tissue specific miRNAs from normalized count data as quality control. (e) Biological validation (n = 4 per group) of the screening data (n = per group). 22 miRNAs were robustly upregulated in both cohorts. (f) Heat map displays row z-score normalized expression data of the 22 miRNA candidates. Fold change > 1.5, adjusted for multiple comparison by FDR (P < 0.05). Minimal counts ≥ 20. (g, h) Bar plots display normalized read counts of the small RNA sequencing form the screening and validation experiment, respectively.

4.2 Profiling of gene regulatory networks in CNS-inflammation

4.2.1 Screening of neuronal miRNA–mRNA networks

To explore the potential impact of the identified deregulated miRNAs on neuronal gene expression, the motor neuronal transcriptome was assessed at healthy and inflamed conditions. miRNAs mainly function on mRNAs by binding complementary sequences in the 3'UTR, thereby inhibiting translation of these transcripts[180] (Figure 4-4, a). To reveal whether mRNA transcripts are regulated by the previously identified inflammation-induced miRNAs, the translating ribosome affinity-purification (TRAP) method, initially developed by *Greengard and Heintz*[274] (Figure 4-4, b), was utilized. The bacterial artificial chromosome (bac) transgenic mouse model *Chat-EGFP/Rpl10a* consists of an EGFP-tagged ribosomal protein L10a under control of a Chat promotor, enabling cell-type specific expression. Analogously to *ChAT-Cre × R26-LSL-tAGO2* (cf. Figure 4-2, a), the tagged ribosome as the functional unit of translation allowed immunopurification of translating mRNAs by α-GFP antibodies from spinal cord motor neurons. For this purpose, healthy (n = 4) and acute EAE-diseased mice were sampled (Figure 4-4, c) and perfused with dissection buffer containing DTT and CHX as described for the miRAP technique. The cervical spinal cords of three mice were pooled, homogenized, lysed and mRNA was either extracted from whole SC or iSC and from MN or iMN by immunoprecipitation. mRNA was subsequently isolated by phenol/guanidine and silica-membrane-based purification of total RNA. The sequencing library was manually prepared with the NEBNext Ultra RNA Library Prep Kit for Illumina (New England Biolabs) and total RNA was subsequently sequenced on an Illumina HiSeq 4000 Analyzer (Figure 4-4, d) by the *Transcriptome and Genome Analysis Laboratory*, Göttingen. The reads were aligned to the *Ensemble mouse reference genome (mm10)* using *STAR* and differential gene expression was analyzed with the R package *DESeq2* (fold change > 1.5, FDR-adjusted $P < 0.05$, analysis by *Dr. Dr. Jan Broder Engler*). As shown in Figure 4-4 e, successful isolation of motor neuron-specific mRNAs was accomplished by TRAP. For this purpose, the FC expression of cell-type specific marker genes relative to whole spinal cord tissue was assessed. An up to 10–fold enrichment was observed for the motor neuronal marker gene Chat, whereas marker genes for oligodendrocytes (*Cnp*), astrocytes (*Gfap*) and immune cells (*Ptprc*, CD45) were not enriched. In total, 2706 genes were found to be downregulated in CNS-inflammation in motor neurons. To further explore, if these transcripts were potential target mRNAs of the 22 newly identified inflammatory miRNAs, they were compared to the computationally predicted targets derived from the public database *TargetScanMouse 7.2* (cumulative weighted context++ score (CWCS) < –0.4). This analysis revealed that 123 downregulated mRNAs were potentially regulated by the 22 previously identified inflammation-induced miRNAs in motor neurons in CNS-inflammation. A network analysis (performed by *Dr. Dr. Jan Broder Engler*) exhibited that certain

genes were potentially regulated by more than one miRNA in inflamed motor neurons (Figure 4-4, f). These hub genes were *Tmem170, Fam96b, Fam199x, Nxph1, St6gal2, Sesn3, Dcun1s4* and *Wasl*. The strongest convergence on mRNA targets was observed for miR-223-3p, miR-199-3p, miR-92a-3p, mir-142-3p.1p/2p, miR-673-5p and miR-146-5p, which together acted on the hub genes *Fam199x, Nxph1, St6gal2, Sesn3, Dcun1d4* and *Wasl,* but also had private targets that were not regulated by another miRNA. Interestingly, the miRNAs miR-155-5p, miR-210-3p, miR-3963, miR-142a-5p, miR-21-3p, miR-143-3p, miR-2137, miR 5099 and miR-147-3p seemed to be less cooperative and rather regulated mRNA targets on their own. Moreover, the dynamic range of miRNA regulation was displayed by the observation that some miRNAs had very few mRNA targets, whereas others regulated many transcripts at the same time (Figure 4-4, f).

To further explore the biological consequence of the miRNA–mRNA network shown in Figure 4-4 f, a gene list enrichment analysis was performed with these targets (*ToppGene Suite*, analysis by *Dr. Dr. Jan Broder Engler*). This analysis revealed a potential involvement of motor neuronal inflammation-induced miRNAs in general neuronal regulatory processes and synaptic signaling (Figure 4-4, g).

In order to disentangle the functional contribution of each miRNA candidate involved in regulating these biological processes in CNS-inflammation in motor neurons, the relative overlap of all predicted and actually downregulated mRNA transcripts was examined (Figure 4-4, h, x-axis, analysis by *Dr. Dr. Jan Broder Engler*). Since some miRNAs were predicted to regulate a big number of mRNAs[166,179], an overrepresentation analysis was integrated into the plot as a metric for miRNA specificity (Figure 4-4, h, y-axis, analysis by *Dr. Dr. Jan Broder Engler*). Thus, miRNAs with a high proportion of predicted targets being downregulated in inflamed neurons were located to the right. Additionally, hypergeometrical testing was used to assess whether an overlap of predicted and actually downregulated targets as big as observed, was due to chance. miRNAs with a low probability of this overlap being due to chance were located to the top. This approach enabled the prioritization of miRNA candidates for further analyses. As shown in Figure 4-4 h, miR-223-5p and miR-92a-3p were statistically most solid in repressing potential mRNA targets ($P = 8.7604 \times 10^{-6}$), while miR-92a-3p had the greater relative overlap of predicted and actually downregulated target transcripts in motor neurons in CNS-inflammation. Together with its robust expression and strong induction in motor neurons in EAE, miR-92a-3p appeared to be a promising candidate for further investigations.

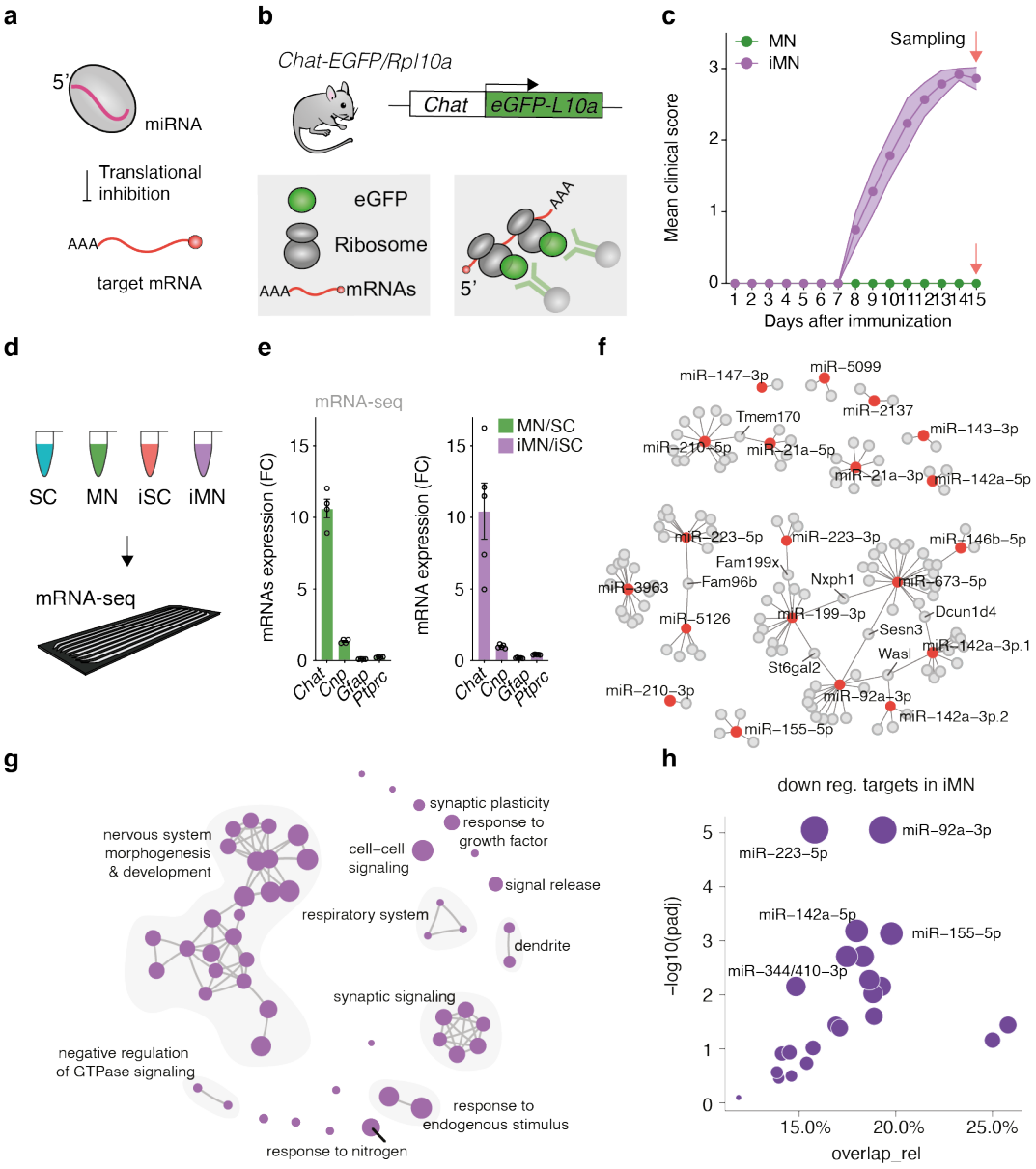

Figure 4-4 A miRNA–mRNA network regulates neuronal genes in CNS-inflammation

a) Scheme shows inhibition of translation by miRNAs. (b) Diagram of the mouse line used to identify deregulated mRNA transcripts in CNS-inflammation. eGFP-tagged 60s ribosomal protein L10a controlled by *Chat* promotor activity, enabled translating ribosome affinity-purification (TRAP) of associated mRNAs from motor neurons. (c, d) mRNAs were isolated at acute EAE (day 15 ± 1, indicated by red arrows) and subsequently sequenced (fold change > 1.5, adjusted for multiple comparison by FDR ($P < 0.05$). (e) mRNA purification shown by FC expression of cell-type specific marker genes (*Chat*, motor neurons; *Cnp*, oligodendrocytes; *Gfap*, astrocytes; *Ptprc*, immune cells) from normalized count data. (f) Interaction network of regulated miRNAs and their predicted, downregulated mRNA targets in inflamed neurons (*TargetScanMouse7.2*, CWCS < –0.4). (g)

Enrichment map of biological processes regulated by candidate miRNAs (gene list enrichment analysis, *ToppGene Suite*). (h) Plot for candidate prioritization. Relative overlap of regulated targets in inflamed motor neurons with all predicted targets for each miRNA candidate. Statistical testing by overrepresentation analysis (hypergeometric test, adjusted for multiple comparison by FDR, $P < 0.05$).

4.2.2 Revealing the miR-92a-3p–*Cpeb3* regulatory network

Analyzing the regulatory potential of miRNAs on motor neuron-specific translation in CNS-inflammation revealed miR-92a-3p as a promising candidate. miR-92a-3p belongs to the miRNA family (miR-25 family) comprising 5 miRNA member that share the same seed region and therefore the same predicted targets[221]. Computational analysis exhibited 854 potential target mRNAs (*TargetScanMouse 7.2*), of which 136 were found to be significantly downregulated in inflamed motor neurons by TRAP (Figure 4-5, a–b). Since miR-92a-3p was the only candidate of the miR-25 family expressed in inflamed motor neurons, it appeared unlikely that other members of the miR-25 family contributed to regulation of the 136 identified mRNAs. However, since the aim of the target analysis was to identify only functionally relevant miR-92a-3p targets, genes which were downregulated upon overexpression of miR-92a-3p were included into the analysis. Therefore, a dataset with downregulated genes caused by adeno-associated virus (AAV)-mediated overexpression of miR-92a-3p in neurons[231] was included into the overlap analysis. The analysis finally revealed 29 miR-92a-3p mRNA targets (Figure 4-5, a–b). A gene list enrichment analysis (*ToppGene Suite*) of these 29 mRNAs showed involvement in regulating neuron-specific biological processes as ‘synaptic signaling’, ‘synaptic plasticity’, ‘exocytosis’, ‘regulation of receptors and vesicles’, ‘ion transport’ and ‘neurogenesis’ as well as general intracellular processes as ‘RNA processing’, ‘lipid- and NO-biosynthesis’ and ‘phosphatidyl inositol-phosphate (PIP)-signaling’ (Figure 4-5, c). The row z-score normalized expression of these 29 mRNAs in healthy and inflamed motor neurons (TRAP data, Figure 4-4) is displayed in Figure 4-5, d. For miRNA target candidate prioritization, the total number of conserved miRNA binding sites (CS) in the 3’UTR and the cumulative weighted context++ score (CWCS), reflecting the predicted efficacy of targeting calculated by the sum of 14 contributing features[179], was analyzed for each miR-92a-3p target (*TargetScanMouse 7.2*). Cpeb3 was observed to be the downregulated mRNA transcript in inflammatory neurons with the strongest miR-92a-3p target prediction, having the highest number of CS and the lowest CWCS. As shown in Figure 4-5 e, the repression of *Cpeb3* mRNA was accompanied by induction of both, the mature miR-92a-3p (miRAP data, Figure 4-3) and its host gene *Mir17HG*[184] (TRAP data, Figure 4-4), resulting in the hypothesis that CNS-inflammation induces expression of *Mir17HG*, which leads to a higher

production of mature miR-92a-3p, which in turn downregulates *Cpeb3* mRNA in motor neurons (Figure 4-5, f).

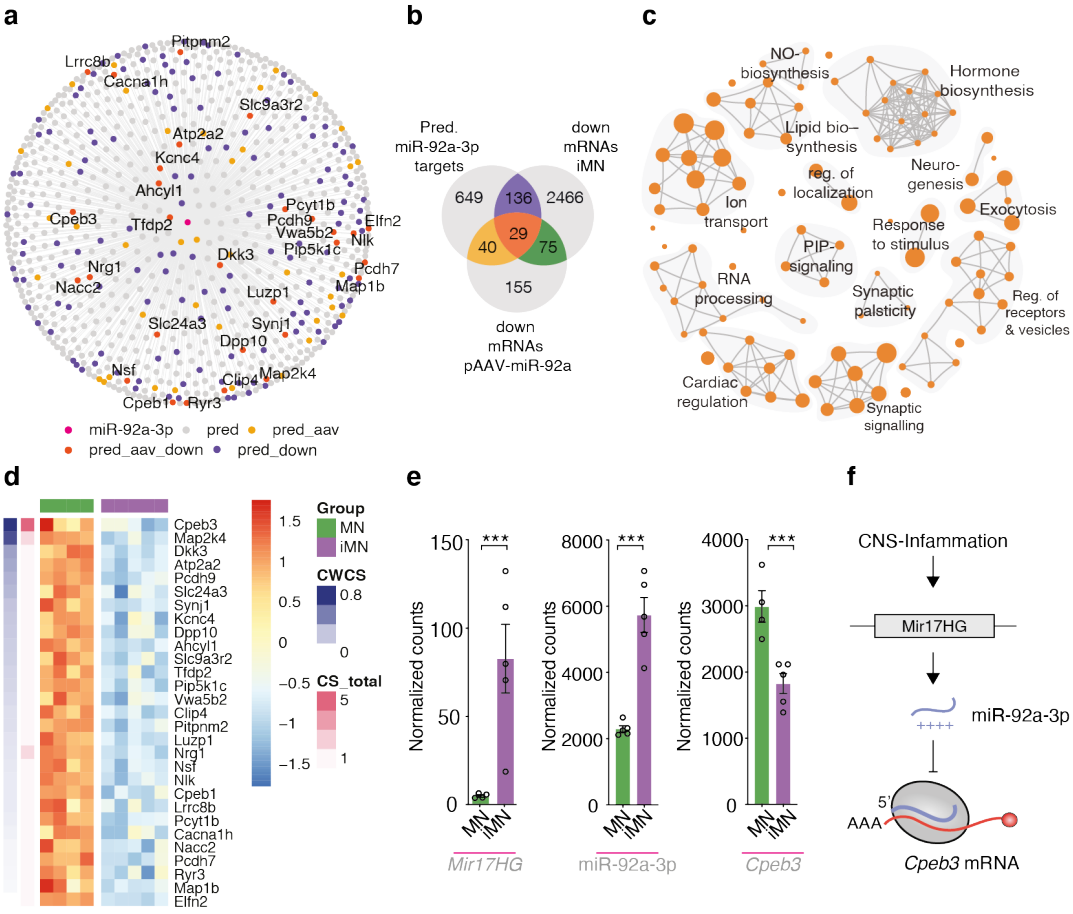

Figure 4-5 Discovery of Cpeb3 by miR-92a-3p target gene prioritization

(a, b) Hairball network and Venn map show color-coded overlap between predicted miR-92a targets (grey; *TargetScanMouse 7.2*) and downregulated genes in inflamed motor neurons (purple; TRAP data, Figure 4-4). Overlapping genes were additionally compared to downregulated genes caused by miR-92a-3p overexpression (data from A. Sakai[231]). 29 genes overlap between all three data sets (orange). (c) Enrichment map shows significant biological process GO terms of the 29 regulated miR-92a-3p genes (*ToppGene Suite*). (d) Heat map of row z-score normalized expression of the 29 miR-92a-3p target genes from inflamed motor neurons (TRAP data). Additionally, the cumulative weighted context++ score (CWCS) and number of total conserved sites (CS) in the 3'UTR of these mRNAs were plotted (*TargetScanMouse 7.2*). (e, f) Hypothesized sequence of events in inflamed motor neurons demonstrating upregulation of *Mir17HG* (TRAP data), causing elevated miR-92a-3p levels (miRAP data) leading to downregulation of *Cpeb3* (TRAP data).

4.2.3 Analysis of neuronal miR-17/92 cluster gene expression

The identified top miRNA candidate miR-92a-3p belongs to the polycistronic miR-17/92 cluster. This cluster consists of 6 miRNA genes (Figure 4-6, a), encoded by *Mir17HG* and transcribed as a single primary transcript[184]. This raised the question, whether the other miR-17/92 cluster miRNAs were also expressed in motor neurons or in other cells of the spinal cord (whole spinal cord) and whether they were also deregulated in CNS-inflammation.

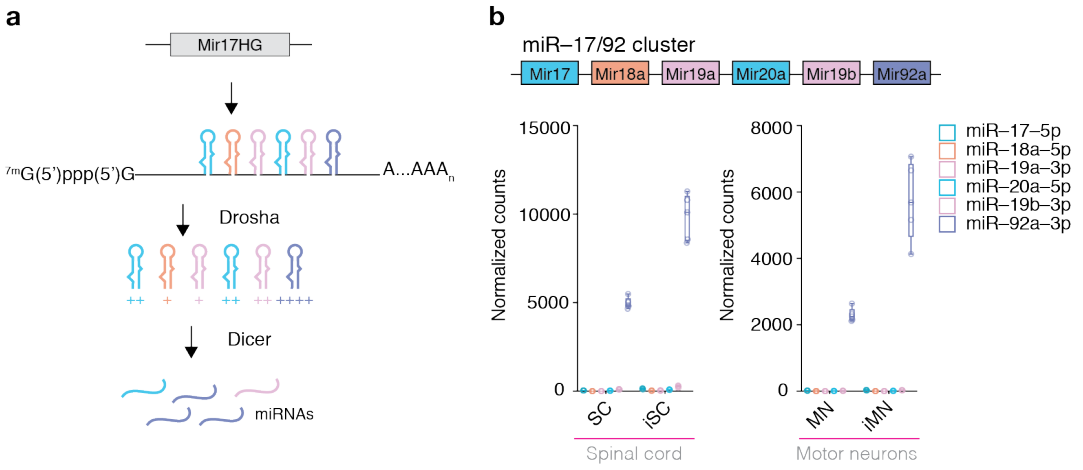

Figure 4-6 Motor neurons express abundant levels of miR-92a-3p

(a) Schematic demonstrates the differential biogenesis of single miRNAs from the precursor mRNA originating the *Mir17HG.* Diverse enzymatic complexes and tertiary structure influence the maturation of miRNAs at different steps. (b) Normalized count data of miR-92a-3p and the other miR-17/92 cluster miRNAs in spinal cord tissue and in motor neurons (miRAP data). The leading strand of each miRNA from the miR-17/92 cluster is shown.

In order to explore the expression pattern of each miRNA gene from the miR-17/92 cluster in all cells of the spinal cord and in motor neurons specifically, the miRAP data were re-analyzed (cf. Figure 4-3). When comparing the normalized miRNA counts of each miR-17/92 cluster member in healthy spinal cord cells and healthy motor neurons, miR-92a-3p had by far the highest expression and was the only robustly EAE-induced miRNA in inflamed motor neurons (Figure 4-6, b). However, miR-92a-3p expression was not restricted to healthy motor neurons but was also expressed by either other neurons or other cell types of the healthy spinal cord. This is indicated by the higher expression level (4969 ± 143) in comparison to motor neurons (2296 ± 94). After induction of EAE, miR-92a-3p upregulation was again higher in inflamed spinal cord (9831± 585) than in inflamed motor neurons (5738 ± 525), suggesting that miR-92a-3p expression is either also induced in other cell types than ChAT expressing motor neurons or originated from tissue-invading immune cells (Figure 4-6, b).

4.3 Validation of the neuronal miR-92a-3p network

4.3.1 Analysis of the transcriptional regulation of miR-92a-3p and *Cpeb3*

As shown above, CNS-inflammation leads to upregulation of miR-92a-3p in motor neurons and other spinal cord cells. Until now, the mechanism behind this induction remained unclear. Therefore, two key pathophysiological features of neurodegeneration in MS and EAE, chronic inflammation and glutamate excitotoxicity[51,109], were utilized as stimulants of neuron-intrinsic stress response networks to investigate the effects on miR-92a-3p expression in primary neurons.

For this purpose, primary cortical mouse neurons were prepared from E16.5 *C57BL/6J* embryos and cultured for ~2 weeks in vitro to achieve neuronal maturation regarding synaptogenesis and connectivity[291]. To limit contamination with glia cells, the cultures were treated with 1 µM AraC to block DNA-synthesis and therefore prevent their proliferation[292]. To mimic CNS-inflammation in vitro mature primary neurons were chronically (24 hours) stimulated with either cytokines[293] or glutamate[294]. The neurons were harvested at DIV 14, total RNA was purified, reverse transcribed and qRT-PCR was performed for mRNAs and miRNAs. TATA-binding protein (*Tbp*)[273] and sno234[271] were used as reference genes to normalize the expression of mRNAs and miRNAs, respectively.

The chronic stimulation of primary cortical neurons with increasing concentrations of glutamate (1 µM, 5 µM, 10 µM, 20 µM) resulted in enhanced mature miR-92a-3p levels in a concentration-dependent manner (Figure 4-7, a). As mentioned above, glutamate excitotoxicity is discussed to be mainly induced by activation of extrasynaptic glutamate receptors[112]. However, stimulation with exogenous glutamate activates potentially both, synaptic and extrasynaptic glutamate receptors[113,115]. Therefore, to examine whether upregulation of miR-92a-3p was due to synaptic activation of glutamate receptors only, cultures were treated with the $GABA_A$ receptor antagonist bicuculline, which leads to a blockade of GABAergic inhibitory inputs, thereby inducing depolarization of the postsynaptic membrane mediated mostly by synaptic, but not extrasynaptic glutamate receptors[112,295]. However, bicuculline treatment (25 µM) for 24 hours did not induce miR-92a-3p in cortical neurons.

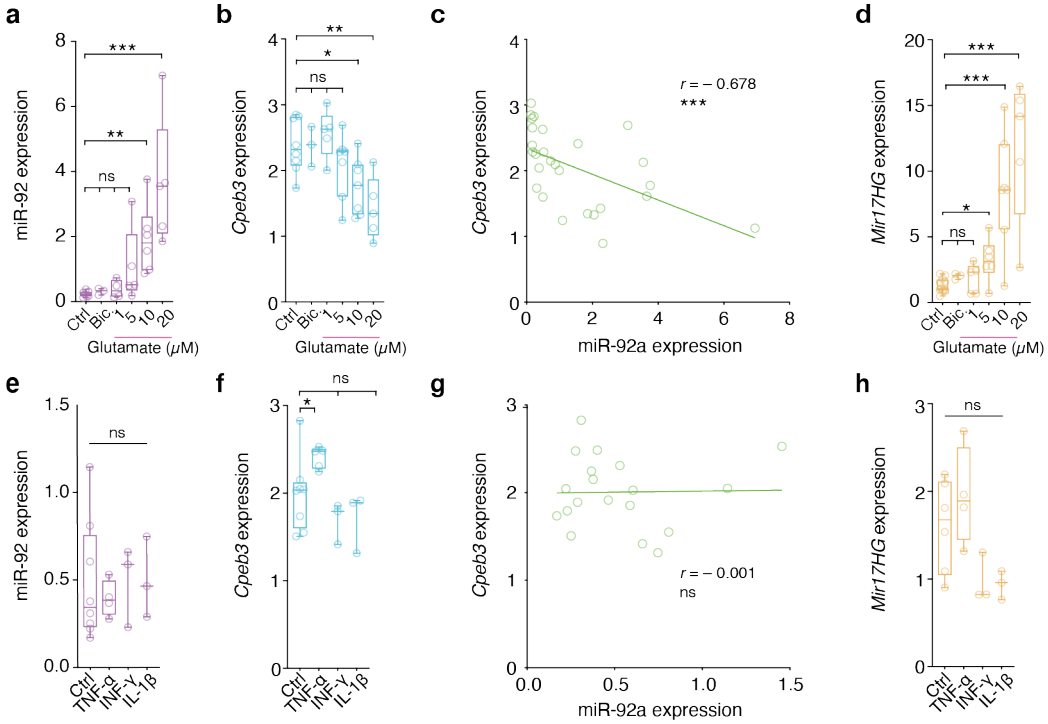

Figure 4-7 Glutamate stimulation induces transcription of miR-92a-3p and reduces Cpeb3

(a, b) qRT-PCR data shows expression of miR-92a-3p (normalized to sno234) and *Cpeb3* (normalized to *Tbp*) after chronic glutamate and bicuculline (25 µM) stimulation (24 hours) in primary cortical mouse neurons (DIV 14). (c) Rank correlation analysis of miR-92a-3p and *Cpeb3* expression upon stimulation with increasing doses of glutamate (two-tailed spearman correlation, $P < 0.05$.). (d) *Tbp* normalized gene expression of *Mir17HG* after chronic glutamate and bicuculline treatment. (e, f) miR-92a-3p and *Cpeb3* expression levels after chronic stimulation with different cytokines (100 ng ml^{-1}). (g) Rank correlation analysis of miR-92a-3p and *Cpeb3* expression after stimulation with cytokines. (h) *Mir17HG* expression levels after stimulation with different cytokines. ROUT outlier identification ($Q = 10\%$), Kruskal–Wallis test (uncorrected Dunn's test), $P < 0.05$.

Following the hypothesis that miR-92a-3p regulates *Cpeb3* mRNA, the expression levels of *Cpeb3* were analyzed. Stimulation with increasing glutamate led to concentration-dependent downregulation of *Cpeb3 (*Figure 4-7, b). As shown by the nonparametric rank correlation analysis (spearman correlation), *Cpeb3* expression negatively corelated *(r* = – 0.678) with increasing miR-92a-3p levels (Figure 4-7, c). In contrast, treatment of cortical neurons with the inflammatory cytokines TNF-α, INF-γ[293] or IL-1β[296] did not result in an induction of miR-92a-3p (Figure 4-7, g) or a correlation with *Cpeb3* expression (Figure 4-7, e, g). Of note, stimulation with TNF-α alone, led to increased *Cpeb3* levels, but had no significant effect on miR-92a-3p expression (Figure 4-7, f), indicating an independent functional role of TNF-α on *Cpeb3* expression. Further, these observations raised the question whether neuronal miR-92a-3p

induction was driven by increased transcription or alteration of the processing machinery upon glutamate induced neuronal toxicity. For this purpose, the expression of the miR-92a-3p precursor gene *Mir17HG* was analyzed. Stimulation of neuronal cell cultures with glutamate led to a concentration-dependent induction of *Mir17HG* (Figure 4-7, d). Concordantly to what was observed for miR-92a-3p expression before, bicuculline treatment and stimulation with the cytokines TNF-α, IFN-γ and IL-1β had no significant effect on gene expression of *Mir17HG* (Figure 4-7, d, h).

4.3.2 Validation of *Cpeb3* regulation by miR-92a-3p

In order to reveal, whether *Cpeb3* downregulation was in fact caused by induced miR-92a-3p expression in neurons (cf. Figure 4-5, e, f) and (cf. Figure 4-7, a–c), a miRNA target gene luciferase reporter assay[297] was performed. The luciferase reporter assay is based on the translational suppression of target genes by miRNA-binding to complementary regions in the 3'UTR (MREs, miRNA response elements)[180]. To allow validation of a functional relationship between a miRNA and a mRNA target, the 3'UTR of firefly luciferase is replaced with the 3'UTR of the target gene, leading to a diminished firefly translation and thus a reduced luminescent signal upon binding of the miRNA (Figure 4-8, b).

For the miRNA target gene luciferase reporter assay miTarget™ 3' UTR miRNA Target Clones were used. To test whether miR-92a-3p physically binds *Cpeb3* 3' UTR and leads to its translational repression, N2a neuronal cells were co-transfected with one of the plasmids (control or reporter vector) and one of LNA miRNA mimics (scramble or miR-92a-3p). The miRCURY LNA™ miRNA mimics are double-stranded RNAs and consist of a guide strand, which is identical to the miRNA and a complementary passenger strand (made up of two RNA strands), which is LNA-based and contains uptake elements such as cholesterol[298] (Figure 4-8, a). Two days after transfection, firefly and renilla luminescence were recorded with a Dual-Glo Luciferase assay system, the firefly luminescent signal (RluC) was normalized to the renilla luminescent signal (FluC) and to the scrambled miRNA control. The firefly luminescence of the control vector co-transfected with miR-92a-3p was comparable to the unspecific scrambled miRNA (P = 0.994) (Figure 4-8, c), whereas a reduced firefly luminescence (P = 0.045) was detected, when the *Cpeb3* 3'UTR reporter vector was co-transfected with the miR-92a-3p in comparison to the scrambled miRNA (Figure 4-8, d). Together, these results show that miR-92a-3p specifically interacts with the 3'UTR of *Cpeb3* and represses its translation.

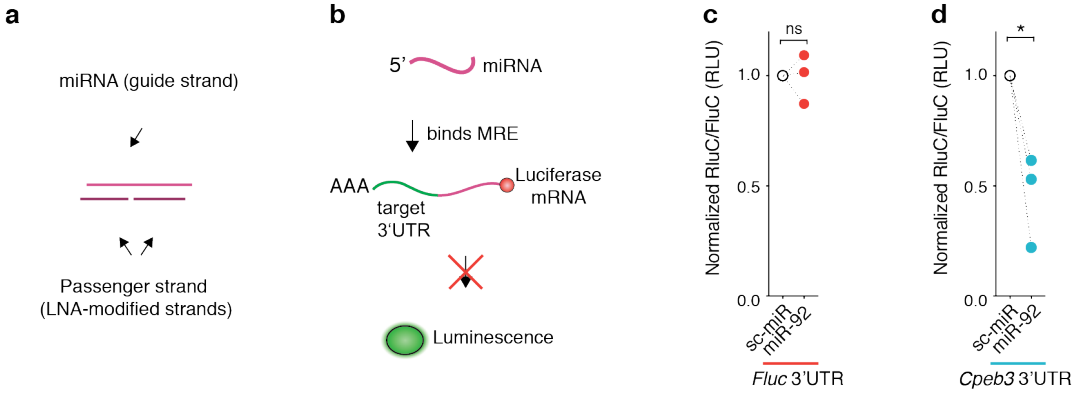

Figure 4-8 Cpeb3 translation is repressed by miR-92a-3p

(a) The graph demonstrates the design of LNA-modified miRNA mimics. (b) Schematic of a miRNA target gene luciferase reporter assay to validate the specific interaction of miRNAs with their mRNA targets. miRNAs bind miRNA response elements (MREs) in the 3'UTR of their targets, leading to inhibition of translation. (c, d) Luminescence (relative luminescent units, RLU) was detected two days after co-transfection of the control or the reporter vector with either the scrambled miRNA control (sc-miR) or the miR-92a-3p mimic (miR-92) in N2a neuronal cells. Firefly luminescence (FluC) was normalized to renilla luminescence (RluC). One sample t test, $P < 0.05$.

4.3.3 Investigation of miR-92a-3p and *Cpeb3* downstream target *Gria1*

As described previously, translation of glutamate ionotropic receptor AMPA type subunit 1 (GluA1) mRNA (*Gria1*) was reported as being re-repressed (activated) by the RNA-binding protein CPEB3 upon neuronal activation[252,299] and re-repressed by miR-92a-3p upon neuronal activity blockade[257]. As shown above, transcription of *Cpeb3* and miR-92a-3p was deregulated in primary neurons exposed to excitotoxic levels of glutamate. Therefore, it was asked whether *Gria1*, which as a Ca^{2+}-selective AMPAR subunit contributes to glutamate excitotoxicity[99,135], was also affected by stimulation with glutamate. To investigate a potential interdependency of miR-92a-3p, *Gria1* and *Cpeb3*, primary cortical neurons were stimulated with either cytokines, bicuculline or increasing doses of glutamate and *Gria1* was subsequently examined by qRT-PCR. This revealed that concordantly to *Cpeb3* expression, glutamate but not bicuculline or cytokines caused a dose-dependent downregulation of *Gria1* expression in primary neurons (Figure 4-9, a, b). This finding was further confirmed by a spearman rank correlation analysis ($r = 0.509$, $P = 0.031$), showing a positive relationship between *Gria1* and *Cpeb3* mRNA (Figure 4-9, c). Conversely, a negative relationship (spearman correlation, $r = -0.780$, $P = 0.002$) between *Gria1* and miR-92a-3p was observed upon glutamate excitotoxicity (Figure 4-9, d). Therefore, it might be that excessive miR-92a-3p expression simultaneously inhibits translation of *Cpeb3* and *Gria1*,

overwriting a possible translational activation of *Gria1* that would be expected upon downregulation of *Cpeb3*.

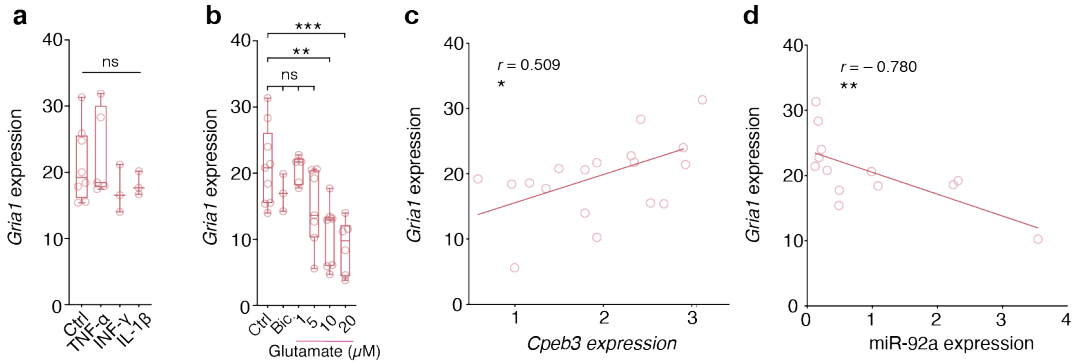

Figure 4-9 Glutamate stimulation reduces Gria1 expression

(a) qRT-PCR data shows *Tbp* normalized expression of *Gria1* after chronic stimulation (24 hours) with different cytokines (100 ng ml·) in primary cortical mouse neurons (DIV 14). ROUT outlier identification (Q = 10%), Kruskal–Wallis test (uncorrected Dunn's test), $P < 0.05$. (b) Chronic stimulation of cortical neurons with bicuculline (25 μM) and different doses of glutamate. (c) Rank correlation analysis of *Gria1* and *Cpeb3* expression upon different doses of glutamate. Two-tailed spearman correlation, $P < 0.05$. (d) Spearman rank correlation analysis of *Gria1* and miR-92a-3p expression upon increasing doses of glutamate.

4.4 Deletion of miR-92a-3p in CNS-inflammation

4.4.1 Characterization of *Mir92-1* knockout mice

In order to study the effect of miR-92a-3p on CNS-inflammation and neurodegeneration *in vivo*, miR-92a-3p knockout mice were utilized. So far, only constitutive *Mir92-1* knockout mice have been generated[232], but no conditional knockout mice that would have allowed a neuron-specific deletion of *Mir92-1* (*Mouse Genome Database*[300]).

As a first step to characterize *Mir92-1* knockout mice, deletion of miR-92a-3p was validated by qRT-PCR. The reported constitutive deletion of the *Mir92-1* locus[232], was verified in immunological (spleen, lymph nodes) and neurological (brain, spinal cord) tissues that were analyzed for miR-92a-3p expression (Figure 4-10, a). All examined tissues showed significant deletion of miR-92a-3p in homozygous knockout mice (miR-17/92$^{\Delta 92/\Delta 92}$) in comparison to wild-type littermates (miR-17/92$^{+/+}$), but no differences in *MIR7HG* expression were observed (Figure 4-10, b), (multiple t test without multiple comparison and without assuming a consistent standard deviation (SD, $P < 0.05$).

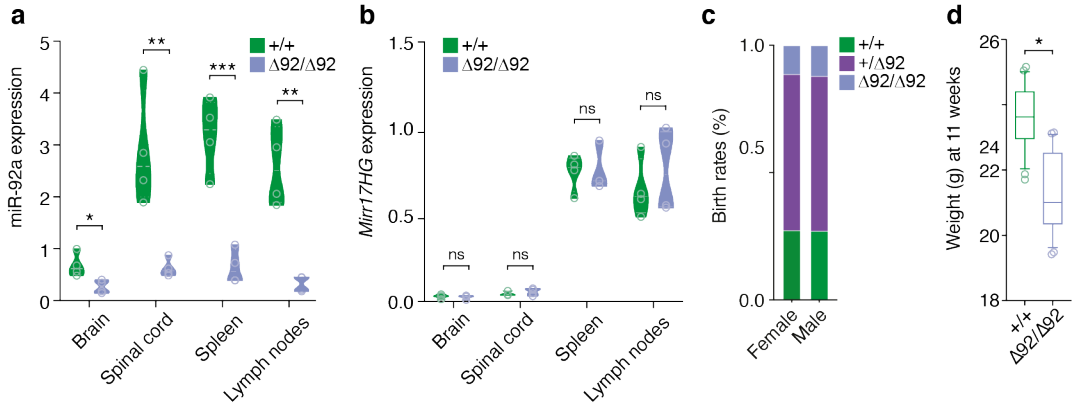

Figure 4-10 Mir92-1 knockout mice exhibit altered birth rates and body weight

(a, b) qRT-PCR data shows expression of miR-92a-3p (normalized to sno234) and its genetic origin *Mir17HG* (normalized to *Tbp*) in different neurological (brain, spinal cord) and immunological (spleen, lymph nodes) tissues in Δ92/Δ92 (miR-17/92$^{\Delta 92/\Delta 92}$) mice and +/+ (miR-17/92$^{+/.}$, wild-type littermates). Multiple t test without correction for multiple comparisons and without assuming a consistent SD, $P < 0.05$. (c) Birth rates and sex distribution (%) of 246 examined littermates originating heterozygous breeding cages. Chi-square test, $P = 0.981$. (d) Body weight of adult Δ92/Δ92 mice (n =16) and +/+ littermates (n =12). Two-tailed Mann–Whitney test, $P = 0.0460$. Box-plot whiskers are drawn to 10th and 90th percentile. Points outside whiskers are shown individually.

Additionally, the breeding rates of heterozygous miR-17/92$^{+/\Delta 92}$ mating cages were characterized. It was observed that miR-17/92$^{\Delta 92/\Delta 92}$ offspring were not born according to mendelian ratios. From all analyzed littermates (n = 246) only 11.8% of expected 25% were miR-17/92$^{\Delta 92/\Delta 92}$ mice (Figure 4-10, c). However, the sex of all littermates among the different genotypes was evenly distributed (chi-square test, $P = 0.981$). Finally, the total body weight (gram) of 11 weeks old miR-17/92$^{\Delta 92/\Delta 92}$ and wild-type littermates was determined. As shown in Figure 4-10 d, miR-17/92$^{\Delta 92/\Delta 92}$ mice were significantly lighter (22.75 ± 0.79 g) than wild-type littermates (24.88 ± 0.88 g).

4.4.2 Effects of *Mir92-1* deletion on clinical disability in EAE

Following characterization of *Mir92-1* knockout mice, the functional impact of miR-92a-3p deletion on CNS-inflammation was analyzed. For this purpose, EAE was induced in miR-17/92$^{\Delta 92/\Delta 92}$ mice (n = 23) and wild-type littermates (n = 26). Deletion of *Mir92-1* led to exacerbated clinical disability in acute and chronic EAE (Figure 4-11, a). The disease onset of miR-17/92$^{\Delta 92/\Delta 92}$ mice occurred in average 1 day later (12.22 ± 0.22) than observed for wild-type littermates (11.23 ± 0.47; two-tailed Mann–Whitney test, P = 0.023), whereas the disease incidence was not changed (Figure 4-11, c). The acute disease peak of miR-17/92$^{\Delta 92/\Delta 92}$ mice

presented as an overshoot of clinical disability, which did not recover to wild-type level (two-tailed Mann–Whitney test, $P = 0.015$). This was also reflected in the average body weight (Figure 4-11, b), showing a stronger loss of body weight in miR-17/92$^{\Delta 92/\Delta 92}$ versus wild-type mice (two-tailed Mann–Whitney test, $P = 0.017$).

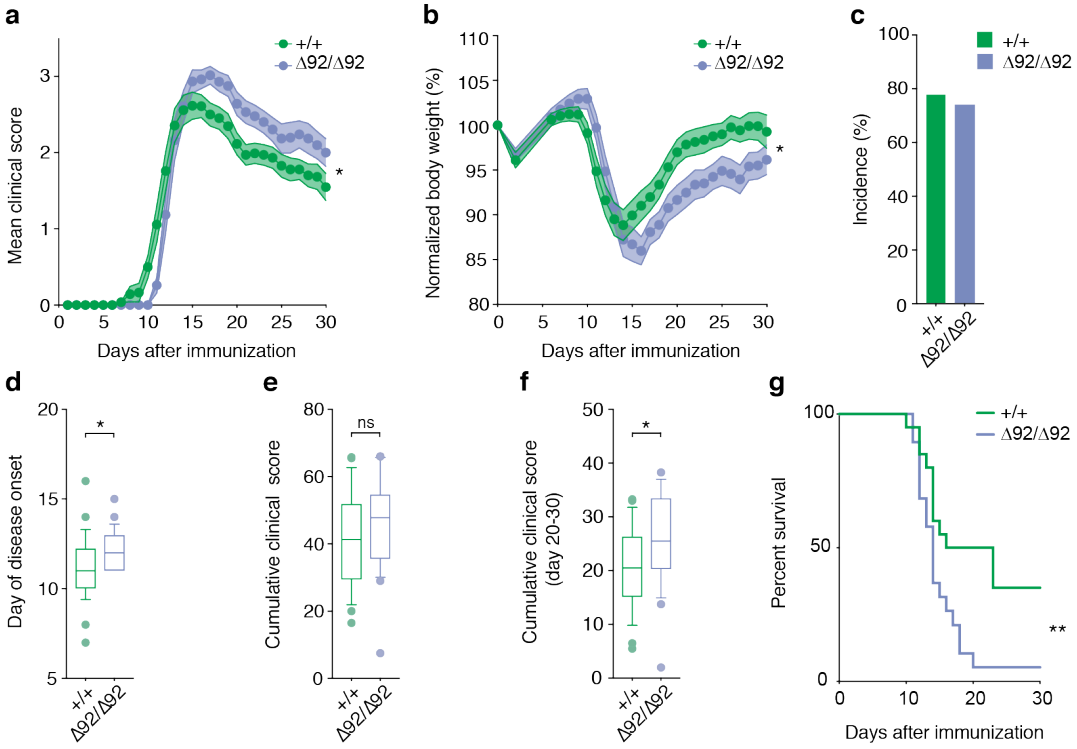

Figure 4-11 Mir92-1 deletion exacerbates clinical disability in EAE

(a) To test the effects of *Mir92-1* deletion on CNS-inflammation *in vivo*, EAE was induced in Δ92/Δ92 and +/+ mice. Mice with either EAE score 5, disease onset ≥ day 17 post immunization or mice without any clinical symptoms were excluded from the analysis. Two-tailed Mann–Whitney test from mean disease onset of all mice (day 11), $P = 0.015$. (b) Normalized body weight (%) of the EAE immunized mice throughout the complete course ($P = 0.017$). (c) EAE-induced disease incidence of Δ92/Δ92 (incidence 74.2%, $n = 31$) and +/+ mice (incidence 78.1%, $n = 32$). Mantel–cox log-rank test, $P = 0.935$. (d) Day of disease onset of Δ92/Δ92 mice (day 12.2, $n = 23$) and +/+ littermates (day 11.2, $n = 26$). Two-tailed Mann–Whitney test, $P = 0.023$. (e) Cumulative clinical disability (total EAE course) of Δ92/Δ92 mice and +/+ littermates ($P = 0.262$). (f) Cumulative clinical disability (chronic EAE course) between Δ92/Δ92 and +/+ mice ($P = 0.0229$). (g) Curves show survival of Δ92/Δ92 and +/+ mice throughout the EAE. Mantel–cox log-rank test, $P = 0.009$.

Additionally, miR-17/92$^{\Delta 92/\Delta 92}$ mice showed a significantly higher cumulative clinical disability in the chronic phase of EAE (day 20–30 post immunization; two-tailed Mann–Whitney test, $P = 0.023$; Figure 4-11) but not over the complete time course ($P = 0.262$). In a third independent

EAE experiment, mice exhibited an extraordinary strong EAE disease course and were therefore analyzed independently (Figure 4-11, g). However, also in this EAE deletion of miR-92a-3p led to a stronger disease course, which was reflected by the significantly reduced survival of miR-17/92$^{\Delta 92/\Delta 92}$ mice in comparison to wild-type littermates (Mantel–Cox log-rank test, $P = 0.009$).

4.4.3 Immunophenotyping of *Mir92-1* knockout EAE

To rule out that the observed exacerbated EAE phenotype in constitutive *Mir92-1* knockout mice was driven by differences in immune response and CNS infiltration, miR-17/92$^{\Delta 92/\Delta 92}$ mice ($n = 4$) and wild-type littermates ($n = 6$) were immunophenotyped. For this purpose, the main CNS resident and CNS invading peripheral immune cell subsets were investigated in EAE (Figure 4-13). Mice were immunized for EAE, perfused with 1X PBS and the CNS dissected at the acute phase (day 15 post immunization). The CNS was subsequently homogenized and the immune cells isolated by a discontinuous percoll-gradient.

First, the absolute numbers of infiltrating and CNS resident immune cells were quantified. Therefore, a fixed fraction of the isolated immune cells was incubated in TruCount® tubes, stained with α-CD45 in order to identify all immune cells and analyzed by flow cytometry. The recorded events were separated into cells and beads. Beads were identified by size and strong fluorescence in FITC and PE, immune cells were identified by size, granularity and by expression of CD45 (shown in the representative gating in Figure 4-12, a). Finally, the ratio of the recorded cell events and bead events allowed to estimate the absolute immune cell number in a given sample. No significant differences in the absolute CNS-infiltrating and resident CD45$^+$ immune cells between miR-17/92$^{\Delta 92/\Delta 92}$ and wild-type mice were detected (two-tailed Mann–Whitney test, $P = 0.7619$), indicating that the exacerbated EAE phenotype was not caused by stronger immune cell infiltration (Figure 4-12, b). To further analyze whether the frequencies of the major immune cell populations were changed in *Mir92-1* knockout mice in EAE, the isolated cells were stained with fluorescently labeled antibodies against specific marker proteins for microglia, neutrophils, macrophages, myeloid dendritic cells (DCs), lymphoid DCs, B cells, CD4$^+$ and CD8$^+$ T cells, natural killer cells (NK) and NK T cells. The different immune cell subsets were identified by a previously established sequential gating strategy (*Dr. Karin Steinbach*)[301] for flow cytometry with minor adjustments (representative gating, Figure 4-13, a).

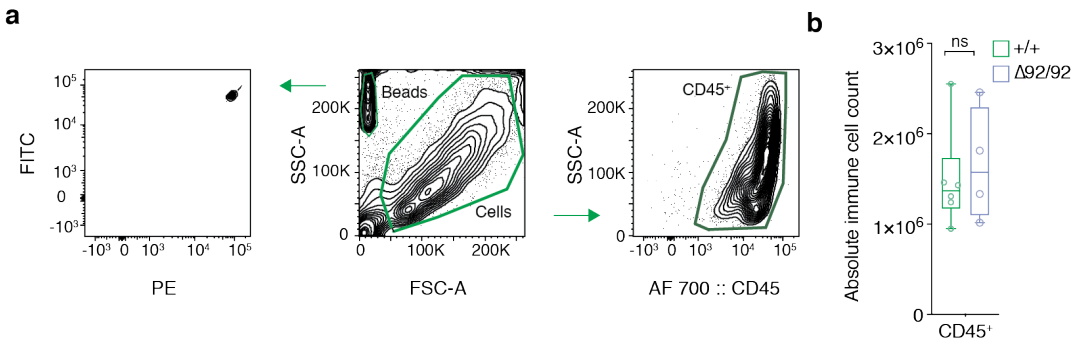

Figure 4-12 CNS immune cell infiltration is not affected by Mir92-1 deletion in acute EAE

(a) Representative gating strategy for flow cytometry to identify the absolute immune cell numbers of Δ92/Δ92 (*n* = 4) mice and +/+ (*n* = 6) littermates at acute EAE (day 15 post immunization). The absolute cell numbers were analyzed via TruCount® tubes. Immune cells were identified by expression of CD45. (b) Quantification of CNS infiltrating and resident CD45^{-} cells from Δ92/Δ92 and +/+mice. Two-tailed Mann–Whitney test, $P = 0.7619$

To analyze the immune cell subpopulation frequencies, all immune cells (CD45^{+}) were identified by first setting a time gate to extract evenly recorded FC events. Single cells were gated according to size (FSC-A) and granularity (SSC-A) and finally identified by CD45 expression. Staining of dead cells (LIVE/DEAD Fixable Dead Cell Stain) allowed identification of living CD45^{+} cells. All other subsets were gated within this population. Neutrophils were identified via Ly6G expression and microglia were discriminated by a lack of Ly6G and expression of CD11b. Their discrimination from macrophages (CD11c^{-} myeloid cells) and myeloid DCs (CD11c^{+} myeloid cells) was accomplished by high instead of intermediate expression of CD45. NKT and NK cells were identified by lack of CD11b expression, but expression of NK1.1. Both subpopulations were discriminated from each other via CD3ε expression. T cells and B cells were identified by CD3ε expression, whereas T cells were considered negative for the B cell marker B220 and further divided into, by expression of, CD4 and CD8. Finally, lymphoid DCs were gated by expression of B220 and CD11c (Figure 4-13, a). In order to achieve graphic visualization of the recorded single-cell events, a uniform manifold approximation and projection (UMAP) algorithm (FlowJo plugin) was applied (Figure 4-13, b). This allowed visual discrimination of the density distribution of single-cell events among cell clusters between miR-17/92$^{\Delta 92/\Delta 92}$ and wild-type mice. To provide the assignment of cell clusters to distinct immune cell populations the events were color-coded according to the manual gates by backgating (Figure 4-13, b). Density shifts between miR-17/92$^{\Delta 92/\Delta 92}$ mice and wild-type littermates were observed within neutrophils, myeloid DCs (CD11c^{+} myeloid cells), CD4^{+} and CD8^{+} T cells as well as NK cells. However, the cluster densities between both analyzed groups appeared to be comparable.

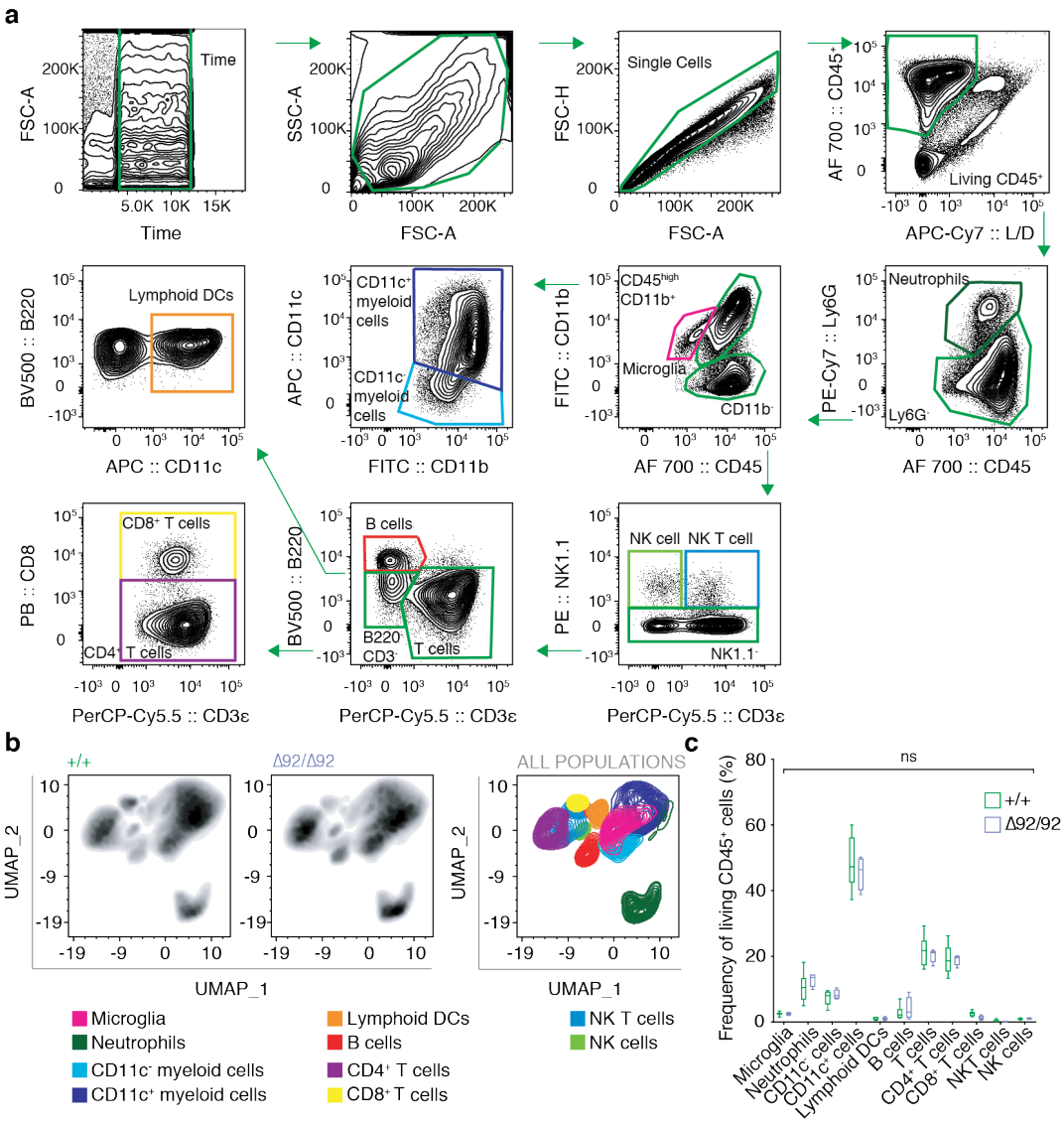

Figure 4-13 CNS immune cell frequencies are not affected by Mir92-1 deletion in acute EAE

(a) Representative FC gating strategy for phenotyping of CNS infiltrating and resident immune cells of Δ92/Δ92 (*n* = 4) and +/+ (*n* = 6) mice at acute EAE (day 15 post immunization). First, a consistent recording of events was filtered by setting a time gate, cells were then identified by size (FSC-A) and granularity (SSC-A), followed by gating on single and living immune cells (CD45 L/D). Sequentially, the major immune cell subtypes (microglia, neutrophils, macrophages, myeloid DCs, lymphoid DCs, B cells, CD4 and CD8 T cells, NK T cells and NK cells) were identified as indicated by arrows (b) Dimensionality reduction with a uniform manifold approximation and projection (UMAP) algorithm of the recorded single-cell events of Δ92/Δ92 and +/+ mice. Cell cluster identities were assigned by backgating (legend, color-coded). (c) Quantification of immune cell subpopulation frequencies between Δ92/Δ92 and +/+ mice. Multiple t test, adjusted for multiple comparisons by FDR ($P < 0.05$).

Finally, the quantification of immune cell population frequencies normalized to all living CD45$^+$ single cells (parent) affirmed variation of certain immune cell populations between miR-17/92$^{\Delta 92/\Delta 92}$ and wild-type mice, but no significant differences were identified (multiple t test, FDR-adjusted $P < 0.05$; Figure 4-13, c). Together, the results show that neither a skewed immune response nor a stronger CNS infiltration caused the observed exacerbated EAE clinical disability in *Mir92-1* knockout mice.

4.4.4 Neurophenotyping of *Mir92-1* knockout EAE

To assess neuropathological changes that were caused by deletion of miR-92a-3p in CNS-inflammation, miR-17/92$^{\Delta 92/\Delta 92}$ mice and wild-type littermates ($n = 6$ per group) were perfused with PFA (4%) at chronic EAE (day 30 post immunization), the spinal cord was dissected and cryosections were prepared in order to investigate axonal damage, neuronal loss and presynaptic synaptopathy by immunohistochemistry[273]. Healthy *C57BL/6J* mice ($n = 3$) were analyzed simultaneously to examine the neuropathological changes of SC and iSC independent of *Mir92-1* deletion. Two different regions, the dorsal column (DC, white matter) and the ventral horn (VH, grey matter) of these animals were analyzed (Figure 4-14, a). Representative confocal images of all groups are displayed in Figure 4-14, b. Neuroaxonal loss was detected by antibodies against phosphorylated (α-SMI-32P) and unphosphorylated neurofilament (α-SMI-31R). The total number of axons was determined by calculating the mean of two images per spinal cord (left and right side of the DC) by an automated counting mask in *Image J* and normalized to the recorded area (Figure 4-14, c). Quantification of axons per mm^2 showed that chronic EAE led to a significant loss of axons in both miR-17/92$^{\Delta 92/\Delta 92}$ and wild-type mice (Kruskal–Wallis test, $P = 0.017$ and $P = 0.029$). However, axonal loss appeared to be independent of *Mir92-1* deletion (Kruskal–Wallis test, $P = 0.807$). To analyze the loss of neuronal somata of the spinal cord VH, cryoslices of the both groups were stained with an α-NeuN antibody. The NeuN$^+$ cells were manually counted and the mean of cells per VH normalized to the analyzed area (per mm^2). This revealed that neuronal somata get lost in chronic EAE in comparison to healthy mice. The neuronal loss was only significant for wild-type mice ($P = 0.007$) but not miR-17/92$^{\Delta 92/\Delta 92}$ mice ($P = 0.073$). However, NeuN$^+$ cell numbers were comparable between miR-17/92$^{\Delta 92/\Delta 92}$ and wild-type mice (Kruskal–Wallis test, $P = 0.272$). Finally, to identify whether synapses were lost in chronic EAE and whether neuronal *Mir92-1* deletion caused synaptic changes, spinal cord ventral horn cryoslices were stained with an α-SYN1/2 antibody. Presynaptic SYN1/2$^+$ puncta were automatically counted in two confocal images per VH side, the mean was calculated and normalized to the recorded area (per µm^2). As shown in Figure 4-14 c, chronic EAE led to a loss of presynaptic terminals in miR-17/92$^{\Delta 92/\Delta 92}$ ($P = 0.031$) and wild-type mice ($P = 0.020$), but showed no differences between miR-17/92$^{\Delta 92/\Delta 92}$ mice and wild-type littermates (Kruskal–Wallis test, $P = 0.846$).

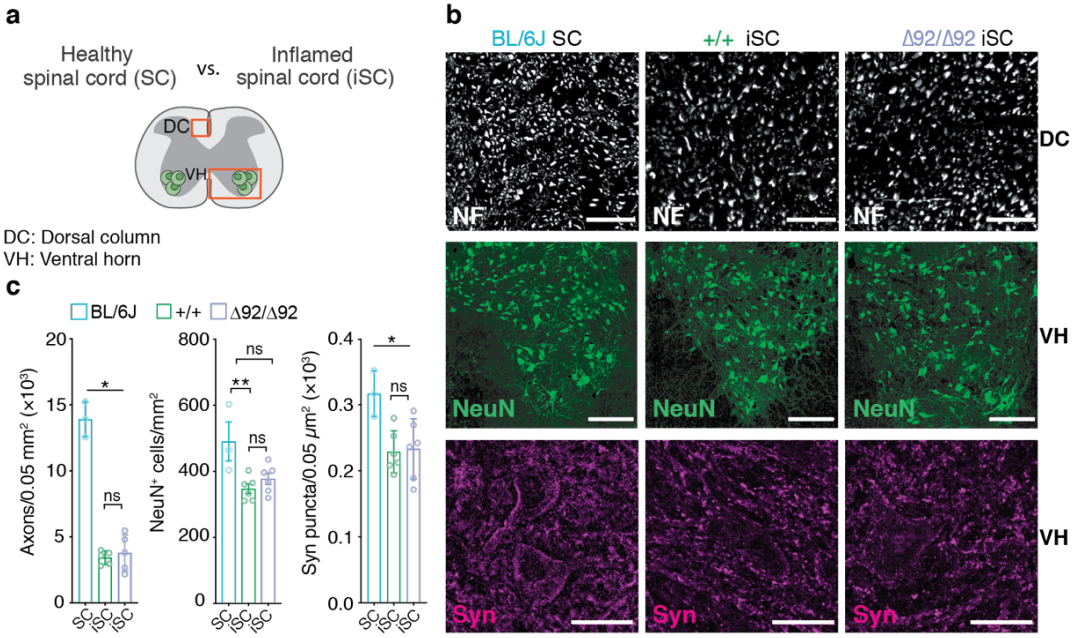

Figure 4-14 Mir92-1 deletion does not affect neuronal, axonal or presynaptic loss in chronic EAE

(a) To analyze neuropathological changes in CNS-inflammation, two different spinal cord regions (DC, dorsal column; VH, ventral horn) were investigated in healthy (SC) and EAE (iSC) spinal cord. (b) Representative confocal images of the different groups stained for unphosphorylated and phosphorylated Neurofilament (NF) with α-SMI-32P and α-SMI-31R antibodies, neuronal somata with α-NeuN antibody and presynaptic terminals with α-SYN1/2 antibody. Scale bar, 25 µm (NF); 150 µm (NeuN); 25 µm (SYN1/2). (c) Quantification of neuropathological investigations between healthy BL/6J and EAE-induced Δ92/Δ92 mice and +/+ littermates. Kruskal–Wallis test (uncorrected Dunn's test), $*P < 0.05$, $**P < 0.01$.

Together, the immunohistochemical analyses of EAE spinal cord revealed that axonal, neuronal and presynaptic loss were comparable between miR-17/92$^{\Delta 92/\Delta 92}$ and wild-type mice in the chronic stage of EAE.

5 Discussion

5.1 Profiling of neuronal miRNAs in CNS-inflammation

5.1.1 Establishment of a transgenic mouse line to study neuronal miRNAs

The first aim of this work was to identify whether neuronal miRNAs are deregulated in CNS-inflammation. Therefore, the transgenic mouse line to profile neuronal miRNAs was established. The immunohistochemical analysis revealed that AGO2-GFP was specifically expressed by spinal cord motor neurons. The miRAP was working reliable as shown by enrichment of miR-218, which is highly expressed by spinal cord motor neurons[287], but no enrichment of non-neuronal miRNAs. Cell type-specific profiling from motor neurons as representative neuronal population to study regulatory miRNA function was chosen for two reasons. The first reason was that ChAT expressing motor neurons are a defined neuronal population, which are mainly involved in mediating hind-limb motor function in mice[302]. In the here utilized mouse model EAE these neurons undergo inflammatory changes, which lead to their dysfunction causing motor disability, which is the major readout for EAE clinical symptoms[283,303]. The second reason was that the mouse line *Chat-EGFP/Rpl10a*[304] enabled studying transcriptional changes of ChAT expressing motor neurons in EAE analogously in order to investigate the mRNA targets that were regulated by the miRNAs in CNS-inflammation in EAE. However, it has to be considered that only AGO2 associated miRNAs were isolated with the established methodology, but not other AGO bound miRNAs. AGO2 is the only Argonaute family member with endonuclease activity[176,305], which can cleave miRNA-silenced mRNA targets and might therefore exert differential function as other AGO family members. AGO1-4 are all expressed within the CNS and are functionally and structurally similar[262,306]. However, it was never thoroughly investigated whether AGO1-4 uniformly mediate miRNA target regulation or whether they are involved in regulating different biological pathways within motor neurons. Nonetheless, it was shown that a distinct group of miRNAs was regulated by AGO2 in the striatum[307], therefore it is likely that AGO2 also plays a defined role within motor neurons. Further, AGO2 was described to be involved in miRNA biogenesis as Dicer, which upon deletion causes motor neuronal degeneration[215]. Finally, AGO2 is by far the best studied AGO protein in mice and the only one that leads to prenatal lethality when deleted[308], therefore plausibly exerting a different function that the other Ago proteins.

Together, the establishment of the transgenic mouse model *ChAT-Cre* × *R26-LSL-tAGO2* was successful and therefore suited to explore motor neuronal miRNA expression, which is associated with AGO2 in CNS-inflammation.

5.1.2 Screening of neuronal miRNAs in CNS-inflammation

An important role of miRNAs in regulating environmental contingencies[164] and their emerging role in motor neuronal development, differentiation and survival[309] indicate that they might also play a prominent role in motor neurons in CNS-inflammation. Screening of motor neuronal miRNAs in CNS-inflammation revealed 22 miRNAs that were all upregulated, which might reflect their biological nature as negative regulators of translation and important opponents of cellular vulnerability towards environmental disturbances[164,310]. Since miRNAs were mainly investigated in whole tissue or in immune cells in EAE, this work specifically aimed at revealing the miRNA expression in neurons. Due to the technical challenges to purify cell-type specific miRNAs, only one other study examined miRNA deregulation in neurons in EAE so far[188]. To isolate neuronal miRNAs, they used laser capture microdissection to mechanically excise neurons from healthy and EAE spinal cord as well as retinal tissue[188]. Interestingly, the here identified motor neuron-specific miRNAs only marginally overlapped with these results. Three motor neuronal miRNAs, miR-142a-5p, miR-203-3p and miR-223-3p were identified by both approaches. However, some decisive points might account for the observed differences in these datasets. First of all, the methodology was very different. Laser capture microdissection is a mechanical procedure, which might induce immediate transcriptional changes[311] thereby impacting the results. Therefore, and due to its serval drawbacks including RNA degradation and sampling limitations, laser capture microdissection is not widely used[312]. However, while microdissection samples all cellular miRNAs, miRAP specifically samples the 'functional pool' of miRNAs that is bound to AGO2 and thereby able to exert regulatory functions. Moreover, miRAP isolates miRNA not only from the cytosol and nucleus as microdissection does, but also captures functional miRNA from neuronal neurites. Therefore, it is plausible that miRNAs, which function predominantly in dendrites, axons and synapses were identified here by miRAP but not targeted by the microdissected motor neuronal cell bodies. Finally, Juźwik et al. compared dissected neurons from three different animals per group, whereas the miRAP in this work was performed from 3 animals per sample and in total 5 samples per group, thereby covering more biological and technical replicates likely manifesting in more robust results. However, miR 223-3p was not found upregulated in retinal neurons, indicating that this miRNA has a specific function in motor neurons in CNS-inflammation. Therefore, research concentrated on the neuroprotective role of miR-223 in CNS-inflammation in EAE[211] and stroke and was shown to regulate expression of glutamate receptors, thereby ameliorating neuronal glutamate responsiveness at the postsynaptic site[212]. miR-223 was shown to ameliorate EAE clinical symptoms, however deletion also affected the immune response of T_H cells[313]. By the here performed miRAP miR-223-3p was identified upregulated, but also its passenger strand miR-223-5p, further consolidating an important role for miR-223 in inflamed

motor neurons. The overrepresentation analysis in this work additionally showed that miR-223-3p and also miR-92a-3p were most likely to effectively regulate their mRNA targets in inflamed motor neurons compared to the other 22 identified miRNA candidates. Recently, a study that performed *in situ* hybridizations showed that miR-92a-3p is highly and almost exclusively expressed by motor neurons of the healthy mouse spinal cord[242]. For miR-92a-3p no EAE deletion had been investigated until now. A strong upregulation of miR-92a-3p in EAE spinal cord homogenate was demonstrated by qRT-PCR previously, but no cell-type specific profiling was performed by the authors. By investigating miR-92a-3p function in splenocytes *in vitro* the upregulation in EAE spinal cord had been hypothetically linked to immune function[240]. However, miRNA profiling studies from EAE splenocytes and MS PBMCs did not report an upregulation of miR-92a-3p[314-316]. Here, it was shown that miR-92a-3p was highly induced by motor neurons in EAE, however which cell type besides motor neurons contributed to increased miR-92a-3p expression in inflamed spinal cord is yet unclear. Nonetheless, it is unlikely that infiltrating immune cells expressed elevated miR-92a-3p. Also, it remains enigmatic why differential expression of miR-92a-3p was not identified in the microdissected motor neurons[188]. In the here reported data set miR-92a-3p was together with miR-223-3p not only most powerful in repressing its predicted targets but also potentially regulated most of its predicted targets compared to the other miRNA candidates. For future experiments the investigation of spatiotemporal expression of miR-92a-3p by *in situ* hybridization of EAE spinal cord would be enlightening. This would enable determining whether its expression differs in motor neuronal somata versus neurites, thereby providing an explanation for the divergent miRNA screening results and additionally hinting towards target specificity and function of miR-92a-3p.

Apparently, many of the 22 deregulated miRNA candidates were previously found deregulated in MS post-mortem brain tissue[206], MS biofluids such as serum, plasma and CSF[151] and tissue of mouse and marmoset EAE[317]. A couple of miRAP-identified motor neuronal candidates were also described as promising biomarkers for MS diagnosis and progression[151,192,194]. However, the expression of most of the miRAP-identified inflammatory miRNAs was not restricted to motor neurons and also identified in other diseases besides MS and EAE previously[259]. Therefore, single miRNAs seem not to be suited as biomarkers for MS or EAE rather than a signature of miRNAs. It appears plausible that these miRNAs are involved in general important cellular stress response networks and were therefore identified in various diseases and different cell types previously. Certainly, a variety of miRNA function is still to be investigated in the future. Nonetheless, these miRNAs seem to represent important regulatory molecules to buffer the motor neuronal contingencies that were caused by CNS-inflammation and might as a signature indicate motor

neuronal loss. Therefore, the here reported results constitute a valuable resource to study the role of neuronal miRNAs in inflammation-induced neurodegeneration.

5.2 Profiling of gene regulatory networks in CNS-inflammation

5.2.1 Screening of neuronal miRNA–mRNA networks

The second aim of this work was to identify the target mRNAs and pathways that were regulated by the in this work identified miRNA signature in inflamed motor neurons. Therefore, motor neuronal mRNAs were profiled by TRAP[274] as reported previously[273]. Interestingly, the network analysis showed that some of these miRNAs closely cooperated on regulating certain 'hub genes', whereas some miRNAs rather functioned on their own and regulated only few targets. The most interesting interaction was observed between miR-92a-3p, miR-223-3p, mir-142-3p, 146b-5p, miR-199a-3p and miR-673-5p, which together acted on the hub genes family with sequence similarity 199, X-linked (*Fam199x)*, neurexophilin-1 *(Nxph1)*, ST6 beta-galactoside alpha-2,6-sialyltransferase 2 (*St6gal2)*, Sestrin 3 (*Sesn3)*, DCN1-like protein 4 (*Dcun1d4)* and WASP like actin nucleation promoting factor (*Wasl).* At a first glance it appears that these genes are involved in neuronal morphological and regenerative processes and were all associated to diseases previously. *Nxph1* and *Wasl* were described to be involved in synaptic morphological processes*. Nxph1* was shown to interact with α-neurexins and to stabilize synapses, thereby modulating short-term plasticity[318]. The neural gene *Wasl* was implicated in cytoskeleton remodeling by regulating actin in dendritic spines and synapses[319]. *Sesn3* was shown to negatively regulate levels of intracellular ROS[320] and is currently investigated as neuroprotective target in Alzheimer's[321]. *St6gal2* and *Dcun1d14* were associated with post-translational protein modifications. *St6gal2* was shown to be a brain-enriched sialyltransferase, which might exert a neuron-specific function[322], whereas *Dcun1d14* was described to function as a ligase for NEDD8 in the neddylation pathway, thereby being involved in protein turnover[323] and described as a risk variant in the development of frontotemporal lobe degeneration[324]. Little is known about the X-linked protein-coding gene *Fam199x*, however it has been recently shown to stabilize ataxin-2 mRNA, which negatively influences toxic TDP-43 aggregation in a mouse model of ALS[260,325]*.* Thus, a miRNA-mediated downregulation of *Fam199x* might be a neuroprotective target for ALS. How this interaction, the expression of these miRNAs and these genes was regulated in motor neurons in CNS-inflammation is yet unknown, however a combinatorial targeting of these miRNAs and their hub genes might uncover unforeseen therapeutic strategies for neurodegenerative diseases.

To identify the biological pathways that the here identified 22 miRNA targets represented, a gene list enrichment analysis was performed. Interestingly, overrepresented gene set clusters, which were potentially downregulated by miRNAs in inflamed motor neurons were basic neuronal pathways that regulate morphological structure and synaptic signaling, rather than immune cell related or cell death pathways as it was described for many here identified miRNAs previously. This demonstrates clearly how important co-profiling of miRNAs and their targets is in order to identify miRNA-mediated cell type-specific function. How exactly the miRNA regulation and cooperation on these pathways was governed in motor neurons in CNS-inflammation and their functional role is unclear and has to be experimentally investigated. Indeed, previous examinations indicate a neuroprotective role of miR-223-3p and miR-92a-3p upregulation however, induction of miR-142a-3p and miR-155-5p seems to be rather neurodegenerative[202,210,257]. However, the chronic cellular stress might also impair regulatory feedback mechanisms that might be responsible for the observed increase in miRNA expression[326]; which is eventually neuroprotective in the beginning of the disease, but emanates in excitotoxicity over time. Therefore, when miRNAs are considered to be used therapeutically the timing of miRNA-based therapy certainly has to be recognized. Until now, the function and interaction of the identified regulatory miRNA network is poorly understood, but constitutes a valuable resource to study complex neuronal miRNA–mRNA networks in a cell-type specific manner in CNS-inflammation.

5.2.2 Revealing the miR-92a-3p–*Cpeb3* regulatory network

To reveal the direct functional contribution of miR-92a-3p in motor neurons in CNS-Inflammation its target genes were identified and prioritized by including evidence for effective experimental downregulation upon miR-92a-3p overexpression[231]. Interestingly, this overlap analysis resulted in 29 potential miR-92a-3p targets, which were significantly downregulated in motor neurons in EAE as shown by TRAP. To reveal whether these targets were involved in the same biological processes, a gene set enrichment analysis was performed. Markedly, these 29 target genes were involved in a huge variety of general intracellular and neuron-specific biological processes, indicating that these genes are ‘multitalented’ regulatory molecules themselves. Therefore, to prioritize predicted miR-92a-3p targets, they were further stratified by the strength of computational evidence to measure miRNA efficacy[179]. Intriguingly, the RNA-binding protein *Cpeb3* was unambiguously qualifying as the top downregulated miR-92a-3p target, with five potential binding sites, in inflamed motor neurons in CNS-inflammation. However, the transcriptional regulation and functional relevance of this network is mostly unknown.

5.2.3 Analysis of neuronal miR-17/92 cluster gene expression

As described above, miR-92a-3p belongs to the polycistronic miR-17/92 cluster, which is encoded by *Mir17HG* and contains five other miRNAs[184]. Since it is believed that cluster-miRNAs are often co-transcribed to cooperate on biological pathways[326,327], the other miR-17/92 cluster miRNAs were analyzed in healthy and inflamed spinal cord and motor neurons (miRNA screening data) to reveal whether they might also regulate translation of motor neuronal genes in CNS-inflammation. A contribution to motor neuronal development and differentiation from other miR-17/92 cluster miRNAs was shown[229,244]. However, it is likely that the expression pattern and function of these miRNAs changed during development and especially during cell stress, as it was described for many miRNAs[164,327]. Concordantly, the analysis revealed that the other miRNA members from that cluster were much less expressed in healthy motor neurons than miR-92a-3p and were also not robustly induced by CNS-inflammation in the two investigated cohorts. Diverse mechanisms to achieve differential cluster miRNA expression have been reported as tertiary structure, miRNA stability as well as biogenesis favoring factors leading to faster processing of the mature miRNA[328]. However, the differential regulation of miR-17/92 cluster miRNAs in differentiated healthy and inflamed motor neurons is poorly understood. The here reported results imply, that miR-92a-3p expression is differentially regulated in healthy and inflamed motor neurons in comparison to the other cluster miRNAs and therefore implies an important cell type-specific function. However, until now the mechanism that drives enhanced miR-92a-3p expression in motor neurons is unknown.

5.3 Validation of the neuronal miR-92a-3p network

5.3.1 Analysis of the transcriptional regulation of miR-92a-3p and *Cpeb3*

The third aim of this work was to validate the identified neuronal miR-92a-3p–*Cpeb3* network. To elucidate the stimulus that was driving motor neuronal miR-92a-3p expression in CNS-inflammation, the effects of two major neuronal stressors that induce neurodegeneration in EAE, extracellular glutamate and pro-inflammatory cytokines[118,329,330] were examined. Fascinatingly, miR-92a-3p expression was induced by only extracellular glutamate in a dose-dependent manner, whereas cytokines did not produce these changes. Therefore, it seems that miR-92a-3p expression was induced upon chronic activation of glutamatergic receptors. Bicuculline did not lead to an upregulation of miR-92a-3p, indicating that extrasynaptic but not synaptic receptor activation[112] induced miR-92a-3p expression. Interestingly, extrasynaptic glutamate receptors were discussed to particularly induce glutamate excitotoxicity[112,113], indicating that miR-92a-3p is involved in rather mediating chronic excitotoxic glutamate stimulation than physiological synaptic

activity. However, miR-92a-3p was also reported to play a role in homeostatic processes in synaptic scaling[257], learning and memory[256] and seems to be regulated in an activity-dependent manner. Upregulation of miR-92a-3p was reported during contextual fear learning[256] in the hippocampus of mice and downregulation of miR-92a-3p was shown upon activity blockade with TTX and AP5 in primary hippocampal neurons[257]. Physiological induction of EPSCs by bicuculline is usually obtained after a few minutes already[112]. However, in this work neurons were sampled after 24 hours to determine miR-92a-3p expression that might have receded upon bicuculline stimulation over time. Further, physiological EPSCs might only induce small local changes of miR-92a-3p expression to regulate homeostatic synaptic processes[256,257,331], which might only be detectable when synaptosomes were isolated by cell fractionation. Even if bicuculline treatment in the experimental setup here did not induce miR-92a-3p, it is not excluded that miR-92a-3p is upregulated also during physiological neuronal activity.

Also, the potential miR-92a-3p target *Cpeb3* was analyzed. Bicuculline and cytokines did not influence on *Cpeb3* levels as observed for miR-92a-3p before. However, *Cpeb3* was significantly downregulated upon increasing doses of extracellular glutamate, which correlated significantly with glutamate-mediated miR-92a-3p upregulation. Therefore, it is possible that *Cpeb3* downregulation was caused by a translational inhibition of miR-92a-3p[175]. However, to validate the effects on glutamate-mediated translational repression by miR-92a-3p the protein levels of CPEB3 had to be investigated additionally. About the regulation of *Cpeb3* mRNA is not much known. Mostly CPEB3 protein levels and its role in hippocampal plasticity in learning and memory was debated. It was described that CPEB3 protein was upregulated 15 minutes after kainate injection[332] in the mouse hippocampus. Further, it was shown that 30 minutes of glutamate stimulation in primary hippocampal neurons, long-term potentiation (LTP) induction in the CA1 and contextual fear conditioning induced the expression of CPEB3[333]. Interestingly, contextual fear conditioning caused CPEB3 oligomerization at the synapse, which was shown to be required for memory of hippocampal contextual fear conditioning[333]. Contrarily, NMDA-mediated degradation of CPEB3 in hippocampal neurons was reported after 1-3 hours previously[254]. Also, a downregulation of CPEB3 was reported after 90 minutes of contextual fear conditioning in the hippocampus[256]. Therefore, it is likely that different types of glutamate receptors as well as strength of neuronal activation differentially effect CPEB3 levels. Since synaptic plasticity requires quick changes in protein expression and composition at the synapse[334] a time-dependent regulation of CPEB3 after neuronal activation is likely. However, the effects on *Cpeb3* mRNA and the mechanisms of *Cpeb3* translation were not addressed in these studies. Also, the long-term effects of glutamate excitotoxicity and CNS-inflammation on CPEB3 expression were not investigated and are mostly unknown. To finally elucidate the interaction of the miR-92a-3p–

Cpeb3 network upon neuronal activity, different glutamate receptor agonists and antagonists as well as different LTP protocols have to be applied and the expression of miR-92a-3p and *Cpeb3* mRNA and protein determined at different acute and chronic time points. Altogether, these results indicate that miR-92a-3p and *Cpeb3* interact and might play a role in physiological glutamatergic signaling and particularly in glutamate excitotoxicity in CNS-inflammation.

Finally, it was investigated here whether miR-92a-3p was transcriptionally regulated by exploring *MiR17HG* levels. *MiR17HG* was transcriptionally induced by only extracellular glutamate in a dose-dependent manner as shown for miR-92a-3p, whereas cytokines and bicuculline did not produce expressional changes. Certainly, it is inquired to identify those factors that drive enhanced *MiR17HG* expression upon extracellular glutamate. Many different transcription factors as myc proto-oncogen, max-interactor 1, signal transducer and activator of transcription 3 and all members of the E2 factor transcription factor family were shown to occupy the *Mir17HG* promoter region and described to regulate *Mir17HG* expression in different cell types and disease[184]. However, nothing is reported for glutamate excitotoxicity in EAE or MS. Interestingly, *Mir17HG* was also significantly induced in inflamed motor neurons as shown by TRAP. Therefore, it is possible that neuronal induction of miR-92a-3p in acute EAE originated increased *Mir17HG* expression that was transcriptionally mediated by extracellular glutamate[184]. Further, it is plausible that this regulation is not specific to EAE or MS, but might also apply to other CNS-diseases where glutamate excitotoxicity plays a role. Future experiments would be to explore and validate the transcription factors as well as epigenetic modifications that related to the induced glutamate-dependent transcription and to elucidate by which type of glutamate receptors these pathways were mediated.

5.3.2 Validation of *Cpeb3* regulation by miR-92a-3p

Secondly, to test whether miR-92a-3p indeed regulated *Cpeb3* levels in neurons a miRNA target gene luciferase reporter assay was performed. By conducting the reporter assay in a neuronal cell line (N2a), a specific translational inhibition of *Cpeb3* by miR-92a-3p interaction with the 3'UTR was validated. An interaction of miR-92a-3p with the *Cpeb3* 3'UTR was also reported by others previously[245,256], corroborating the in this work obtained results. Until now a functional link between miR-92a-3p and *Cpeb3* has only been shown in hippocampal fear learning. It was demonstrated that miR-92a-3p expression is induced upon contextual fear conditioning in the hippocampus of mice, accompanied by a downregulation of CPEB3[256]. Interestingly, injection of a miR-92a-3p inhibitor led to increased CPEB3 and impaired contextual fear conditioning[256]. This functional link of the miR-92a-3p–*Cpeb3* network was only shown for hippocampal leaning so far, however the function of this network in CNS-inflammation is still to be investigated.

5.3.3 Investigation of the miR-92a-3p and *Cpeb3* downstream target *Gria1*

To elucidate a potential functional role of the miR-92a-3p–*Cpeb3* network in neurons the expression of a mutual downstream target of miR-92a-3p and CPEB3 was examined. miR-92a-3p was shown to regulate expression of *Gria1* during homeostatic synaptic scaling in excitatory hippocampal neurons[257]. It was shown, that upon activity blockade a downregulation of miR-92a-3p led to a decreased translational repression of *Gria1* and thereby increased AMPA receptor subunit GluA1 expression at the postsynaptic site. However, it was not investigated whether activation of synaptic glutamate receptors induced miR-92a-3p expression vice versa, which would lead to reduced translation of *Gria1*[257]. Here, it was shown that *Gria1* was downregulated upon excitotoxic levels of glutamate and negatively correlated with miR-92a-3p upregulation, indicating a possible relationship. Interestingly, CPEB3 was shown to act as a translational repressor of *Gria1*[246,251,252]. However, in this work neuronal *Cpeb3* and *Gria1* expression positively correlated upon stimulation with extracellular glutamate. It might be that the miR-92a-3p–*Cpeb3* network builds a feedback loop that tightly controls the expression levels of GluA1, most likely in an activity-dependent manner. In this feedback loop, CPEB3 would constitute the molecular switch, which expression is controlled by activity-regulated miR-92a-3p. Induction of miR-92a-3p would reduce CPEB3 levels, leading to a re-repression of *Gria1* and its translation, whereas remaining miR-92a-3p would outbalance *Gria1 by* preventing surplus translation. Such miRNA networks were suggested to be much more common in neurons than translational repression of single genes[335]. Upon excitotoxic glutamate, this feedback loop might be disturbed by excessive miR-92a-3p overexpression, thereby inducing a shut-down of GluA1 and CPEB3. This shut-down might prove to be neuroprotective by reducing glutamate-mediated downstream events, similar to what was reported for miR-223-3p previously[212]. A functional link between reduced *Cpeb3* and *Grai1* expression levels might be, that CPEB3 plays a role in mediating *Gria1* transport to the synapse[253]. However, whether *Gria1* expression was functionally linked to miR-92a-3p or to *Cpeb3* expression is still to be validated. An important factor that impedes interpretation of these results is that only mRNA levels but not the protein levels of CPEB3 and GluA1 were investigated upon glutamate stimulation in this work. Further, CPEB3 functionality is highly determined by post-transitional modifications and aggregation[248-250], which also had to be examined to better understand the regulatory impact on *Gria1*. Certainly, it has to be considered that a possible physiological feedback loop between miR-92a-3p, *Cpeb3* and *Gria1* might differentiate from chronic glutamate excitotoxicity and other neurodegenerative mechanisms in CNS-inflammation. It might be possible that the downregulation of CPEB3 and GluA1 were simultaneously mediated by induced miR-92a-3p upon neurotoxic levels of extracellular glutamate, but exerted different neuroprotective effects. Relating thereto, CPEB3

aggregation was reported upon overt neuronal stimulation[248,249], therefore it might be that CPEB3 also aggregates upon excessive extracellular glutamate and might thus promote neurodegeneration as reported for different proteins in primary neurodegenerative diseases[40,41] and for EAE and MS recently[273]. Nevertheless, the proposed hypotheses are still to be thoroughly investigated.

However, miR-92a-3p-mediated post-transcriptional regulation of *Cpeb3* seems to be a powerful tool to eventually mediate various neuronal changes as translation of different postsynaptic genes inter alia *Gria1* and might exert important neuronal function in glutamate excitotoxicity and CNS-inflammation. Therefore, it is highly interesting to further investigate the functional relationship between the miR-92a-3p–*Cpeb3* network and potential neuroprotective downstream effects as translational regulation of *Gria1* in inflamed motor neurons in EAE.

5.4 Deletion of miR-92a-3p in CNS-inflammation

5.4.1 Characterization of *Mir92-1* knockout mice

The fourth aim of this work was to identify whether miR-92a-3p deletion had a functional impact on CNS-inflammation. The initial publication that designed and reported the miR-17/92$^{\Delta 92/\Delta 92}$ mice observed no phenotypic changes nor differences in the development and numbers of B cells and T cells[232]. However, as also mentioned by the authors some of the phenotypic deficiencies resulted in more severe phenotypes during backcrossing into a pure *C57BL/6* genetic background, since the miR-17/92$^{\Delta 92/\Delta 92}$ mice were created in mixed *B6-129* mice[232]. Later, it was published that miR-17/92$^{\Delta 92/\Delta 92}$ mice were much lighter and had a skeletal deficiency[237]. Therefore, prior to EAE induction miR-17/92$^{\Delta 92/\Delta 92}$ knockout mice were carefully characterized here. By analyzing the mean weight of adult mice, a significant decrease of weight was observed. Further, miR-17/92$^{\Delta 92/\Delta 92}$ mice were not born according to mendelian ratios as their heterozygous and homozygous littermates, indicating a developmental defect that might prefer abortion of miR-17/92$^{\Delta 92/\Delta 92}$ mice. A difference in newborn male and female mice was not observed. However, it has to be recognized that the miR-17/92$^{\Delta 92/\Delta 92}$ phenotype might impact on functional studies. Additionally, miR-17/92$^{\Delta 92/\Delta 92}$ knockout mice were validated by qRT-PCR and showed significant deletion of miR-92a-3p in neurological (CNS) and immunological tissues (spleen, lymph nodes). Importantly, no compensational expression of *Mir17HG* was observed.

5.4.2 Effects of *Mir92-1* deletion on clinical disability in EAE

Deletion of miR-92a-3p in miR-17/92$^{\Delta 92/\Delta 92}$ mice resulted in exacerbated clinical disability in comparison to wild-type littermates, which presented as an overshoot of disability in the acute

phase and diminished recovery of symptoms in the chronic phase in two independent EAE experiments. The exacerbated clinical symptoms were further accompanied by a higher relative weight loss and impaired recovery of the starting weight. Deletion of miR-92a-3p showed a robust, but moderate increase in EAE clinical disability, implicating that the regulatory miR-92a-3p network is required in order to sustain homeostatic cellular function. However, it is yet unclear, by which mechanisms miR-92a-3p deletion led to increased disability in EAE. As mentioned before, previous investigations indicate a neuroprotective function of miR-92a-3p overexpression. It is possible, that miR-92a-3p would act neuroprotective by repressing CPEB3 and GluA1 expression upon high levels of extracellular glutamate, which were identified in EAE[118], thereby ameliorating glutamate excitotoxicity and neuronal loss. However, as mentioned above functionality of miR-92a-3p was postulated in nervous as well as immunological tissue[240,256]. Thus, the cellular components and cell types contributing to the here observed phenotype were investigated in immune cell populations and neurons.

5.4.3 Immunophenotyping of *Mir92-1* knockout EAE

The effects of miR-92a-3p deletion on immune cell function were analyzed to identify the cell types that were implicated in the exacerbated EAE clinical disability. Unfortunately, no neuron-specific miR-92a-3p knockout existed to directly investigate the neuronal function of miR-92a-3p on CNS-inflammation, which was the primary interest of this work. However, to rule out involvement of miR-92a-3p in immune responses in EAE, miR-17/92$^{\Delta 92/\Delta 92}$ mice had to be immunophenotyped. However, no significant differences in either total immune cell numbers (CD45^{+}), absolute numbers of each immune cell subpopulation nor significant differences in immune cell type frequencies were identified between miR-17/92$^{\Delta 92/\Delta 92}$ and wild-type mice. A functional role of miR-92a-3p was shown in murine T_H and T_H17 cells in EAE[240]. In the here utilized FC panel T_H17 cells were not specifically investigated, however infiltrating CD4^{+} T cell subsets were not changed in absolute numbers or frequencies between miR-17/92$^{\Delta 92/\Delta 92}$ and wild-type mice. Also, no differences in the absolute numbers and frequencies of CNS-infiltrating B cells were observed, in which miR-92a-3p was described to be involved during development[336]. However, it is not excluded that with a more fine-grained FC panel the numbers and frequencies of different immune cell populations would differ from the herewith reported results. Nonetheless, this would rather refer to the numbers of immune cell subpopulations than to the differences observed between miR-17/92$^{\Delta 92/\Delta 92}$ and wild-type mice, since the cell populations in both groups were analyzed in the exact same way. Further, no activation markers as CD44, CD69 or CD25 were included in the utilized FC panel, therefore no conclusions regarding a differential activation status in miR-17/92$^{\Delta 92/\Delta 92}$ mice can be made. However, to enter the CNS most of the infiltrated immune cells are activated anyways, therefore the implication of activation markers would not

necessarily add valuable insights[337]. Relating thereto it was shown that miR-92a-3p overexpression in $CD4^+$ T cells rather leads to their activation as shown by increased IFN-γ production[240], implying that the activation status of T_H cells would be decreased and not enhanced in miR-17/92$^{\Delta 92/\Delta 92}$ mice. Therefore, such changes are unlikely to have caused exacerbated clinical disability in EAE upon miR-92a-3p deletion. Further, miRNA profiling in RRMS PBMCs[315] or EAE splenocytes[317] did not report differential expression of miR-92a-3p, implicating no function of this miRNA in immune responses in CNS-inflammation, maintaining the here obtained results.

5.4.4 Neurophenotyping of *Mir92-1* knockout EAE

Lastly, the effects of miR-92a-3p deletion on neurodegeneration were analyzed to identify the neuron-specific effects of miR-92a-3p that were proposed in this work. Therefore, mice were examined after 30 days of EAE. However, no significant differences in neuronal impairment on a morphological level were identified between both groups that would correlate with the clinical EAE symptomatology overserved in miR-17/92$^{\Delta 92/\Delta 92}$ mice. It is nevertheless possible that a potential exacerbated neuronal impairment in miR-17/92$^{\Delta 92/\Delta 92}$ mice would rather be detectable at acute EAE when the spinal cord was massively inflamed and when the significant induction of miR-92a-3p was observed. However, also healthy miR-17/92$^{\Delta 92/\Delta 92}$ mice had to be neurophenotyped, since a role of miR-92a-3p was shown during neuronal development and differentiation. It was shown that miR-92a-3p regulated the transition of radial glia cells to intermediate progenitors, which then symmetrically divide into post-mitotic neurons[235]. It was shown that knockout of the miR-17/92 cluster also led to increased levels of intermediate progenitors, thereby most likely producing more post-mitotic neurons[235,338]. However as shown for motor neurons, specific deletion of the miR-17/92 cluster led to aberrant generation of motor neurons during development, but induced degeneration in differentiated motor neurons[244]. Altogether, it would be informative to examine whether healthy miR-17/92$^{\Delta 92/\Delta 92}$ mice showed differences in the number of motor neurons and other neuronal population of the spinal cord in comparison to wild-type littermates and whether differentiated motor neurons that lack miR-92a-3p were less protected against neurodegenerative processes in CNS-inflammation. Importantly, examination of postsynapses had to be included into the pathological analysis, since the postulated miR-92a-3p network is believed to mainly regulate postsynaptic genes[257,331]. However, it is still possible that functional neuronal impairment due to loss of regulatory miR-92a-3p is rather observed on a molecular level and does not manifest into morphological changes or neuronal loss. Therefore, electrophysiological examinations would provide insight into a functional impairment of neurons in healthy and EAE-induced miR-17/92$^{\Delta 92/\Delta 92}$ mice and wild-type littermates.

5.5 Therapeutic potential of motor neuronal miRNAs

miRNA targeting approaches were investigated mainly to debilitate the inflammatory insults that drive development of EAE[207,339], even if a dual role in immune and nervous system regulation was shown for many here identified miRNAs[202,210]. Still only few reports focused on neuroprotective miRNA targeting. As described above, miRNAs seem to particularly play a functional role in motor neurons[309]. Many of the miRAP-identified inflammation-induced motor neuronal miRNAs were induced from very low or even no expression. On the contrary, four miRNAs had a high expression in healthy motor neurons already, implying an important physiological function without inflammation. Among these miRNAs were miR-92a-3p and miR-143-3p and have all been associated with MS[187,194] and EAE before[188,206,240]. Further, they were previously associated with neuronal function and motor neuron diseases, particularly with ALS[242,340,341], maintaining an important functional role in motor neuronal integrity and survival. Interestingly, miR-143-3p was associated with ALS and found deregulated upon TDP-43 mutation in a mouse model of ALS[342]. In this work it was shown that miR-143-3p is highly induced by CNS-inflammation but particularly expressed by healthy motor neurons. Therefore, it is possible that upregulated miR-143-3p in serum and CSF of ALS patients originated unspecific motor neuronal degeneration[341,343]. Some reports indicated a deleterious role of miR-143-3p in motor neuron disease due to its pro-apoptotic function in cancer[344], however the function in ALS is yet unclear. A recent study used ASOs to markedly increase survival of motor neurons and associated motor functions in a mouse and rat model of ALS by reducing ataxin-2 levels, which were shown to suppress toxic aggregation of TDP-43[260]. Since TDP-43 aggregation occurs in nearly all cases of ALS[345], ASO targeting of ataxin-2 might represent a broadly effective therapy for ALS in humans. However, these insights indicate that miR-143-3p modulation might be a valuable therapeutic strategy to directly reduce levels of TDP-43 and ameliorate motor neuronal death in ALS. However, miR-143-3p deregulation was also reported for MS. A biomarker study identified miR-143-3p as negatively correlating with lesion-based brain tissue destruction in two independent cohorts, thereby termed ‘protective’ miRNA[194]. Concordantly, miR-143-3p levels correlated negatively with brain tissue damage and minimal cognitive impairment in Alzheimer’s patients and were found to be decreased in vascular dementia in comparison to HCs[346]. miR-143-3p was ascribed a potential role in neuroprotection and repair by regulating proliferation, survival and differentiation of neuronal stem cells[347]. Together, all hints towards a neuroprotective role of miR-143-3p, however the contribution to (motor) neuronal survival in CNS-inflammation in EAE and MS is still to be investigated.

In general miRNA targeting as a therapeutic strategy is appealing, since a network of regulation and homeostatic buffering[164,180] would be provided instead of disturbing functionality of single molecules, proteins or receptors, which might be interfering in general brain function[120]. The here identified highly expressed motor neuronal miRNAs miR-143-3p and miR-92a-3p implicate an important functional role in motor neuronal integrity and survival and might be suited as therapeutic targets by stabilizing their expression to prevent motor neuronal damage or loss in MS.

5.6 Outlook

5.6.1 Functional relevance of the miR-92a-3p–*Cpeb3* network in CNS-inflammation

First, to identify the direct neuroprotective effects of miR-92a-3p the survival of primary neurons that were overexpressed with miR-92a-3p and exposed to neuroinflammatory stimuli as toxic levels of glutamate have to be assessed. Secondly, miR-92a-3p-mediated CPEB3 downregulation has to be verified. Therefore, CPEB3 expression has to be examined in miR-92a-3p overexpressing primary neurons as well as in EAE spinal cord motor neurons of miR-17/92$^{\Delta 92/\Delta 92}$ mice and wild-type littermates. To finally elucidate whether proposed downregulation of *Cpeb3* exerts improved neuronal survival in CNS-inflammation, neuron-specific CPEB3 knockout mice[252] have to be induced with EAE and their clinical outcome determined. Finally, the effects of a potential neuroprotective CPEB3 downregulation by lack of regulation of synaptic mRNAs, lack of synaptic transport of these mRNAs or reduced CPEB3 aggregation as observed for proteins in primary neurodegenerative diseases[348] and for EAE and MS[273] is still to be investigated. Importantly, deregulation of the miR-92a-3p–*Cpeb3* network has to be validated in MS patients by staining neuronal miR-92a-3p and *Cpeb3* mRNA and protein, as well as CPEB3 aggregation in post-mortem tissue.

Basically, two different neuroprotective strategies could be persecuted to achieve CPEB3 downregulation. First, miR-92a-3p overexpression by a miRNA mimic or virus-mediated delivery could be applied to target *Cpeb3* or rather a broader spectrum of deregulated targets and pathways. Secondly, *Cpeb3* might be targeted directly by a specifically designed ASOs that would more effectively inhibit *Cpeb3* translation without off-target effects that could occur upon therapeutic application of miR-92a-3p. Lastly, CPEB3 function might be also targeted directly by application of the RNA oligomer SELEX 1904, which was shown to compete with binding of its target mRNAs[246,299]. If a neuroprotection by CPEB3 inhibition proves effective in reducing neuronal dysfunction and improves clinical disability in EAE, this approach might be a novel therapeutic strategy for MS patients.

5.6.2 Final remarks

Altogether, this work offers a starting point in investigating complex epigenetic and transcriptomic regulatory networks in CNS-inflammation. This work constitutes a valuable resource to study neuronal as well as motor neuron-specific miRNA function, the role of downregulated neuronal genes and pathways and complex miRNA–mRNA networks in inflammation-induced neurodegeneration. Importantly, this work offers potential miRNA-based therapy that might re-balance neuronal signaling and eventually modulate glutamate downstream events to act neuroprotective without disrupting endogenous brain function. However, the strategy of this work was to rather investigate miRNA-regulated pathways in order to identify cell type-specific molecules such as CPEB3, which might in the future constitute a beneficial therapeutic target for neurodegeneration in MS and EAE.

6 Summary

Multiple sclerosis (MS) is characterized by immune cell infiltration, axonal demyelination and neurodegeneration. Excessive activation of the glutamatergic pathway accompanies MS pathophysiology resulting in neuronal stress response networks with alteration of neuronal signaling, thereby perpetuating neurodegeneration and consecutive neurological deficits. A fundamental mechanism to respond to changes in the cellular environment is coordination of translation by microRNAs (miRNAs). However, it remains unclear to which extend miRNAs orchestrate neuronal gene expression and determine consecutive neurodegeneration in central nervous system (CNS)-inflammation. By targeted profiling of neuronal transcriptome and miRNome in CNS-inflammation it was demonstrated here that genes involved in neuronal regulatory processes and synaptic signaling were significantly underrepresented, while at the same time newly identified inflammation-induced miRNAs were predicted to target these mRNA transcripts. It was shown in this work that miR-92a-3p was highly expressed in healthy motor neurons and transcriptionally upregulated by extracellular glutamate. Luciferase reporter assays validated cytoplasmic polyadenylation element-binding protein 3 (*Cpeb3*) mRNA as a miR-92a-3p target. Further, deletion of miR-92a-3p in the MS mouse model experimental autoimmune encephalomyelitis (EAE) led to exacerbated neurological disability, but unchanged immune cell infiltration, implying a neuronal function of miR-92a-3p induction. Yet, the neuronal substrate of miR-92a-3p deletion that caused exacerbated clinical disability in CNS-inflammation is still to be investigated. In future studies, the interaction network of miR-92a-3p and *Cpeb3* and their implications for neuronal survival in CNS-inflammation and glutamate excitotoxicity will be investigated in mouse models and validated in MS patients. Together, this work offers a new approach for deciphering the contribution of miRNA networks to synaptic function and neuronal integrity in CNS-inflammation with possible implications for the treatment of MS-associated neurodegeneration.

7 Bibliography

1 Lassmann, H. Multiple Sclerosis Pathology: Evolution of Pathogenetic Concepts. *Brain Pathol* **15**, 217-222 (2006).

2 Lublin, F. History of modern multiple sclerosis therapy. *J Neurol* **252**, iii3-iii9 (2005).

3 Popescu, B. F. G., Pirko, I. & Lucchinetti, C. F. Pathology of Multiple Sclerosis: Where Do We Stand? *Continuum (Minneap Minn)* **19**, 901-921 (2013).

4 Compston, A. & Coles, A. Multiple sclerosis. *Lancet* **372**, 1502-1517 (2008).

5 Calabrese, M. *et al.* Exploring the origins of grey matter damage in multiple sclerosis. *Nat Rev Neurosci* **16**, 147-158 (2015).

6 Friese, M. A., Schattling, B. & Fugger, L. Mechanisms of neurodegeneration and axonal dysfunction in multiple sclerosis. *Nat Rev Neurol* **10**, 225-238 (2014).

7 Filippo, M. D., Portaccio, E., Mancini, A. & Calabresi, P. Multiple sclerosis and cognition: synaptic failure and network dysfunction. *Nat Rev Neurosci* **19**, 599-609 (2018).

8 Brownlee, W. J., Hardy, T. A., Fazekas, F. & Miller, D. H. Diagnosis of multiple sclerosis: progress and challenges. *Lancet* **389**, 1336-1346 (2017).

9 Collaborators, G. B. D. C. R. D. *et al.* Global, regional, and national deaths, prevalence, disability-adjusted life years, and years lived with disability for chronic obstructive pulmonary disease and asthma, 1990–2015: a systematic analysis for the Global Burden of Disease Study 2015. *Lancet Respir Med* **5**, 691-706 (2017).

10 Dendrou, C. A., Fugger, L. & Friese, M. A. Immunopathology of multiple sclerosis. *Nat Rev Immunol* **15**, 545-558 (2015).

11 Sand, I. K. Classification, diagnosis, and differential diagnosis of multiple sclerosis. *Curr Opin Neurol* **28**, 193-205 (2015).

12 Reich, D. S., Lucchinetti, C. F. & Calabresi, P. A. Multiple Sclerosis. *New Engl J Med* **378**, 169-180 (2018).

13 Stys, P. K. Pathoetiology of multiple sclerosis: are we barking up the wrong tree? *F1000prime Reports* **5**, 20 (2013).

14 Trapp, B. D. & Nave, K.-A. Multiple sclerosis: an immune or neurodegenerative disorder? *Annu Rev Neurosci* **31**, 247-269 (2008).

15 Belbasis, L., Bellou, V., Evangelou, E., Ioannidis, J. P. A. & Tzoulaki, I. Environmental risk factors and multiple sclerosis: an umbrella review of systematic reviews and meta-analyses. *Lancet Neurol* **14**, 263-273 (2015).

16 Marrie, R. A. Environmental risk factors in multiple sclerosis aetiology. *Lancet Neurol* **3**, 709-718 (2004).

17 Leray, E., Moreau, T., Fromont, A. & Edan, G. Epidemiology of multiple sclerosis. *Rev Neurol* **172**, 3-13 (2015).

18 Rooks, M. G. & Garrett, W. S. Gut microbiota, metabolites and host immunity. *Nat Rev Immunol* **16**, 341-352 (2016).

19 Berer, K. *et al.* Commensal microbiota and myelin autoantigen cooperate to trigger autoimmune demyelination. *Nature* **479**, 538-541 (2011).

20 Gödel, C. *et al.* Perturbation of gut microbiota decreases susceptibility but does not modulate ongoing autoimmune neurological disease. *J Neuroinflamm* **17**, 79 (2020).

21 Berer, K. *et al.* Gut microbiota from multiple sclerosis patients enables spontaneous autoimmune encephalomyelitis in mice. *Proc National Acad Sci* **114**, 10719-10724 (2017).

22 Tremlett, H., Bauer, K. C., Appel-Cresswell, S., Finlay, B. B. & Waubant, E. The gut microbiome in human neurological disease: A review: Gut Microbiome. *Ann Neurol* **81**, 369-382 (2017).

23 Mestre, L. *et al.* Manipulation of Gut Microbiota Influences Immune Responses, Axon Preservation, and Motor Disability in a Model of Progressive Multiple Sclerosis. *Front Immunol* **10**, 1374 (2019).

24 Gandy, K. A. O., Zhang, J., Nagarkatti, P. & Nagarkatti, M. The role of gut microbiota in shaping the relapse-remitting and chronic-progressive forms of multiple sclerosis in mouse models. *Sci Rep* **9**, 6923 (2019).

25 Cardona-Gómez, G., Mendez, P., DonCarlos, L. L., Azcoitia, I. & Garcia-Segura, L. M. Interactions of estrogens and insulin-like growth factor-I in the brain: implications for neuroprotection. *Brain Res Rev* **37**, 320-334 (2001).

26 Cooper, G. S. & Stroehla, B. C. The epidemiology of autoimmune diseases. *Autoimmun Rev* **2**, 119-125 (2003).

27 Confavreux, C., Hutchinson, M., Hours, M., Cortinovis-Tourniaire, P. & Moreau, T. Rate of Pregnancy-Related Relapse in Multiple Sclerosis. *New Engl J Medicine* **339**, 285-291 (1998).

28 Engler, J. B. *et al.* Glucocorticoid receptor in T cells mediates protection from autoimmunity in pregnancy. *P Natl Acad Sci* **114**, E181-E190 (2017).

29 Ribbons, K. *et al.* Male Sex Is Independently Associated with Faster Disability Accumulation in Relapse-Onset MS but Not in Primary Progressive MS. *Plos One* **10**, e0122686 (2015).

30 Confavreux, C., Vukusic, S., Moreau, T. & Adeleine, P. Relapses and Progression of Disability in Multiple Sclerosis. *New Engl J Med* **343**, 1430-1438 (2000).

31 Shastry, B. S. SNP alleles in human disease and evolution. *J Hum Genet* **47**, 0561-0566 (2002).

32 Canto, E. & Oksenberg, J. R. Multiple sclerosis genetics. *Mult Scler J* **24**, 75-79 (2017).

33 Hollenbach, J. A. & Oksenberg, J. R. The immunogenetics of multiple sclerosis: A comprehensive review. *J Autoimmun* **64**, 13-25 (2015).

34 Trowsdale, J. & Knight, J. C. Major histocompatibility complex genomics and human disease. *Annu Rev Genom Hum G* **14**, 301-323 (2013).

35 Kular, L. *et al.* DNA methylation as a mediator of HLA-DRB1*15:01 and a protective variant in multiple sclerosis. *Nat Commun* **9**, 2397 (2018).

36 Briggs, F. B. S. *et al.* Genome-wide association study of severity in multiple sclerosis. *Genes Immun* **12**, 615-625 (2011).

37 Baranzini, S. E. *et al.* Genome-wide association analysis of susceptibility and clinical phenotype in multiple sclerosis. *Hum Mol Genet* **18**, 767-778 (2009).

38 Baranzini, S. E. *et al.* Genetic variation influences glutamate concentrations in brains of patients with multiple sclerosis. *Brain* **133**, 2603-2611 (2010).

39 Farh, K. K.-H. *et al.* Genetic and epigenetic fine mapping of causal autoimmune disease variants. *Nature* **518**, 337-343 (2014).

40 Soto, C. & Pritzkow, S. Protein misfolding, aggregation, and conformational strains in neurodegenerative diseases. *Nat Neurosci* **21**, 1332-1340 (2018).

41 Jucker, M. & Walker, L. C. Propagation and spread of pathogenic protein assemblies in neurodegenerative diseases. *Nat Neurosci* **21**, 1341-1349 (2018).

42 Barkhof, F., Calabresi, P. A., Miller, D. H. & Reingold, S. C. Imaging outcomes for neuroprotection and repair in multiple sclerosis trials. *Nat Rev Neurol* **5**, 256-266 (2009).

43 Chard, D. T. *et al.* Brain atrophy in clinically early relapsing–remitting multiple sclerosis. *Brain* **125**, 327-337 (2002).

44 Lucchinetti, C. F. *et al.* Inflammatory cortical demyelination in early multiple sclerosis. *New Engl J Med* **365**, 2188-2197 (2011).

45 Dutra, R. C. *et al.* Spatial reference memory deficits precede motor dysfunction in an experimental autoimmune encephalomyelitis model: The role of kallikrein–kinin system. *Brain Behav Immun* **33**, 90-101 (2013).

46 Scalfari, A. *et al.* The natural history of multiple sclerosis: a geographically based study 10: relapses and long-term disability. *Brain J Neurol* **133**, 1914-1929 (2010).

47 Mandolesi, G. *et al.* Synaptopathy connects inflammation and neurodegeneration in multiple sclerosis. *Nat Rev Neurol* **11**, 711-724 (2015).

48 Hauser, S. L. & Oksenberg, J. R. The Neurobiology of Multiple Sclerosis: Genes, Inflammation, and Neurodegeneration. *Neuron* **52**, 61-76 (2006).

49 Simmons, S. B., Pierson, E. R., Lee, S. Y. & Goverman, J. M. Modeling the heterogeneity of multiple sclerosis in animals. *Trends Immunol* **34**, 410-422 (2013).

50 Gold, R., Linington, C. & Lassmann, H. Understanding pathogenesis and therapy of multiple sclerosis via animal models: 70 years of merits and culprits in experimental autoimmune encephalomyelitis research. *Brain* **129**, 1953-1971 (2006).

51 Frischer, J. M. *et al.* The relation between inflammation and neurodegeneration in multiple sclerosis brains. *Brain* **132**, 1175-1189 (2009).

52 Venken, K. *et al.* Natural Naive $CD4^+$ $CD25^+$ CD127 low Regulatory T Cell (Treg) Development and Function Are Disturbed in Multiple Sclerosis Patients: Recovery of Memory Treg Homeostasis during Disease Progression. *J Immunol* **180**, 6411-6420 (2008).

53 Willing, A. *et al.* CD8 + MAIT cells infiltrate into the CNS and alterations in their blood frequencies correlate with IL-18 serum levels in multiple sclerosis: Clinical immunology. *Eur J Immunol* **44**, 3119-3128 (2014).

54 Abrahamsson, S. V. *et al.* Non-myeloablative autologous haematopoietic stem cell transplantation expands regulatory cells and depletes IL-17 producing mucosal-associated invariant T cells in multiple sclerosis. *Brain J Neurol* **136**, 2888-2903 (2013).

55 Correale, J. & Villa, A. Role of $CD8^+$ $CD25^+$ $Foxp3^+$ regulatory T cells in multiple sclerosis. *Ann Neurol* **67**, 625-638 (2010).

56 Lassmann, H. Multiple Sclerosis Pathology. *Cold Spring Harb Perspect Med* **8**, a028936 (2018).

57 McMurran, C. E., Jones, C. A., Fitzgerald, D. C. & Franklin, R. J. M. CNS Remyelination and the Innate Immune System. *Frontiers Cell Dev Biology* **4**, 38 (2016).

58 Prinz, M., Priller, J., Sisodia, S. S. & Ransohoff, R. M. Heterogeneity of CNS myeloid cells and their roles in neurodegeneration. *Nat Neurosci* **14**, 1227-1235 (2011).

59 Howell, O. W. *et al.* Meningeal inflammation is widespread and linked to cortical pathology in multiple sclerosis. *Brain J Neurol* **134**, 2755-2771 (2011).

60 Lucchinetti, C. *et al.* Heterogeneity of multiple sclerosis lesions: Implications for the pathogenesis of demyelination. *Ann Neurol* **47**, 707-717 (2000).

61 Leypoldt, F., Armangue, T. & Dalmau, J. Autoimmune encephalopathies: Autoimmune encephalopathies. *Ann N Y Acad Sci* **1338**, 94-114 (2014).

62 Brändle, S. M. *et al.* Distinct oligoclonal band antibodies in multiple sclerosis recognize ubiquitous self-proteins. *Proc Natl Acad Sci* **113**, 7864-7869 (2016).

63 Wherry, E. J. T cell exhaustion. *Nat Immunol* **12**, 492-499 (2011).

64 Ponath, G., Park, C. & Pitt, D. The Role of Astrocytes in Multiple Sclerosis. *Front Immunol* **9**, 217 (2018).

65 Maggi, P. *et al.* The formation of inflammatory demyelinated lesions in cerebral white matter: Inflammatory Brain Lesions. *Ann Neurol* **76**, 594-608 (2014).

66 Liddelow, S. A. *et al.* Neurotoxic reactive astrocytes are induced by activated microglia. *Nature* **541**, 481-487 (2017).

67 Correale, J. The role of microglial activation in disease progression. *Mult Scler J* **20**, 1288-1295 (2014).

68 Aguzzi, A., Barres, B. A. & Bennett, M. L. Microglia: Scapegoat, Saboteur, or Something Else? *Science* **339**, 156-161 (2013).

69 Tan, Y.-L., Yuan, Y. & Tian, L. Microglial regional heterogeneity and its role in the brain. *Mol Psychiatr* **25**, 351-367 (2019).

70 Herranz, E. *et al.* The neuroinflammatory component of gray matter pathology in multiple sclerosis. *Ann Neurol* **80**, 776-790 (2016).

71 Mahmoud, S., Gharagozloo, M., Simard, C. & Gris, D. Astrocytes Maintain Glutamate Homeostasis in the CNS by Controlling the Balance between Glutamate Uptake and Release. *Cells* **8**, 184 (2019).

72 Ludwin, S. K., Rao, V. T. S., Moore, C. S. & Antel, J. P. Astrocytes in multiple sclerosis. *Mult Scler J* **22**, 1114-1124 (2016).

73 Correale, J. & Farez, M. F. The Role of Astrocytes in Multiple Sclerosis Progression. *Front Neurol* **6**, 180 (2015).

74 Airas, L., Nylund, M. & Rissanen, E. Evaluation of Microglial Activation in Multiple Sclerosis Patients Using Positron Emission Tomography. *Front Neurol* **9**, 181 (2018).

75 Filippo, M. D. *et al.* Persistent activation of microglia and NADPH oxidase drive hippocampal dysfunction in experimental multiple sclerosis. *Sci Rep* **6**, 20926 (2016).

76 Habbas, S. *et al.* Neuroinflammatory TNF α Impairs Memory via Astrocyte Signaling. *Cell* **163**, 1730-1741 (2015).

77 Kornek, B. *et al.* Multiple Sclerosis and Chronic Autoimmune Encephalomyelitis. *Am J Pathol* **157**, 267-276 (2000).

78 Rivers, T. M., Sprunt, D. H. & Berry, G. P. Observations on attempts to produce acute disseminated encephalomyelitis in monkeys. *J Exp Med* **58**, 39-53 (1933).

79 Kipp, M. *et al.* Experimental in vivo and in vitro models of multiple sclerosis: EAE and beyond. *Mult Scler Relat Disord* **1**, 15-28 (2012).

80 Mount, C. W. & Monje, M. Wrapped to Adapt: Experience-Dependent Myelination. *Neuron* **95**, 743-756 (2017).

81 Miller, S. D. & Karpus, W. J. Experimental Autoimmune Encephalomyelitis in the Mouse. *Curr Protoc Immunol* **77**, Unit 15.11 (2007).

82 Stromnes, I. M. & Goverman, J. M. Active induction of experimental allergic encephalomyelitis. *Nat Protoc* **1**, 1810-1819 (2006).

83 Brown, D. A. & Sawchenko, P. E. Time course and distribution of inflammatory and neurodegenerative events suggest structural bases for the pathogenesis of experimental autoimmune encephalomyelitis. *J Comp Neurol* **502**, 236-260 (2007).

84 Friese, M. A. *et al.* The value of animal models for drug development in multiple sclerosis. *Brain* **129**, 1940-1952 (2006).

85 Constantinescu, C. S., Farooqi, N., O'Brien, K. & Gran, B. Experimental autoimmune encephalomyelitis (EAE) as a model for multiple sclerosis (MS). *Brit J Pharmacol* **164**, 1079-1106 (2011).

86 Clements, R. J., McDonough, J. & Freeman, E. J. Distribution of parvalbumin and calretinin immunoreactive interneurons in motor cortex from multiple sclerosis post-mortem tissue. *Exp Brain Res* **187**, 459-465 (2008).

87 Musella, A., Mandolesi, G., Mori, F., Gentile, A. & Centonze, D. Linking synaptopathy and gray matter damage in multiple sclerosis. *Multiple Scler* **22**, 146-149 (2016).

88 Mandolesi, G., Grasselli, G., Musumeci, G. & Centonze, D. Cognitive deficits in experimental autoimmune encephalomyelitis: neuroinflammation and synaptic degeneration. *Neurol Sci* **31**, S255-259 (2010).

89 Peterson, J. W., Bö, L., Mörk, S., Chang, A. & Trapp, B. D. Transected neurites, apoptotic neurons, and reduced inflammation in cortical multiple sclerosis lesions: Cortical Lesions in MS. *Ann Neurol* **50**, 389-400 (2001).

90 Wegner, C., Esiri, M. M., Chance, S. A., Palace, J. & Matthews, P. M. Neocortical neuronal, synaptic, and glial loss in multiple sclerosis. *Neurology* **67**, 960-967 (2006).

91 Marques, K. B., Santos, L. M. B. & Oliveira, A. L. R. Spinal motoneuron synaptic plasticity during the course of an animal model of multiple sclerosis. *Eur J Neurosci* **24**, 3053-3062 (2006).

92 Mandolesi, G. *et al.* Interleukin-1 Alters Glutamate Transmission at Purkinje Cell Synapses in a Mouse Model of Multiple Sclerosis. *J Neurosci* **33**, 12105-12121 (2013).

93 Geurts, J. J. G. *et al.* Expression patterns of Group III metabotropic glutamate receptors mGluR4 and mGluR8 in multiple sclerosis lesions. *J Neuroimmunol* **158**, 182-190 (2005).

94 Meldrum, B. S. Glutamate as a Neurotransmitter in the Brain: Review of Physiology and Pathology. *J Nutrition* **130**, 1007S-1015S (2000).

95 Zhou, Y. & Danbolt, N. C. Glutamate as a neurotransmitter in the healthy brain. *J Neural Transm* **121**, 799-817 (2014).

96 Platt, S. R. The role of glutamate in central nervous system health and disease – A review. *Vet J* **173**, 278-286 (2007).

97 Madden, D. R. The structure and function of glutamate receptor ion channels. *Nat Rev Neurosci* **3**, 91-101 (2002).

98 Traynelis, S. F. *et al.* Glutamate receptor ion channels: structure, regulation, and function. *Pharmacol Rev* **62**, 405-496 (2010).

99 Liu, S. J. & Zukin, R. S. Ca2+-permeable AMPA receptors in synaptic plasticity and neuronal death. *Trends Neurosci* **30**, 126-134 (2007).

100 Dong, X.-x., Wang, Y. & Qin, Z.-h. Molecular mechanisms of excitotoxicity and their relevance to pathogenesis of neurodegenerative diseases. *Acta Pharmacol Sin* **30**, 379-387 (2009).

101 Tzschentke, T. M. Glutamatergic mechanisms in different disease states: overview and therapeutical implications - An introduction. *Amino Acids* **23**, 147-152 (2002).

102 Lissin, D. V. *et al.* Activity differentially regulates the surface expression of synaptic AMPA and NMDA glutamate receptors. *Proc National Acad Sci* **95**, 7097-7102 (1998).

103 Nakagawa, T. Structures of the AMPA receptor in complex with its auxiliary subunit cornichon. *Science* **366**, 1259-1263 (2019).

104 Midgett, C. R., Gill, A. & Madden, D. R. Domain architecture of a calcium-permeable AMPA receptor in a ligand-free conformation. *Front Mol Neurosci* **4**, 56 (2012).

105 Wang, M. *et al.* Direct interaction between GluR2 and GAPDH regulates AMPAR-mediated excitotoxicity. *Mol Brain* **5**, 13 (2012).

106 Contractor, A. & Swanson, G. T. The Receptors. 99-158 (2008).

107 Bowie, D. Ionotropic Glutamate Receptors & CNS Disorders. *CNS Neurol Disord Drug Targets* **7**, 129-143 (2008).

108 Wang, Y. & Qin, Z.-H. Molecular and cellular mechanisms of excitotoxic neuronal death. *Apoptosis* **15**, 1382-1402 (2010).

109 Kostic, M., Zivkovic, N. & Stojanovic, I. Multiple sclerosis and glutamate excitotoxicity. *Rev Neurosci* **24**, 71-88 (2013).

110 Hardingham, G. E., Chawla, S., Johnson, C. M. & Bading, H. Distinct functions of nuclear and cytoplasmic calcium in the control of gene expression. *Nature* **385**, 260-265 (1997).

111 Bading, H. Transcription-dependent neuronal plasticity: The nuclear calcium hypothesis. *Eur J Biochem* **267**, 5280-5283 (2000).

112 Hardingham, G. E., Fukunaga, Y. & Bading, H. Extrasynaptic NMDARs oppose synaptic NMDARs by triggering CREB shut-off and cell death pathways. *Nat Neurosci* **5**, 405-414 (2002).

113 Hardingham, G. E. & Bading, H. Synaptic versus extrasynaptic NMDA receptor signalling: implications for neurodegenerative disorders. *Nat Rev Neurosci* **11**, 682-696 (2010).

114 Zhou, X., Hollern, D., Liao, J., Andrechek, E. & Wang, H. NMDA receptor-mediated excitotoxicity depends on the coactivation of synaptic and extrasynaptic receptors. *Cell Death Dis* **4**, e560 (2013).

115 Choquet, D. Linking Nanoscale Dynamics of AMPA Receptor Organization to Plasticity of Excitatory Synapses and Learning. *J Neurosci* **38**, 9318-9329 (2018).

116 Santos, A. E. *et al.* Excitotoxicity mediated by Ca2+-permeable GluR4-containing AMPA receptors involves the AP-1 transcription factor. *Cell Death Differ* **13**, 652-660 (2005).

117 Lewerenz, J. & Maher, P. Chronic Glutamate Toxicity in Neurodegenerative Diseases-What is the Evidence? *Front Neurosci* **9**, 469 (2015).

118 Pitt, D., Werner, P. & Raine, C. S. Glutamate excitotoxicity in a model of multiple sclerosis. *Nat Med* **6**, 67-70 (2000).

119 Luchtman, D. *et al.* In vivo and in vitro effects of multiple sclerosis immunomodulatory therapeutics on glutamatergic excitotoxicity. *J Neurochem* **136**, 971-980 (2016).

120 Villoslada, P., Arrondo, G., Sepulcre, J., Alegre, M. & Artieda, J. Memantine induces reversible neurologic impairment in patients with MS. *Neurology* **72**, 1630-1633 (2008).

121 Paul, C. & Bolton, C. Modulation of Blood-Brain Barrier Dysfunction and Neurological Deficits during Acute Experimental Allergic Encephalomyelitis by the N -Methyl-d-aspartate Receptor Antagonist Memantine. *J Pharmacol Exp Ther* **302**, 50-57 (2002).

122 Werner, P., Pitt, D. & Raine, C. S. Multiple sclerosis: Altered glutamate homeostasis in lesions correlates with oligodendrocyte and axonal damage. *Ann Neurol* **50**, 169-180 (2001).

123 Azevedo, C. J. *et al.* In vivo evidence of glutamate toxicity in multiple sclerosis. *Ann Neurol* **76**, 269-278 (2014).

124 Piani, D., Frei, K., Do, K. Q., Cuénod, M. & Fontana, A. Murine brain macrophages induce NMDA receptor mediated neurotoxicity in vitro by secreting glutamate. *Neurosci Lett* **133**, 159-162 (1991).

125 Sarchielli, P., Greco, L., Floridi, A., Floridi, A. & Gallai, V. Excitatory Amino Acids and Multiple Sclerosis. *Arch Neurol* **60**, 1082 (2003).

126 MacMillan, E. L. *et al.* Progressive multiple sclerosis exhibits decreasing glutamate and glutamine over two years. *Mult Scler* **22**, 112-116 (2015).

127 Hädel, S., Wirth, C., Rapp, M., Gallinat, J. & Schubert, F. Effects of age and sex on the concentrations of glutamate and glutamine in the human brain. *J Magnetic Reson Imaging* **38**, 1480-1487 (2013).

128 Sitges, M., Guarneros, A. & Nekrassov, V. Effects of carbamazepine, phenytoin, valproic acid, oxcarbazepine, lamotrigine, topiramate and vinpocetine on the presynaptic $Ca2^{+}$ channel-mediated release of [^{3}H]glutamate: Comparison with the Na^{+} channel-mediated release. *Neuropharmacology* **53**, 854-862 (2007).

129 Freria, C. M., Zanon, R. G., Santos, L. M. B. & Oliveira, A. L. R. Major histocompatibility complex class I expression and glial reaction influence spinal motoneuron synaptic plasticity during the course of experimental autoimmune encephalomyelitis. *J Comp Neurology* **518**, 990-1007 (2010).

130 Dutta, R. *et al.* Mitochondrial dysfunction as a cause of axonal degeneration in multiple sclerosis patients. *Ann Neurol* **59**, 478-489 (2006).

131 Falco, A., Pennucci, R., Brambilla, E. & Curtis, I. d. Reduction in parvalbumin-positive interneurons and inhibitory input in the cortex of mice with experimental autoimmune encephalomyelitis. *Exp Brain Res* **232**, 2439-2449 (2014).

132 Smith, T., Groom, A., Zhu, B. & Turski, L. Autoimmune encephalomyelitis ameliorated by AMPA antagonists. *Nat Med* **6**, 62-66 (2000).

133 Groom, A. J., Ith, T. & Turski, L. Multiple Sclerosis and Glutamate. *Ann Ny Acad Sci* **993**, 229-275 (2003).

134 Zhai, D. *et al.* Blocking GluR2-GAPDH ameliorates experimental autoimmune encephalomyelitis. *Ann Clin Transl Neur* **2**, 388-400 (2015).

135 Carriedo, S. G., Sensi, S. L., Yin, H. Z. & Weiss, J. H. AMPA Exposures Induce Mitochondrial Ca 2^{+} Overload and ROS Generation in Spinal Motor Neurons In Vitro. *J Neurosci* **20**, 240-250 (2000).

136 Carriedo, S. G., Yin, H. Z. & Weiss, J. H. Motor Neurons Are Selectively Vulnerable to AMPA/Kainate Receptor-Mediated Injury In Vitro. *J Neurosci* **16**, 4069-4079 (1996).

137 Rothstein, J. D. & Kuncl, R. W. Neuroprotective Strategies in a Model of Chronic Glutamate-Mediated Motor Neuron Toxicity. *J Neurochem* **65**, 643-651 (2002).

138 Rothstein, J. D., Jin, L., Dykes-Hoberg, M. & Kuncl, R. W. Chronic inhibition of glutamate uptake produces a model of slow neurotoxicity. *Proc National Acad Sci* **90**, 6591-6595 (1993).

139 Netzahualcoyotzi, C. & Tapia, R. Degeneration of spinal motor neurons by chronic AMPA-induced excitotoxicity in vivo and protection by energy substrates. *Acta Neuropathol Commun* **3**, 27 (2015).

140 Banke, T. G. *et al.* Control of GluR1 AMPA Receptor Function by cAMP-Dependent Protein Kinase. *J Neurosci* **20**, 89-102 (2000).

141 Erausquin, G. A. d. *et al.* Nuclear Translocation of Nuclear Transcription Factor- κ B by α -Amino-3-hydroxy-5-methyl-4-isoxazolepropionic Acid Receptors Leads to Transcription of p53 and Cell Death in Dopaminergic Neurons. *Mol Pharmacol* **63**, 784-790 (2003).

142 Furukawa, K. & Mattson, M. P. The Transcription Factor NF- κ B Mediates Increases in Calcium Currents and Decreases in NMDA- and AMPA/Kainate-Induced Currents Induced by Tumor Necrosis Factor- α in Hippocampal Neurons. *J Neurochem* **70**, 1876-1886 (2002).

143 Evonuk, K. S. *et al.* Reduction of AMPA receptor activity on mature oligodendrocytes attenuates loss of myelinated axons in autoimmune neuroinflammation. *Sci Adv* **6**, eaax5936 (2020).

144 Gallo, V. & Ghiani, C. A. Glutamate receptors in glia: new cells, new inputs and new functions. *Trends Pharmacol Sci* **21**, 252-258 (2000).

145 Ceprian, M. & Fulton, D. Glial Cell AMPA Receptors in Nervous System Health, Injury and Disease. *Int J Mol Sci* **20**, 2450 (2019).

146 Berezikov, E. Evolution of microRNA diversity and regulation in animals. *Nat Rev Genet* **12**, 846-860 (2011).

147 Lee, R. C., Feinbaum, R. L. & Ambros, V. The C. elegans heterochronic gene lin-4 encodes small RNAs with antisense complementarity to lin-14. *Cell* **75**, 843-854 (1993).

148 Pasquinelli, A. E. *et al.* Conservation of the sequence and temporal expression of let-7 heterochronic regulatory RNA. *Nature* **408**, 86-89 (2000).

149 Pauli, A., Rinn, J. L. & Schier, A. F. Non-coding RNAs as regulators of embryogenesis. *Nat Rev Genet* **12**, 136-149 (2011).

150 Esteller, M. Non-coding RNAs in human disease. *Nat Rev Genetics* **12**, 861-874 (2011).

151 Piket, E., Zheleznyakova, G. Y., Kular, L. & Jagodic, M. Small non-coding RNAs as important players, biomarkers and therapeutic targets in multiple sclerosis: A comprehensive overview. *J Autoimmun* **101**, 17-25 (2019).

152 Yue, F. *et al.* A comparative encyclopedia of DNA elements in the mouse genome. *Nature* **515**, 355-364 (2014).

153 Zeng, Y. & Cullen, B. R. Recognition and cleavage of primary microRNA transcripts. *Methods Mol Biol* **342** 49-56 (2006).

154 Kim, J. *et al.* A MicroRNA Feedback Circuit in Midbrain Dopamine Neurons. *Science* **317**, 1220-1224 (2007).

155 Hébert, S. S. *et al.* Genetic ablation of Dicer in adult forebrain neurons results in abnormal tau hyperphosphorylation and neurodegeneration. *Hum Mol Genet* **19**, 3959-3969 (2010).

156 Shin, D., Shin, J.-Y., McManus, M. T., Ptácek, L. J. & Fu, Y.-H. Dicer ablation in oligodendrocytes provokes neuronal impairment in mice. *Ann Neurol* **66**, 843-857 (2009).

157 Ling, S.-C. *et al.* ALS-associated mutations in TDP-43 increase its stability and promote TDP-43 complexes with FUS/TLS. *P Natl Acad Sci* **107**, 13318-13323 (2010).

158 Edbauer, D. *et al.* Regulation of Synaptic Structure and Function by FMRP-Associated MicroRNAs miR-125b and miR-132. *Neuron* **68**, 161 (2010).

159 Waterson, R. H., Lander, E. S. & Wilson, R. K. Initial sequence of the chimpanzee genome and comparison with the human genome. *Nature* **437**, 69-87 (2005).

160 Franchini, L. F. & Pollard, K. S. Human evolution: the non-coding revolution. *Bmc Biol* **15**, 89 (2017).

161 Laurent, J. M., Pinglay, S., Mitchell, L. & Brosh, R. Probing the dark matter of the human genome with big DNA. *Biochem* **41**, 46-48 (2019).

162 Nowakowski, T. J. *et al.* Regulation of cell-type-specific transcriptomes by microRNA networks during human brain development. *Nat Neurosci* **21**, 1784-1792 (2018).

163 Cao, X., Yeo, G., Muotri, A. R., Kuwabara, T. & Gage, F. H. Noncoding RNAs in the mammalian central nervous system. *Annu Rev Neurosci* **29**, 77-103 (2006).

164 Kosik, K. S. MicroRNAs and Cellular Phenotypy. *Cell* **143**, 21-26 (2010).

165 Friedman, R. C., Farh, H. K., Burge, C. B. & Bartel, D. P. Most mammalian mRNAs are conserved targets of microRNAs. *Genome Res* **19**, 92-105 (2008).

166 Gebert, L. F. R. & MacRae, I. J. Regulation of microRNA function in animals. *Nat Rev Mol Cell Bio* **20**, 21-37 (2018).

167 Ameres, S. L. & Zamore, P. D. Diversifying microRNA sequence and function. *Nat Rev Mol Cell Biol* **14**, 475-488 (2013).

168 Cai, X., Hagedo, C. H. & Cullen, B. R. Human microRNAs are processed from capped, polyadenylated transcripts that can also function as mRNAs. *RNA* **10**, 1957-1966 (2004).

169 Denli, A. M., Tops, B. B. J., Plasterk, R. H. A., Ketting, R. F. & Hannon, G. J. Processing of primary microRNAs by the Microprocessor complex. *Nature* **432**, 231-235 (2004).

170 Gregory, R. I. *et al.* The Microprocessor complex mediates the genesis of microRNAs. *Nature* **432**, 235-240 (2004).

171 Yi, R., Qin, Y., Macara, I. G. & Cullen, B. R. Exportin-5 mediates the nuclear export of pre-microRNAs and short hairpin RNAs. *Gene Dev* **17**, 3011-3016 (2003).

172 Bartel, D. P. MicroRNAs. *Cell* **116**, 281-297 (2004).

173 Grimson, A. *et al.* MicroRNA Targeting Specificity in Mammals: Determinants beyond Seed Pairing. *Mol Cell* **27**, 91-105 (2007).

174 Gu, S., Jin, L., Zhang, F., Sarnow, P. & Kay, M. A. Biological basis for restriction of microRNA targets to the 3' untranslated region in mammalian mRNAs. *Nat Struct Mol Biol* **16**, 144-150 (2009).

175 Guo, H., Ingolia, N. T., Weissman, J. S. & Bartel, D. P. Mammalian microRNAs predominantly act to decrease target mRNA levels. *Nature* **466**, 835-840 (2010).

176 Jonas, S. & Izaurralde, E. Towards a molecular understanding of microRNA-mediated gene silencing. *Nat Rev Genet* **16**, 421-433 (2015).

177 Liu, J. *et al.* Argonaute2 Is the Catalytic Engine of Mammalian RNAi. *Science* **305**, 1437-1441 (2004).

178 Tang, G., Reinhart, B. J., Bartel, D. P. & Zamore, P. D. A biochemical framework for RNA silencing in plants. *Gene Dev* **17**, 49-63 (2003).

179 Agarwal, V., Bell, G. W., Nam, J.-W. & Bartel, D. P. Predicting effective microRNA target sites in mammalian mRNAs. *Elife* **4**, e05005 (2015).

180 Bartel, D. P. MicroRNAs: Target Recognition and Regulatory Functions. *Cell* **136**, 215-233 (2009).

181 Selbach, M. *et al.* Widespread changes in protein synthesis induced by microRNAs. *Nature* **455**, 58-63 (2008).

182 Uhlmann, S. *et al.* Global microRNA level regulation of EGFR-driven cell-cycle protein network in breast cancer. *Mol Syst Biol* **8**, 570 (2012).

183 Park, C. Y., Choi, Y. S. & McManus, M. T. Analysis of microRNA knockouts in mice. *Hum Mol Genet* **19**, R169-175 (2010).

184 Mogilyansky, E. & Rigoutsos, I. The miR-17/92 cluster: a comprehensive update on its genomics, genetics, functions and increasingly important and numerous roles in health and disease. *Cell Death Differ* **20**, 1603-1614 (2013).

185 Neilsen, C. T., Goodall, G. J. & Bracken, C. P. IsomiRs – the overlooked repertoire in the dynamic microRNAome. *Trends Genet* **28**, 544-549 (2012).

186 Ros, X. *et al.* Structural Differences between Pri-miRNA Paralogs Promote Alternative Drosha Cleavage and Expand Target Repertoires. *Cell Rep* **26**, 447-459.e444 (2019).

187 Junker, A. *et al.* MicroRNA profiling of multiple sclerosis lesions identifies modulators of the regulatory protein CD47. *Brain* **132**, 3342-3352 (2009).

188 Juźwik, C. A. *et al.* Neuronal microRNA regulation in Experimental Autoimmune Encephalomyelitis. *Sci Rep* **8**, 13437 (2018).

189 Backes, C., Meese, E. & Keller, A. Specific miRNA Disease Biomarkers in Blood, Serum and Plasma: Challenges and Prospects. *Mol Diagn Ther* **20**, 509-518 (2016).

190 Gandhi, R. *et al.* Circulating MicroRNAs as biomarkers for disease staging in multiple sclerosis: Circulating MicroRNAs in MS. *Ann Neurol* **73**, 729-740 (2013).

191 Regev, K. *et al.* Comprehensive evaluation of serum microRNAs as biomarkers in multiple sclerosis. *Neurol Neuroimmunol Neuroinflamm* **3**, e296 (2016).

192 Regev, K. *et al.* Identification of MS-specific serum miRNAs in an international multicenter study. *Neurol Neuroimmunol Neuroinflamm* **5**, e491 (2018).

193 Ebrahimkhani, S. *et al.* Exosomal microRNA signatures in multiple sclerosis reflect disease status. *Sci Rep* **7**, 14293 (2017).

194 Regev, K. *et al.* Association Between Serum MicroRNAs and Magnetic Resonance Imaging Measures of Multiple Sclerosis Severity. *Jama Neurol* **74**, 275 (2017).

195 Wang, L. & Zhang, L. Circulating MicroRNAs as Diagnostic Biomarkers for Motor Neuron Disease. *Front Neurosci* **14**, 354 (2020).

196 Cheng, L., Sharples, R. A., Scicluna, B. J. & Hill, A. F. Exosomes provide a protective and enriched source of miRNA for biomarker profiling compared to intracellular and cell-free blood. *J Extracell Vesicles* **3**, 23743 (2014).

197 Prada, I. & Meldolesi, J. Binding and Fusion of Extracellular Vesicles to the Plasma Membrane of Their Cell Targets. *Int J Mol Sci* **17**, 1296 (2016).

198 Andaloussi, S. E. L., Mäger, I., Breakefield, X. O. & Wood, M. J. A. Extracellular vesicles: biology and emerging therapeutic opportunities. *Nat Rev Drug Discov* **12**, 347-357 (2013).

199 Chaudhuri, A. *et al.* TNFα and IL-1β modify the miRNA cargo of astrocyte shed extracellular vesicles to regulate neurotrophic signaling in neurons. *Cell Death Dis* **9**, 363 (2018).

200 Prada, I. *et al.* Glia-to-neuron transfer of miRNAs via extracellular vesicles: a new mechanism underlying inflammation-induced synaptic alterations. *Acta Neuropathol* **135**, 529-550 (2018).

201 Dickens, A. M. *et al.* Astrocyte-shed extracellular vesicles regulate the peripheral leukocyte response to inflammatory brain lesions. *Sci Signal* **10**, eaai7696 (2017).

202 Mandolesi, G. *et al.* miR-142-3p Is a Key Regulator of IL-1β-Dependent Synaptopathy in Neuroinflammation. *J Neurosci* **37**, 546-561 (2016).

203 Waschbisch, A. *et al.* Glatiramer Acetate Treatment Normalizes Deregulated microRNA Expression in Relapsing Remitting Multiple Sclerosis. *Plos One* **6**, e24604 (2011).

204 Keller, A. *et al.* Multiple Sclerosis: MicroRNA Expression Profiles Accurately Differentiate Patients with Relapsing-Remitting Disease from Healthy Controls. *Plos One* **4**, e7440 (2009).

205 Arruda, L. C. M. *et al.* Autologous hematopoietic SCT normalizes miR-16, -155 and -142-3p expression in multiple sclerosis patients. *Bone Marrow Transpl* **50**, 380-389 (2014).

206 Lescher, J. *et al.* MicroRNA regulation in experimental autoimmune encephalomyelitis in mice and marmosets resembles regulation in human multiple sclerosis lesions. *J Neuroimmunol* **246**, 27-33 (2012).

207 Murugaiyan, G., Beynon, V., Mittal, A., Joller, N. & Weiner, H. L. Silencing microRNA-155 ameliorates experimental autoimmune encephalomyelitis. *J Immunol* **187**, 2213-2221 (2011).

208 Vigorito, E., Kohlhaas, S., Lu, D. & Leyland, R. miR-155: an ancient regulator of the immune system. *Immunol Rev* **253**, 146-157 (2013).

209 Rodríguez-Galán, A., Fernández-Messina, L. & Sánchez-Madrid, F. Control of Immunoregulatory Molecules by miRNAs in T Cell Activation. *Front Immunol* **9**, 2148 (2018).

210 Gaudet, A. D. *et al.* miR-155 Deletion in Mice Overcomes Neuron-Intrinsic and Neuron-Extrinsic Barriers to Spinal Cord Repair. *J Neurosci* **36**, 8516-8532 (2016).

211 Morquette, B. *et al.* MicroRNA-223 protects neurons from degeneration in experimental autoimmune encephalomyelitis. *Brain* **142**, 2979-2995 (2019).

212 Harraz, M. M., Eacker, S. M., Wang, X., Dawson, T. M. & Dawson, V. L. MicroRNA-223 is neuroprotective by targeting glutamate receptors. *Proc National Acad Sci* **109**, 18962-18967 (2012).

213 Verma, P., Augustine, G. J., Ammar, M.-R., Tashiro, A. & Cohen, S. M. A neuroprotective role for microRNA miR-1000 mediated by limiting glutamate excitotoxicity. *Nat Neurosci* **18**, 379-385 (2015).

214 Schaefer, A. *et al.* Cerebellar neurodegeneration in the absence of microRNAs. *J Exp Med* **204**, 1553-1558 (2007).

215 Haramati, S. *et al.* miRNA malfunction causes spinal motor neuron disease. *P Natl Acad Sci* **107**, 13111-13116 (2010).

216 Griffiths-Jones, S., Grocock, R. J., Dongen, S. v., Bateman, A. & Enright, A. J. miRBase: microRNA sequences, targets and gene nomenclature. *Nucleic Acids Res* **34**, D140-D144 (2006).

217 Kozomara, A., Birgaoanu, M. & Griffiths-Jones, S. miRBase: from microRNA sequences to function. *Nucleic Acids Res* **47**, D155-D162 (2018).

218 He, M. *et al.* Cell-Type-Based Analysis of MicroRNA Profiles in the Mouse Brain. *Neuron* **73**, 35-48 (2012).

219 Jin, J. *et al.* miR-17-92 Cluster Regulates Adult Hippocampal Neurogenesis, Anxiety, and Depression. *Cell Rep* **16**, 1653-1663 (2016).

220 Kiezun, A. *et al.* miRviewer: a multispecies microRNA homologous viewer. *Bmc Res Notes* **5**, 92 (2012).

221 Sárközy, M., Kahán, Z. & Csont, T. A myriad of roles of miR-25 in health and disease. *Oncotarget* **9**, 21580-21612 (2018).

222 Brancati, G. & Großhans, H. An interplay of miRNA abundance and target site architecture determines miRNA activity and specificity. *Nucleic Acids Res* **46**, 3259-3269 (2018).

223 Kohram, F. *et al.* Cell type-dependent functions of microRNA-92a. *J Cell Biochem* **119**, 5798-5804 (2018).

224 Ventura, A. *et al.* Targeted Deletion Reveals Essential and Overlapping Functions of the miR-17~92 Family of miRNA Clusters. *Cell* **132**, 875-886 (2008).

225 Xiao, C. *et al.* Lymphoproliferative disease and autoimmunity in mice with increased miR-17-92 expression in lymphocytes. *Nat Immunol* **9**, 405-414 (2008).

226 Chen, C. *et al.* Dysregulated MicroRNA Involvement in Multiple Sclerosis by Induction of T Helper 17 Cell Differentiation. *Front Immunol* **9**, 1256 (2018).

227 Kouchkovsky, D. d. *et al.* microRNA-17-92 regulates IL-10 production by regulatory T cells and control of experimental autoimmune encephalomyelitis. *J Immunol* **191**, 1594-1605 (2013).

228 Garza-Manero, S., Arias, C., Bermúdez-Rattoni, F., Vaca, L. & Zepeda, A. Identification of age- and disease-related alterations in circulating miRNAs in a mouse model of Alzheimer's disease. *Front Cell Neurosci* **9**, 53 (2015).

229 Tung, Y.-T. *et al.* Mir-17~92 Confers Motor Neuron Subtype Differential Resistance to ALS-Associated Degeneration. *Cell Stem Cell* **25**, 193-209.e197 (2019).

230 Kannu, P. *et al.* Post-axial polydactyly type A2, overgrowth and autistic traits associated with a chromosome 13q31.3 microduplication encompassing miR-17-92 and GPC5. *Eur J Med Genet* **56**, 452-457 (2013).

231 Sakai, A. *et al.* MicroRNA cluster miR-17-92 regulates multiple functionally related voltage-gated potassium channels in chronic neuropathic pain. *Nat Commun* **8**, 16079 (2017).

232 Han, Y.-C. *et al.* An allelic series of miR-17~92–mutant mice uncovers functional specialization and cooperation among members of a microRNA polycistron. *Nat Genet* **47**, 766-775 (2015).

233 Jiang, S. *et al.* Molecular dissection of the miR-17-92 cluster's critical dual roles in promoting Th1 responses and preventing inducible Treg differentiation. *Blood* **118**, 5487-5497 (2011).

234 Zhang, Y. *et al.* The MicroRNA-17-92 Cluster Enhances Axonal Outgrowth in Embryonic Cortical Neurons. *J Neurosci* **33**, 6885-6894 (2013).

235 Bian, S. *et al.* MicroRNA cluster miR-17-92 regulates neural stem cell expansion and transition to intermediate progenitors in the developing mouse neocortex. *Cell Rep* **3**, 1398-1406 (2013).

236 Pontual, L. d. *et al.* Germline deletion of the miR-17~92 cluster causes skeletal and growth defects in humans. *Nat Genet* **43**, 1026-1030 (2011).

237 Penzkofer, D. *et al.* Phenotypic Characterization of miR-92a–/– Mice Reveals an Important Function of miR-92a in Skeletal Development. *Plos One* **9**, e101153 (2014).

238 Khuu, C., Utheim, T. P. & Sehic, A. The Three Paralogous MicroRNA Clusters in Development and Disease, miR-17-92, miR-106a-363, and miR-106b-25. *Sci* **2016**, 1-10 (2016).

239 Wang, Y., Luo, J., Zhang, H. & Lu, J. microRNAs in the Same Clusters Evolve to Coordinately Regulate Functionally Related Genes. *Mol Biol Evol* **33**, 2232-2247 (2016).

240 Rezaei, N. *et al.* MicroRNA-92a Drives Th1 Responses in the Experimental Autoimmune Encephalomyelitis. *Inflammation* **42**, 235-245 (2018).

241 Siedlecki-Wullich, D. *et al.* Altered microRNAs related to synaptic function as potential plasma biomarkers for Alzheimer's disease. *Alzheimer's Res Ther* **11**, 46 (2019).

242 Campos-Melo, D., Hawley, Z. C. E. & Strong, M. J. Dysregulation of human NEFM and NEFH mRNA stability by ALS-linked miRNAs. *Mol Brain* **11**, 43 (2018).

243 Yang, T. *et al.* miR-92 Suppresses Robo1 Translation to Modulate Slit Sensitivity in Commissural Axon Guidance. *Cell Rep* **24**, 2694-2708.e2696 (2018).

244 Tung, Y.-T. *et al.* Mir-17~92 Governs Motor Neuron Subtype Survival by Mediating Nuclear PTEN. *Cell Rep* **11**, 1305-1318 (2015).

245 Morgan, M., Iaconcig, A. & Muro, A. F. CPEB2, CPEB3 and CPEB4 are coordinately regulated by miRNAs recognizing conserved binding sites in paralog positions of their 3′-UTRs. *Nucleic Acids Res* **38**, 7698-7710 (2010).

246 Huang, Y.-S., Kan, M.-C., Lin, C.-L. & Richter, J. D. CPEB3 and CPEB4 in neurons: analysis of RNA-binding specificity and translational control of AMPA receptor GluR2 mRNA. *Embo J* **25**, 4865-4876 (2006).

247 Ford, L., Ling, E., Kandel, E. R. & Fioriti, L. CPEB3 inhibits translation of mRNA targets by localizing them to P bodies. *Proc National Acad Sci* **116**, 18078-18087 (2019).

248 Drisaldi, B. *et al.* SUMOylation Is an Inhibitory Constraint that Regulates the Prion-like Aggregation and Activity of CPEB3. *Cell Rep* **11**, 1694-1702 (2015).

249 Pavlopoulos, E. *et al.* Neuralized1 activates CPEB3: a function for nonproteolytic ubiquitin in synaptic plasticity and memory storage. *Cell* **147**, 1369-1383 (2011).

250 Kaczmarczyk, L. *et al.* New Phosphospecific Antibody Reveals Isoform-Specific Phosphorylation of CPEB3 Protein. *Plos One* **11**, e0150000 (2016).

251 Huang, Y. S., Jung, M. Y., Sarkissian, M. & Richter, J. D. N-methyl-D-aspartate receptor signaling results in Aurora kinase-catalyzed CPEB phosphorylation and alphaCaMKII mRNA polyadenylation at synapses. *Embo J* **21**, 2139-2148 (2002).

252 Chao, H.-W. *et al.* Deletion of CPEB3 Enhances Hippocampus-Dependent Memory via Increasing Expressions of PSD95 and NMDA Receptors. *J Neurosci* **33**, 17008-17022 (2013).

253 Peng, S.-C., Lai, Y.-T., Huang, H.-Y., Huang, H.-D. & Huang, Y.-S. A novel role of CPEB3 in regulating EGFR gene transcription via association with Stat5b in neurons. *Nucleic Acids Res* **38**, 7446-7457 (2010).

254 Wang, C. F. & Huang, Y. S. Calpain 2 Activated through N-Methyl-D-Aspartic Acid Receptor Signaling Cleaves CPEB3 and Abrogates CPEB3-Repressed Translation in Neurons. *Mol Cell Biol* **32**, 3321-3332 (2012).

255 Hodgman, R., Tay, J., Mendez, R. & Richter, J. D. CPEB phosphorylation and cytoplasmic polyadenylation are catalyzed by the kinase IAK1/Eg2 in maturing mouse oocytes. *Dev Camb Engl* **128**, 2815-2822 (2001).

256 Vetere, G. *et al.* Selective inhibition of miR-92 in hippocampal neurons alters contextual fear memory. *Hippocampus* **24**, 1458-1465 (2014).

257 Letellier, M. *et al.* miR-92a regulates expression of synaptic GluA1-containing AMPA receptors during homeostatic scaling. *Nat Neurosci* **17**, 1040-1042 (2014).

258 Lane, R. M. *et al.* Translating Antisense Technology into a Treatment for Huntington's Disease. *Methods Mol Biol* **1780**, 497-523 (2018).

259 Peng, Y. & Croce, C. M. The role of MicroRNAs in human cancer. *Signal Transduct Target Ther* **1**, 15004 (2016).

260 Becker, L. A. *et al.* Therapeutic reduction of ataxin-2 extends lifespan and reduces pathology in TDP-43 mice. *Nature* **544**, 367-371 (2017).

261 Lee, Y. *et al.* miR-19, miR-101 and miR-130 co-regulate ATXN1 levels to potentially modulate SCA1 pathogenesis. *Nat Neurosci* **11**, 1137-1139 (2008).

262 Kosik, K. S. The neuronal microRNA system. *Nat Rev Neurosci* **7**, 911-920 (2006).

263 Sood, P., Krek, A., Zavolan, M., Macino, G. & Rajewsky, N. Cell-type-specific signatures of microRNAs on target mRNA expression. *Proc National Acad Sci* **103**, 2746-2751 (2006).

264 Kay, M. A. State-of-the-art gene-based therapies: the road ahead. *Nat Rev Genet* **12**, 316-328 (2011).

265 Melo, S. *et al.* Small molecule enoxacin is a cancer-specific growth inhibitor that acts by enhancing TAR RNA-binding protein 2-mediated microRNA processing. *P Natl Acad Sci* **108**, 4394-4399 (2011).

266 Saito, Y. *et al.* Specific activation of microRNA-127 with downregulation of the proto-oncogene BCL6 by chromatin-modifying drugs in human cancer cells. *Cancer Cell* **9**, 435-443 (2006).

267 Lujambio, A. *et al.* Genetic Unmasking of an Epigenetically Silenced microRNA in Human Cancer Cells. *Cancer Res* **67**, 1424-1429 (2007).

268 Lu, Y. *et al.* A single anti-microRNA antisense oligodeoxyribonucleotide (AMO) targeting multiple microRNAs offers an improved approach for microRNA interference. *Nucleic Acids Res* **37**, e24 (2009).

269 Doyle, J. P. *et al.* Application of a translational profiling approach for the comparative analysis of CNS cell types. *Cell* **135**, 749-762 (2008).

270 Dunn, T. B. Normal and Pathologic Anatomy of the Reticular Tissue in Laboratory Mice, With a Classification and Discussion of Neoplasms. *J Natl Cancer Inst* **14**, 1281-1433 (1954).

271 Kalpachidou, T., Kummer, K. K., Mitrić, M. & Kress, M. Tissue Specific Reference Genes for MicroRNA Expression Analysis in a Mouse Model of Peripheral Nerve Injury. *Front Mol Neurosci* **12**, 283 (2019).

272 Schwarzenbach, H., Silva, A. M. d., Calin, G. & Pantel, K. Data Normalization Strategies for MicroRNA Quantification. *Clin Chem* **61**, 1333-1342 (2015).

273 Schattling, B. *et al.* Bassoon proteinopathy drives neurodegeneration in multiple sclerosis. *Nat Neurosci* **22**, 887-896 (2019).

274 Heiman, M., Kulicke, R., Fenster, R. J., Greengard, P. & Heintz, N. Cell type-specific mRNA purification by translating ribosome affinity purification (TRAP). *Nat Protoc* **9**, 1282-1291 (2014).

275 Capece, V. *et al.* Oasis: online analysis of small RNA deep sequencing data. *Bioinformatics* **31**, 2205-2207 (2015).

276 Love, M. I., Huber, W. & Anders, S. Moderated estimation of fold change and dispersion for RNA-seq data with DESeq2. *Genome Biol* **15**, 550 (2014).

277 Chen, J., Bardes, E. E., Aronow, B. J. & Jegga, A. G. ToppGene Suite for gene list enrichment analysis and candidate gene prioritization. *Nucleic Acids Res* **37**, W305-311 (2009).

278 Merico, D., Isserlin, R., Stueker, O., Emili, A. & Bader, G. D. Enrichment map: a network-based method for gene-set enrichment visualization and interpretation. *Plos One* **5**, e13984 (2010).

279 Dobin, A. *et al.* STAR: ultrafast universal RNA-seq aligner. *Bioinformatics* **29**, 15-21 (2012).

280 Liao, Y., Smyth, G. K. & Shi, W. featureCounts: an efficient general purpose program for assigning sequence reads to genomic features. *Bioinformatics* **30**, 923-930 (2013).

281 Fath, T., Ke, Y. D., Gunning, P., Götz, J. & Ittner, L. M. Primary support cultures of hippocampal and substantia nigra neurons. *Nat Protoc* **4**, 78-85 (2008).

282 Wujek, J. R. *et al.* Axon Loss in the Spinal Cord Determines Permanent Neurological Disability in an Animal Model of Multiple Sclerosis. *J Neuropathol Exp Neurolol* **61**, 23-32 (2002).

283 Vogt, J. *et al.* Lower motor neuron loss in multiple sclerosis and experimental autoimmune encephalomyelitis. *Ann Neurol* **66**, 310-322 (2009).

284 Bjartmar, C., Kidd, G., M□rk, S., Rudick, R. & Trapp, B. D. Neurological disability correlates with spinal cord axonal loss and reducedN-acetyl aspartate in chronic multiple sclerosis patients. *Ann Neurol* **48**, 893-901 (2000).

285 Filippi, M. *et al.* A spinal cord MRI study of benign and secondary progressive multiple sclerosis. *J Neurol* **243**, 502-505 (1996).

286 Bjartmar, C., Wujek, J. R. & Trapp, B. D. Axonal loss in the pathology of MS: consequences for understanding the progressive phase of the disease. *J Neurol Sci* **206**, 165-171 (2003).

287 Thiebes, K. P. *et al.* miR-218 is essential to establish motor neuron fate as a downstream effector of Isl1–Lhx3. *Nat Commun* **6**, 7718 (2015).

288 Pan, D. *et al.* A Neuron-Specific Host MicroRNA Targets Herpes Simplex Virus-1 ICP0 Expression and Promotes Latency. *Cell Host Microbe* **15**, 446-456 (2014).

289 Yuva-Aydemir, Y., Simkin, A., Gascon, E. & Gao, F.-B. MicroRNA-9: Functional evolution of a conserved small regulatory RNA. *RNA Biol* **8**, 557-564 (2011).

290 Zhou, B., Wang, S., Mayr, C., Bartel, D. P. & Lodish, H. F. miR-150, a microRNA expressed in mature B and T cells, blocks early B cell development when expressed prematurely. *Proc National Acad Sci* **104**, 7080-7085 (2007).

291 Lesuisse, C. & Martin, L. J. Long-term culture of mouse cortical neurons as a model for neuronal development, aging, and death. *J Neurobiol* **51**, 9-23 (2002).

292 Seibenhener, M. L. & Wooten, M. W. Isolation and culture of hippocampal neurons from prenatal mice. *J Vis Exp* **65**, 3634 (2012).

293 Clarkson, B. D. S., Kahoud, R. J., McCarthy, C. B. & Howe, C. L. Inflammatory cytokine-induced changes in neural network activity measured by waveform analysis of high-content calcium imaging in murine cortical neurons. *Sci Rep* **7**, 9037 (2017).

294 Ha, J. S., Lee, C.-S., Maeng, J.-S., Kwon, K.-S. & Park, S. S. Chronic glutamate toxicity in mouse cortical neuron culture. *Brain Res* **1273**, 138-143 (2009).

295 Ivanov, A. *et al.* Opposing role of synaptic and extrasynaptic NMDA receptors in regulation of the extracellular signal-regulated kinases (ERK) activity in cultured rat hippocampal neurons: Synaptic and extrasynaptic NMDAR in ERK activation. *J Physiol* **572**, 789-798 (2006).

296 Lin, C.-C. & Edelson, B. T. New Insights into the Role of IL-1β in Experimental Autoimmune Encephalomyelitis and Multiple Sclerosis. *J Immunol* **198**, 4553-4560 (2017).

297 Jin, Y., Chen, Z., Liu, X. & Zhou, X. Evaluating the microRNA targeting sites by luciferase reporter gene assay. *Methods Mol Biol* **935**, 117-127 (2012).

298 Hagedorn, P. H. *et al.* Locked nucleic acid: modality, diversity, and drug discovery. *Drug Discov Today* **23**, 101-114 (2017).

299 Savtchouk, I. *et al.* Topological Regulation of Synaptic AMPA Receptor Expression by the RNA-Binding Protein CPEB3. *Cell Reports* **17**, 86-103 (2016).

300 Bult, C. J. *et al.* Mouse Genome Database (MGD) 2019. *Nucleic Acids Res* **47**, D801-D806 (2018).

301 Steinbach, K. Role of autoimmune inflammation and impaired neuroregeneration in the pathogenesis of experimental autoimmune encephalomyelitis. *Diss* (2011)

302 Bácskai, T., Rusznák, Z., Paxinos, G. & Watson, C. Musculotopic organization of the motor neurons supplying the mouse hindlimb muscles: a quantitative study using Fluoro-Gold retrograde tracing. *Brain Struct Funct* **219**, 303-321 (2013).

303 Bannerman, P. G. *et al.* Motor neuron pathology in experimental autoimmune encephalomyelitis: studies in THY1-YFP transgenic mice. *Brain* **128**, 1877-1886 (2005).

304 Heiman, M. *et al.* A translational profiling approach for the molecular characterization of CNS cell types. *Cell* **135**, 738-748 (2008).

305 Diederichs, S. & Haber, D. A. Dual Role for Argonautes in MicroRNA Processing and Posttranscriptional Regulation of MicroRNA Expression. *Cell* **131**, 1097-1108 (2007).

306 Lewkowicz, P. *et al.* Dysregulated RNA-Induced Silencing Complex (RISC) Assembly within CNS Corresponds with Abnormal miRNA Expression during Autoimmune Demyelination. *J Neurosci* **35**, 7521-7537 (2015).

307 Schaefer, A. *et al.* Argonaute 2 in dopamine 2 receptor-expressing neurons regulates cocaine addiction. *J Exp Med* **207**, 1843-1851 (2010).

308 Morita, S. *et al.* One Argonaute family member, Eif2c2 (Ago2), is essential for development and appears not to be involved in DNA methylation. *Genomics* **89**, 687-696 (2007).

309 Hawley, Z. C. E., Campos-Melo, D., Droppelmann, C. A. & Strong, M. J. MotomiRs: miRNAs in Motor Neuron Function and Disease. *Front Mol Neurosci* **10**, 127 (2017).

310 McNeill, E. & Van Vactor, D. MicroRNAs Shape the Neuronal Landscape. *Neuron* **75**, 363-379 (2012).

311 Spriggs, K. A., Bushell, M. & Willis, A. E. Translational regulation of gene expression during conditions of cell stress. *Mol Cell* **40**, 228-237 (2010).

312 Sow, F. B., Gallup, J. M., Sacco, R. E. & Ackermann, M. R. Laser Capture Microdissection Revisited as a Tool for Transcriptomic Analysis: Application of an Excel-Based qPCR Preparation Software (PREXCEL-Q). *Int J Biomed Sci* **5**, 105-124 (2009).

313 Cantoni, C. *et al.* Mir-223 regulates the number and function of myeloid-derived suppressor cells in multiple sclerosis and experimental autoimmune encephalomyelitis. *Acta Neuropathol* **133**, 61-77 (2016).

314 Lindberg, R. L. P., Hoffmann, F., Mehling, M., Kuhle, J. & Kappos, L. Altered expression of miR-17-5p in CD4+ lymphocytes of relapsing-remitting multiple sclerosis patients. *Eur J Immunol* **40**, 888-898 (2010).

315 Fenoglio, C. *et al.* Expression and genetic analysis of miRNAs involved in CD4+ cell activation in patients with multiple sclerosis. *Neurosci Lett* **504**, 9-12 (2011).

316 Sanders, K. A. *et al.* Next-generation sequencing reveals broad down-regulation of microRNAs in secondary progressive multiple sclerosis CD4+ T cells. *Clin Epigenetics* **8**, 87 (2016).

317 Venkatesha, S. H., Dudics, S., Song, Y., Mahurkar, A. & Moudgil, K. D. The miRNA Expression Profile of Experimental Autoimmune Encephalomyelitis Reveals Novel Potential Disease Biomarkers. *Int J Mol Sci* **19**, 3990 (2018).

318 Born, G. *et al.* Modulation of synaptic function through the α-neurexin-specific ligand neurexophilin-1. *P Natl Acad Sci* **111**, E1274-1283 (2014).

319 Wegner, A. M. *et al.* N-wasp and the arp2/3 complex are critical regulators of actin in the development of dendritic spines and synapses. *J Biol Chem* **283**, 15912-15920 (2008).

320 Zamkova, M., Khromova, N., Kopnin, B. P. & Kopnin, P. Ras-induced ROS upregulation affecting cell proliferation is connected with cell type-specific alterations of HSF1/SESN3/p21Cip1/WAF1 pathways. *Cell Cycle* **12**, 826-836 (2013).

321 Wang, M. *et al.* Recent Insights into the Biological Functions of Sestrins in Health and Disease. *Cell Physiol Biochem* **43**, 1731-1741 (2017).

322 Lehoux, S. *et al.* Transcriptional regulation of the human ST6GAL2 gene in cerebral cortex and neuronal cells. *Glycoconj J* **27**, 99-114 (2009).

323 Kim, A. Y. *et al.* SCCRO (DCUN1D1) is an essential component of the E3 complex for neddylation. *J Biol Chem* **283**, 33211-33220 (2008).

324 Villa, C. *et al.* DCUN1D1 is a risk factor for frontotemporal lobar degeneration. *Eur J Neurol* **16**, 870-873 (2009).

325 Yokoshi, M. *et al.* Direct Binding of Ataxin-2 to Distinct Elements in 3′ UTRs Promotes mRNA Stability and Protein Expression. *Mol Cell* **55**, 186-198 (2014).

326 Ebert, M. S. & Sharp, P. A. Roles for MicroRNAs in Conferring Robustness to Biological Processes. *Cell* **149**, 515-524 (2012).

327 Leung, A. K. L. & Sharp, P. A. MicroRNA Functions in Stress Responses. *Mol Cell* **40**, 205-215 (2010).

328 Concepcion, C. P., Bonetti, C. & Ventura, A. The MicroRNA-17-92 Family of MicroRNA Clusters in Development and Disease. *Cancer J* **18**, 262-267 (2012).

329 Gogoleva, V. S. *et al.* Cytokines as Mediators of Neuroinflammation in Experimental Autoimmune Encephalomyelitis. *Biochem Biokhimiia* **83**, 1089-1103 (2018).

330 Centonze, D. *et al.* Inflammation Triggers Synaptic Alteration and Degeneration in Experimental Autoimmune Encephalomyelitis. *J Neurosci* **29**, 3442-3452 (2009).

331 Hu, Z. *et al.* miR-191 and miR-135 are required for long-lasting spine remodelling associated with synaptic long-term depression. *Nat Commun* **5**, 3263 (2014).

332 Stephan, J. S. *et al.* The CPEB3 Protein Is a Functional Prion that Interacts with the Actin Cytoskeleton. *Cell Rep* **11**, 1772-1785 (2015).

333 Fioriti, L. *et al.* The Persistence of Hippocampal-Based Memory Requires Protein Synthesis Mediated by the Prion-like Protein CPEB3. *Neuron* **86**, 1433-1448 (2015).

334 Rosenberg, T. *et al.* The roles of protein expression in synaptic plasticity and memory consolidation. *Front Mol Neurosci* **7**, 86 (2014).

335 Tsang, J., Zhu, J. & Oudenaarden, A. v. MicroRNA-Mediated Feedback and Feedforward Loops Are Recurrent Network Motifs in Mammals. *Mol Cell* **26**, 753-767 (2007).

336 Li, Y. *et al.* The miR-17-92 cluster expands multipotent hematopoietic progenitors whereas imbalanced expression of its individual oncogenic miRNAs promotes leukemia in mice. *Blood* **119**, 4486-4498 (2012).

337 Goverman, J. Autoimmune T cell responses in the central nervous system. *Nat Rev Immunol* **9**, 393-407 (2009).

338 Noctor, S. C., Martínez-Cerdeño, V. & Kriegstein, A. R. Contribution of Intermediate Progenitor Cells to Cortical Histogenesis. *Arch Neurol* **64**, 639-642 (2007).

339 Centonze D. miR-142-3p as Potential Biomarker of Synaptopathy in MS. *Case Medical Res* (2019).

340 Parisi, C. *et al.* Dysregulated microRNAs in amyotrophic lateral sclerosis microglia modulate genes linked to neuroinflammation. *Cell Death Dis* **4**, e959 (2013).

341 Waller, R. *et al.* Small RNA Sequencing of Sporadic Amyotrophic Lateral Sclerosis Cerebrospinal Fluid Reveals Differentially Expressed miRNAs Related to Neural and Glial Activity. *Front Neurosci* **11**, 731 (2018).

342 Freischmidt, A., Müller, K., Ludolph, A. C. & Weishaupt, J. H. Systemic dysregulation of TDP-43 binding microRNAs in amyotrophic lateral sclerosis. *Acta Neuropathol Commun* **1**, 42 (2013).

343 Waller, R. *et al.* Serum miRNAs miR-206, 143-3p and 374b-5p as potential biomarkers for amyotrophic lateral sclerosis (ALS). *Neurobiol Aging* **55**, 123-131 (2017).

344 Wu, X.-L. *et al.* MicroRNA-143 suppresses gastric cancer cell growth and induces apoptosis by targeting COX-2. *World J Gastroentero* **19**, 7758 (2013).

345 Ling, S.-C., Polymenidou, M. & Cleveland, D. W. Converging mechanisms in ALS and FTD: disrupted RNA and protein homeostasis. *Neuron* **79**, 416-438 (2013).

346 Dong, H. *et al.* Serum MicroRNA Profiles Serve as Novel Biomarkers for the Diagnosis of Alzheimer's Disease. *Dis Markers* **2015**, 1-11 (2015).

347 Rani, N. *et al.* A Primate lncRNA Mediates Notch Signaling during Neuronal Development by Sequestering miRNA. *Neuron* **90**, 1174-1188 (2016).

348 Ross, C. A. & Poirier, M. A. Protein aggregation and neurodegenerative disease. *Nat Med* **10**, S10-S17 (2004).

Confirmation of correctness of the English language

Brenna Fearey (MSc Neuroscience and Cognition)

Bei der Schilleroper 10

22767 Hamburg

I hereby confirm that the Dissertation of Iris Winkler is written in correct English.

Brenna Fearey Place, Date

Affidavit

I hereby confirm that this dissertation is my own written work and that I have used no sources and aids other than indicated.

Iris Winkler Place, Date

Acknowledgement

I thank Prof. Dr. Manuel Alexander Friese for the great supervision, his support, the scientific discussions and scientific freedom in working at this exciting cutting-edge project in preclinical science. I am very thankful to have visited diverse leading scientific conferences and workshops to present my work and improve and expand my soft skills as well as for being a part of the DFG *Schwerpunktprogramm* SPP 1738.

I thank Prof. Dr. Christian Lohr for co-supervising my work and together with Prof. Matthias Kneussel, Prof. Dr. Boris Fehse and Dr. Guido Hermey for being my thesis committee, supporting the project with their experience and helpful ideas.

Many thanks to Dr. Dr. Jan Broder Engler for his expertise and support, great ideas, for his aestheticism and critical view as well as for being a role model in the INIMS lab. Many thanks for the bioinformatic contributions to this work and the proof-reading.

I thank Dr. Ole Pless and Dr. Benjamin Schattling for the financial and scientific initiation of this interesting project.

I heartily thank all members of the lab for the scientific and non-scientific discussions and the good atmosphere in the laboratory. Special thanks to Lukas Bal for his support in this work.

Many thanks to Simone Träger, Simone Bauer, Vanessa Vieira and Nina Kursave for the technical support and help.

I am very grateful for everybody who supported me in the last years and from whom I got to learn. I especially thank all the people in my life– my friends and my family.